

**WIND POWER GENERATION AND INTEGRATION INTO A LOW-
COST FRESH PRODUCE PRESERVATION TECHNOLOGY: A CASE
OF A RENEWABLE ENERGY INTEGRATION INTO AN
EVAPORATIVE COOLING SYSTEM**

P Mthethwa

Submitted in partial fulfilment of the
requirements for the degree of MScEng

Bioresources Engineering
School of Engineering
University of KwaZulu-Natal
Pietermaritzburg
South Africa
June 23

Supervisor: Prof TS Workneh

Co-supervisor: Dr A Kassim

DECLARATION ON PLAGIARISM

I, Perm Mthethwa, declare that:

- (a) The research reported in this thesis, except where otherwise indicated, is my original work.
- (b) This thesis has not been submitted for any degree or examination at any other university.
- (c) This thesis does not contain text, data, figures, pictures, graphs or tables from another document, unless it is specifically acknowledged as being sourced from the original document. Where other sources have been quoted, then:
 - i) their words have been paraphrased/re-written, and the general information attributed to them has been referenced, and
 - ii) where their exact words have been used, their writing has been placed inside quotation marks, and referenced.
- (d) Where I have reproduced a publication, of which I am an author, co-author or editor, I have indicated in detail which part of the publication was actually written by myself alone and have fully referenced such publications.
- (e) This document does not contain text, graphics or tables copied and pasted from the Internet, unless they are specifically acknowledged, and the source is detailed, both in the document and in the References section.

Signed: 

Date: 20/12/2022

Supervis 

Date: 21/12/2022

Co-supervisor:

Date:

ABSTRACT

Smallholder farmers in developing countries experience high-postharvest losses (PHL) estimated around 23% during the transportation of fruit and vegetables. This is due to the inappropriate storage facilities that are unable to maintain optimum environmental conditions which are specific to the fresh produce. This situation arises because smallholder farmers cannot afford the available mobile cooling technologies such as refrigerated trucks since they are energy-intensive which makes them have high running costs in addition to the associated high investment costs. Consequently, smallholder farmers resort to utilizing small vehicles to transport fresh produce without air conditioning to cool the environment. These vehicles usually have an environment mainly characterized by high temperature and low relative humidity which are undesirable conditions for fresh produce. The power supply is a great challenge for mobile cooling technologies. As the main energy source, mobile cooling technologies use petrol and diesel to power the systems. These energy sources are costly, rapidly depleting, and detrimental to the atmosphere. Renewable energy sources such as biomass, solar and wind energy are promising technologies to substitute fossil fuels to power cooling technologies. Using renewable energy sources reduces the high incurring costs of operating a cooling technology, which ultimately reduces the purchase or lease costs. Since there is high airflow on the road associated with moving vehicles, this study aims to design and develop a small wind turbine to power an evaporative cooling system (ECS) during the transportation of fruit and vegetables in KwaZulu-Natal. The design of the wind turbine is done with the assistance of the Blade Element Momentum (BEM) theory, QBlade and MATLAB Simulink modelling software. A prototype of the wind turbine was designed, developed and tested on a moving vehicle between Pietermaritzburg and Estcourt. The wind turbine is 600 mm in diameter and made of three PVC pipe material blades connected by a 60 x 2 mm diameter mild steel plate hub protected by an 800 x 800 x 500 mm mild steel protective casing. The wind turbine was tested against three vehicle speeds of 60, 80, and 100 km.h⁻¹, and the two opening levels, level 1 at 45° and level 2 at 80° relative to the louvre mechanism frame. The results of this study revealed that the power output is significantly influenced ($p < 0.001$) by both the vehicle speed and louvre opening level. The power output of 113.4, 159.6 and 210.0 W per hour was observed for the vehicle speed of 60, 80 and 100 km.h⁻¹, respectively, on louvre opening level 1. Further, the power output of 142.8, 268.8 and 294.0 W per hour was observed for a wind speed of 60, 80, and 100 km.h⁻¹, respectively on louvre opening level 2. This shows

that higher wind speeds (vehicle speeds) obtain higher power output which account for the small size of the wind turbine rotor. The maximum power of 294 W was obtained at a vehicle speed of 100 km.h⁻¹ (27.78 m.s⁻¹), for louvre opening level 2 which achieved a maximum power coefficient of 0.49. With the assistance of the 600 W, 230 VAC power inverter, these power outputs are sufficient to provide power to a 600 W load (ECS unit). A study of the wind turbine integrated with a 53 m³ evaporative cooler at the Ukulinga research farm was also performed to assess the capability of the wind turbine to provide power to the cooling system. Grid electricity was used as a control measure to assess the performance of the wind turbine. The performance of the wind turbine and grid powered ECS unit was assessed by determining the temperature drop, the relative humidity increase and the cooling efficiency. The temperature inside the ECS unit varied between 24.65 – 31.87 °C with a temperature drop range of 2.85 °C to 10.59 °C from the ambient temperature while using the wind turbine as the power source. The relative humidity of the wind turbine-powered ECS unit ranged between 57.8 – 88.77 % with a relative humidity increase range varying between 21.66 – 29.04 %. For the grid-powered ECS unit, the temperature inside the storage unit ranged between 23.71 – 25.23 °C. Then the temperature drop was found to be 3.91 – 15.75 °C. While being powered by the grid the ECS unit, the inside relative humidity increase varied between 28.52 – 47.66 %. The cooling efficiency varied between 12.62 – 59.78 % and 14.26 – 55.93 % for the wind turbine and grid electricity power source, respectively. The wind turbine performance assessed in terms of the temperature drop and relative humidity increase control in the ECS unit was comparable to that observed with the grid electricity power source. Therefore, the designed wind turbine can be used as a primary or alternate source of electricity to power an ECS unit or any mobile cooling technologies when the wind turbine is correctly sized according to the power requirement of the cooling technology electrical components following the path used in this study.

DECLARATION ON PUBLICATION

This section contains work that is published or to be published based on this research study.

Published manuscript

Mthethwa, P., Workneh, T.S. and Kassim, A. 2022. Small wind turbine blade optimisation and design using QBlade for integration into a low-cost fresh produce preservation technology. *Acta Horticulturae* 1349 (5) (417-426)

Manuscript Impress

Mthethwa, P., Workneh, T.S. and Kassim, A. 2023. Other alternative energy sources that could be utilized towards the operation of evaporative coolant structures most especially in rural communities where there is no electricity. In ed. Workneh, TS, *Engineering Principles, Modelling and Economics of Evaporative Coolers*. Chapter 8. Elsevier Science & Technology, Oxford, United Kingdom.

Mthethwa, P., Workneh, T.S. and Kassim, A. 2023. Renewable Energy Integration into a Low-Cost Evaporative Cooling System for Fresh Produce Storage. In ed. Workneh, TS, *Engineering Principles, Modelling and Economics of Evaporative Coolers*. Chapter 9. Elsevier Science & Technology, Oxford, United Kingdom.

ACKNOWLEDGEMENTS

I would like to extend my profound appreciation to the following people and parties who were instrumental in the success of this research study:

- My supervisor, Prof. TS Workneh and co-supervisor Dr A Kassim who granted me this opportunity. I am forever grateful for the academic support, guidance and trust you put in me.
- The technical staff, Mr Mazibuko, Mr Nxumalo and Mr Hlatshwayo for the technical support during the construction and testing phase as well as material procurement, I could not have done it without all of you.
- Other UKZN staff personnel, the Howard electrical engineering department for helping with the generator, the PMB nursery team for helping with the vacuum blower and anyone else who was instrumental in the success of this project.
- My family, for the emotional support, motivation and assistance throughout this journey, it does not go unseen.
- My friends, in and outside of the engineering field who were always encouraging, listening and ready to step-in and help at any time. Especially Sihle Mfusi for the electrical knowledge, and Steven Cossa for the procurement of the generator
- The WORNEH JW NELSON and SEYOUM UKZN scholarship for funding this project
- The God Almighty through which all things are possible, I could not have come this far without Your protection and wisdom. I am forever grateful.
- Lastly, I would like to dedicate this thesis to both my late mother, OY Mthethwa and father, NJ Mthethwa.

LIST OF ABBREVIATIONS AND SYMBOLS

Abbreviation	Term	Page
AC	Alternating Current	23
AOA	Angle of Attack	27
AR	Aspect Ratio between the Blade Length tip chord	34
BEM	Blade Element Momentum	7
CFRP	Carbon Fibre Reinforced Polymers	35
CO ₂	Carbon Dioxide	4
COP	Coefficient of Performance	16
CSP	Concentrated Solar Panels	17
DC	Direct Current	23
DEC	Direct Evaporative Cooling	12
DFIG	Doubly-Fed Induction Generator	22
EC	Evaporative Cooling	2
ECS	Evaporative Cooling System	4
FS	Fixed Speed	21
FV	Fruit and Vegetables	1
GFRP	Glass Fibre Reinforced Polymers	35
GHG	Greenhouse Gases	4
HAWT	Horizontal Axis Wind Turbine	26
IAC + EC	Indirect air cooling and evaporation cooling	13
IDEC	Indirect/Direct Evaporative Cooling	12
IEC	Indirect Evaporative Cooling	12
IEC	International Electrochemical Commission	18
IIR	International Institute of Refrigeration	1
Li-ion	Lithium ion	24

NFRP	Natural Fibre Reinforced Polymers	35
PHL	Post-harvest Losses	1
PMSG	Permanent Magnet Synchronous Generator	20
PV	Photovoltaic	17
PVC	Polyvinyl Chloride	35
RE	Renewable Energy	2
RES	Renewable Energy Sources	3
RH	Relative Humidity	1
TSR	Tip Speed Ratio	21
SCIG	Squirrel Cage Induction Generator	22
SDGs	Sustainable Development Goals	4
SPECSS	Solar Power Evaporative Cooling Storage System	16
SRG	Switched Reluctance General	22
SWOT	Strength, Weaknesses, Opportunities and Threats	35
SWT	Small Wind Turbines	5
VAWT	Vertical Axis Wind Turbine	26
VRLA	Value-regulated Lead Acid	24
VS	Variable Speed	21
WT	Wind Turbine	5

Symbol	Meaning	Page
a	Axial Induction Factor	28
a'	Tangential Induction Factor	28
A	Swept Area	19
β	Pitch Angle	32
B	Number of Blades	30
φ	Inflow Angle	30

σ	Solidity factor	29
α	Angle of Attack	31
α_{stall}	Inflow Angle at Stall Onset	34
C	Chord Length	35
C_D	Drag Coefficient	32
$C_{D, \text{stall}}$	Drag Coefficient	34
C_e	Exposure factor	27
C_L	Lift Coefficient	32
$(C_L)_D$	Design Lift Coefficient	32
$C_{L, \text{stall}}$	Lift Coefficient	34
C_x	Normal Load Coefficient	29
C_y	Tangential Load Coefficient	29
C_p	Power Output	19
F	Hub-tip Loss Factor	29
F_D	Drag Force	31
F_L	Lift Force	31
I	Current	25
L	Blade Length	30
ρ	Air Density	19
P_A	Aerodynamic Power Output	25
P_{tot}	Total Power Output	25
R	Radius of the Rotor	32
R	Radial Distance from Hub to Blade Section	31
Re	Reynolds number	34
T_w	Wet Bulb Temperature	39
T	Time	25
R	Radial Distance from the Hub to the Blade Element	22
λ	Tip Speed Ratio	18
λ_D	Design Tip Speed Ratio	32
ν	Kinematic viscosity of Air	35
V_1	Undisturbed Wind Speed	19
V_a	Air Speed	31
V_c	Vehicle speed	31

ω	Rotational Speed	31
V	Voltage	25
W	Velocity of Incoming Flow	34

TABLE OF CONTENTS

	Page
DECLARATION ON PLAGIARISM	ii
ABSTRACT	iii
DECLARATION ON PUBLICATION	v
ACKNOWLEDGEMENTS	vi
SUPERVISOR'S APPROVAL	Error! Bookmark not defined.
LIST OF ABBREVIATIONS AND SYMBOLS	vii
LIST OF FIGURES	xiv
LIST OF TABLES	xvii
1. INTRODUCTION	1
1.1 Outline of Dissertation Structure.....	7
1.2 References	7
2. LITERATURE REVIEW ON COOLING TECHNOLOGIES AND RENEWABLE ENERGY SOURCES APPLICABLE TO THE COLD CHAIN	11
2.1 Cooling Technologies.....	11
2.2 Renewable Energy Sources	16
2.2.1 Biomass	16
2.2.2 Solar energy	17
2.2.3 Wind energy	18
2.2.4 Wind energy power	19
2.2.5 Energy conversion system.....	20
2.2.6 Electric generator.....	22
2.2.1 Bridge rectifier.....	23
2.2.2 Power inverter	24
2.2.3 Battery power storage.....	24
2.3 Wind Turbine Power Generation	25
2.3.1 Turbine rotor geometry.....	26
2.3.2 Rotor blades design through Blade Element Momentum (BEM) theory	26
2.4 Integration of Renewable Energy on Cooling Technologies and Vehicles.....	38
2.5 Theoretical Framework	38

2.5.1	Wind turbine performance parameters	38
2.5.2	Evaporative cooling system performance parameters	39
2.6	Discussion and Conclusion	40
2.7	References	42
3.	WIND TURBINE MODELLING USING BLADE ELEMENT MOMENTUM THEORY, QBLADE AND MATLAB-SIMULINK.....	47
	Abstract	47
3.1	Introduction	48
3.2	Wind Turbine Blade Design Using the Blade Element Momentum (BEM) Theory	49
3.3	Modelling the Wind Turbine Blades using QBlade	60
3.3.1	Modelling on QBlade	60
3.3.2	Results and discussion.....	63
3.4	Modelling the Wind Turbine using MATLAB Simulink.....	65
3.4.1	Results and discussion.....	67
3.5	Conclusion.....	68
3.6	References	69
4.	DEVELOPMENT AND EVALUATION OF A PORTABLE SMALL WIND TURBINE	71
	Abstract	71
4.1	Introduction	71
4.2	Material and Methods.....	73
4.2.1	Study site and climatic data	74
4.2.2	Design considerations and specifications	74
4.2.3	Description of the wind turbine	75
4.2.4	Wind turbine experimental design.....	79
4.2.5	Determination of the power output.....	82
4.2.6	Determination of the power coefficient.....	83
4.3	Data Collection and Analysis	83
4.4	Results and Discussion.....	83
4.4.1	Relationship between vehicle speed and incoming wind speed	83
4.4.2	Power output of the wind turbine	86
4.4.3	Power coefficient of the wind turbine	91
4.5	Wind Turbine Prototype Costs	92

4.6	Conclusion.....	92
4.7	References	93
5.	PERFORMANCE ANALYSIS OF AN EVAPORATIVE COOLER UNIT POWERED BY A WIND TURBINE	96
	Abstract.....	96
5.1	Introduction	96
5.2	Material and Methods.....	98
5.2.1	Study site and climatic data	98
5.2.2	Description of the evaporative cooling system powered by a wind turbine.....	99
5.2.3	Sample preparation.....	100
5.3	Experimental Design	100
5.4	Comparison of Wind Turbine and Grid Powered Evaporative Cooler Performance.....	101
5.5	Results and Discussion.....	102
5.5.1	Temperature.....	102
5.5.2	Relative humidity (RH)	105
5.5.3	Cooling efficiency	106
5.6	Conclusion.....	108
5.7	References	109
6.	CONCLUSIONS AND RECOMMEDATIONS	111
6.1	Conclusion.....	111
6.2	Recommendations	113
7.	APPENDIX.....	114

LIST OF FIGURES

	Page
Figure 2.1 A small wind turbine configuration (Harrouz <i>et al.</i> , 2016)	21
Figure 2.2 Wind energy conversion sytems (Ofualagba and Ubeku, 2008)	22
Figure 2.3 Cross-sectional view of each wind electrical power generator type (Harrouz <i>et al.</i> , 2016).	23
Figure 2.4 Three-phase bridge rectifier circuit (Sakui and Fujita, 1994).	24
Figure 2.5 Rotor geometries (a) horizontal and (b) vertical wind turbine (Goriounov, 2013)	26
Figure 2.6 Labelled wind turbine components, hub and blades (Koç <i>et al.</i> , 2016).	27
Figure 2.7 Blade element section with all angles, forces and planes on the blade element section defined (Berger and Kühn, 2015)	29
Figure 2.8 Parameters for wind turbine design (Raj <i>et al.</i> , 2016)	39
Figure 3.1 Power curve of a wind turbine (Cole, 2022)	51
Figure 3.2 SG6043 airfoil section design	53
Figure 3.3 Lift coefficient (C_L) vs angle of attack (α) for SG6043 airfoil section at different Reynolds number (Re)	54
Figure 3.4 Drag coefficient (C_D) vs angle of attack (α) for SG6043 airfoil section at different Reynolds number (Re)	55
Figure 3.5 Lift to drag ratio (C_L / C_D) vs angle of attack (α) for SG6043 airfoil section at different Reynolds number (Re)	55
Figure 3.6 SG6043 airfoil section design created on QBlade	60
Figure 3.7 Blade length design showing the airfoil section of each blade element	61
Figure 3.8 Lift coefficient, C_L and lift to drag ratio, C_L / C_D versus angle of attack, α curves	62
Figure 3.9 Rotor blade design on QBlade	63
Figure 3.10 Power output versus design wind speed	64
Figure 3.11 Power coefficient, C_p variation with TSR for different wind speeds	64
Figure 3.12 Mechanical power output variation with rotor rotational speed for different wind speeds	65
Figure 3.13 Modelling of the wind turbine using MATLAB Simulink	66
Figure 3.14 Turbine power characteristic curve (pitch angle = 7°)	68

Figure 4.1	Annotated small wind turbine design.....	75
Figure 4.2	Top, front, left, and isometric view of the wind turbine design.....	76
Figure 4.3	Louver mechanism to control airflow into the wind turbine.	76
Figure 4.4	Wind turbine blades made of PVC material with magnified hub design.....	78
Figure 4.5	Energy conversion system of the small wind turbine	78
Figure 4.6	(a) Isometric view and (b) inside of a designed portable evaporative cooler unit powered by a small wind turbine	79
Figure 4.7	Side view of an ECS unit powered by a wind turbine mounted on a bakkie.....	79
Figure 4.8	Experimental design to determine the accumulated power output of a wind turbine	80
Figure 4.9	Small wind turbine prototype mounted on a bakkie	81
Figure 4.10	(a) Effect of vehicle speed on accumulated power, (b) Effect of louvre opening level on accumulated power, (c) Accumulated power over one-hour duration, (d) Accumulated power over time for different vehicle speeds and louvre opening leve	90
Figure 4.11	Power coefficient for different vehicle speeds.....	91
Figure 4.12	Power coefficient for different vehicle speeds.....	92
Figure 5.1	Top view of the evaporative cooler unit powered by the wind turbine showing different positions of the HOBO data loggers in the storage chamber.	100
Figure 5.2	Temperature and relative humidity data collection with tomato sample using a HOBOWare data logger sensor.....	100
Figure 5.3	Experimental design to assess the performance of an evaporative cooler unit with different power source using tomato testing sample.....	101
Figure 5.4	Temperature at different locations of the evaporative cooler unit using wind energy power source	103
Figure 5.5	Temperature at different locations of the evaporative cooler unit using grid energy power source	104
Figure 5.6	Relative humidity at different locations of the evaporative cooler unit using wind energy power source	106
Figure 5.7	Relative humidity at different locations of the evaporative cooler unit using grid energy power source	106
Figure 5.8	Cooling efficiency of (a) the wind turbine powered ECS unit and (b) the grid powered ECS unit	108
Figure 7.1	(a) 1st level opening and (b) 2nd level opening of the louvre mechanism	116

Figure 7.2 Small wind turbine prototype.....	117
--	-----

LIST OF TABLES

	Page
Table 2.1 Summary of advantages, disadvantages and characteristics of different cooling technologies (Sibanda and Workneh, 2020b)	15
Table 2.2 Summary of the wind turbine performance studies by various researchers	19
Table 2.3 Summary of the cut-in, rated, and cut-out wind speed of small wind turbine	30
Table 2.4 Material properties of CFRP, GFRP and PVC	36
Table 2.5 SWOT Analysis of materials for rotor blades (Kale <i>et al.</i> , 2015)	37
Table 3.1 Initial design parameters of the small wind turbine	49
Table 3.2 Inflow angle and angle of attack at different blade elements	52
Table 3.3 C_L , C_D and C_L/C_D values for Re at 200 000 for each angle of attack at different blade elements operating post-stall and during stall conditions.	53
Table 3.4 SG6043 airfoil section data, including curve plots according to Reynolds number, N_{crit} and max C_L/C_D with the corresponding	54
Table 3.5 Tip-hub loss factor, F	56
Table 3.6 Chord length and solidity factor for different elements along the blade length 57	
Table 3.7 Normal loads coefficient, tangential loads coefficient, axial and tangential induction factor along the blade length	58
Table 3.8 Relative wind speed, axial force, tangential force, torque and power output for each blade element.	59
Table 3.9 Horizontal axis wind turbine blade design on QBlade	61
Table 3.10 Input parameters for modelling the wind turbine on MATLAB Simulink	65
Table 3.11 Electrical generator specifications	67
Table 3.12 Input parameters in MATLAB Simulink wind turbine model	67
Table 4.1 Chord length for different sections of the PVC pipe blade length	77
Table 4.2 Generator specifications	81
Table 4.3 Rotor specifications	81
Table 4.4 Technical specification of the turbine	82
Table 4.5 Wind speed data collection from a moving car at different vehicle travelling speeds	84
Table 4.6 Theoretic apparent wind speed	85

Table 4.7	External and internal wind speed at different louvre opening level	86
Table 7.1	Lead-acid voltage and charge capacity (Beale, 2022)	114
Table 7.2	Battery charge measurements	114
Table 7.3	Average voltage readings at different opening levels of the louvre mechanism for different vehicle speed.....	115
Table 7.4	Accumulated power of the small wind turbine with different louvre opening level subjected to different vehicle speeds.....	116

1. INTRODUCTION

Smallholder farmers have the potential to become commercial, but constraints along the supply chain such as quality deterioration and quantity loss cost them not only their fresh produce but profit (Murthy *et al.*, 2009; Elik *et al.*, 2019). Moreover, this pressures them to sell faster to intermediaries at low prices to prevent fresh produce from deteriorating (Sibanda and Workneh, 2020a; Sibanda and Workneh, 2020b). Smallholder farmers are defined as resource-poor farmers with regard to fertilizers, herbicides, water and labour (Louw and Jordaan, 2016). A further distinction of these farmers is the small farming land, low production volume and low capital input cost (Mpandeli and Maponya, 2014). In developing countries it is estimated that about 23% of post-harvest losses (PHL) of fruit and vegetables (FV) occurring during storage and transportation are mainly because of the absence of cooling technologies as reported by the International Institute of Refrigeration (IIR) in 2009 (Elik *et al.*, 2019). Regardless of the challenges, smallholder farmers contribute to 80% of the FV production (Sibanda and Workneh, 2020a; Sibanda and Workneh, 2020b).

Cooling is one of the conventional methods used to preserve perishable commodities in order to keep their quality whilst elongating the shelf life (Sibanda and Workneh, 2020a; Sibanda and Workneh, 2020b). Immediately after harvest, the farm produce begins to deteriorate due to fast metabolic rate caused by exposure to high ambient temperature and low relative humidity (RH) along the supply chain. This subjects the fresh FV to faster physiological, chemical and enzymatic changes than in a controlled micro-environment (Raut *et al.*, 2019). Thus, introducing cooling technologies for FVs helps control the storage conditions by maintaining low temperatures and high relative humidity (RH) in the micro-environment around fresh produce to help keep their quality longer (Sibanda and Workneh, 2020b).

Over the years, the population in urban areas has tremendously increased, with an estimated 59.8% of the total South African population in 2008 residing in urban areas and recently 67.35% in 2020, with an increase of approximately 2 - 2.5% each year (Louw *et al.*, 2008; Maja and Ayano, 2021). Alongside this population growth in the cities, there is an associated food demand increase. This food demand must be met by the supermarket retail chain and agro-processors whose fruit and vegetables (fresh produce) are supplied by large commercial farms and local or distant small-scale farmers. While commercial farmers have the resources to get

their produce to the market with the proper refrigerated transportation, smallholder farmers struggle to get their fresh produce to the market while maintaining its high quality using the appropriate cooling technology.

Smallholder farmers transport FVs using open-air vehicles, which gives rise to the degradation of the fresh produce, putting them at a disadvantage with the market (supermarket) and may result in losing their contracts. Over time, this weakens the small-scale farmers' link to the market. Various studies have shown that smallholder farmers can contribute massively to the supply chain of fresh produce, but due to the instability in their food quality and quantity, they have a fragile and strained relationship with the fresh produce market sector and agro-processors (Louw *et al.*, 2008; Magesa *et al.*, 2020). As a result, smallholder farmers cannot grow in size nor become commercial. Food quality losses are caused by mechanical injury, mishandling during transportation, micro infections, wilting and fast ripening due to high-temperature conditions and the absence of mobile cooling technology in the case of transportation (Louw and Jordaan, 2016).

Various studies have shown that smallholder farmers struggle with the acquisition of an appropriate cooling technology to utilize during the transportation of FVs amongst other factors that may fuel food quality losses (Elik *et al.*, 2019). Louw and Jordaan (2016), in one of their studies stated that some of the logistical and infrastructural risks along the supply chain include changes in transport, communication, degraded and undependable transport, physical destruction and labour disputes affecting transportation. In a study conducted by Mpandeli and Maponya (2014), it was found that small-scale farmers experience many challenges. These include being unable to acquire productive resources, the high price of inputs such as fertilizers and herbicides, difficulty in gaining market access and lastly, the cost of transport. Gogo *et al.* (2018) also mentioned in their study that most fresh produce loss is caused by absence of appropriate fresh produce preservation, post-harvest treatment and cold storage facilities, lack of proper transportation facilities, improper packaging, and lack of efficient food handling techniques.

In developing countries food loss occurs mainly during the initial stages of the supply chain, with slight loss during the consumption stage (Kitinoja *et al.*, 2011). Amongst most researchers, cost and lack of appropriate cooling storage facilities and transportation are the most common challenges faced by smallholder farmers, thus a need to get into more detail and attempt to

resolve this ordeal for smallholder farmers. The issue of inappropriate transport presented along the supply chain is more evident in the study done by Cheron and Workneh (2020), where tomato fruits collected as a sample for research purposes were transported in trucks with no refrigeration over long distances from different areas in the Limpopo province to Pietermaritzburg in KwaZulu-Natal for pre-treatment and storage under ambient and cold storage conditions. The tomatoes were transported through different routes with different road conditions as well as climatic conditions, which proves the unavailability and relative unaffordability of mobile cooling technologies for long distance use.

As previously mentioned, smallholder farmers are unable to acquire appropriate mobile cooling technologies to utilize during transit. Even a mobile cooling technology like the refrigeration system is out of reach for smallholder farmers because of high energy input and investment costs. This is because refrigerated trucks utilize the vehicle's petrol or diesel to power its systems. In an attempt to make the cooling technologies available and affordable to smallholder farmers, the solution is to reduce the dependence of operating the cooling technology on the vehicle energy supply line and introduce renewable energy as a power source, thus reducing the incurring costs of the energy supply to the cooling unit (Njoroge *et al.*, 2018). To resolve the energy supply crisis for existing cooling technologies, different authors have looked at the use of renewable energy sources to power cooling storage units. Solar and wind energy along with biomass are some of the renewable energy resources applicable for use in transportation (Benedek *et al.*, 2018; Sibanda and Workneh, 2020a; Sibanda and Workneh, 2020b). Then the potential cooling technologies used in transport include mechanical refrigeration, vacuum, hydro, forced-air and evaporative cooling (EC) system (Nkolisa *et al.*, 2018a; Sibanda and Workneh, 2020a; Sibanda and Workneh, 2020b)

Besides the fact that petrol and diesel are expensive and constantly on a price rise, fossil fuels have become unappealing to the world due to their significant carbon emissions resulting in extreme global warming and climate change which in turn affects the livelihood of the society (Singh and Ahmed, 2013; Kabir *et al.*, 2018). Moreover, fossil fuels are depleting at an alarming rate, thus fuelling the drive for the implementation of renewable energy resources (RES) to power systems in transportation (Fontes and Freires, 2018; Hossain, 2020b). Unlike non-renewable fossil fuels, renewable energy (RE) resources are easily replenishable and abundant. RE resources are a clean energy source, mitigate climate change and, therefore, are environmentally friendly (Benedek *et al.*, 2018). As part of the 17 Sustainable Development

Goals (SDGs) put together by the United Nations for Agenda 2030, goal 7 states the need to make available affordable, reliable, sustainable and modern energy for all since the impact of the previously stated challenges has been more prominent in the recent years (Nurunnabi *et al.*, 2020).

While refrigeration is the most reliable and efficient cooling method, it is relatively expensive (Rai and Tassou, 2017; Sibanda and Workneh, 2020a; Sibanda and Workneh, 2020b). As previously discussed, smallholder farmers cannot afford to transport their FVs using refrigerated trucks along the supply chain, instead, they resort to using farm bakkies to transport their farm produce (Sibanda and Workneh, 2020a; Sibanda and Workneh, 2020b). This causes deterioration in the quality of fresh produce, thus resulting in high monetary losses for the sustenance of the farm business. Moreover, the storage capacity of most refrigerated trucks is considerably large for the volume of FV produced and transported by an individual smallholder farmer, which results in unnecessary extra expenses. Thus, the need to explore and develop other mobile cooling technologies to store FV since high PHL negatively affect food security. In total, PHLs are estimated to be around 30 - 50% throughout the value chain though it can vary with crop types and environmental conditions (Elik *et al.*, 2019; Sibanda and Workneh, 2020a; Sibanda and Workneh, 2020b).

In the past few years, Sibanda and Workneh (2020a); Sibanda and Workneh (2020b) have been engaged in research specifically focused on the evaporative cooling system (ECS) as the solution to PHLs, and with all cooling technologies, they have found that continuous power supply is an issue. Refrigerated trucks utilize auxiliary diesel engines to generate energy to power their systems (Rai and Tassou, 2017). In approximation, vehicles contribute about 19% of global energy use and 23% carbon dioxide (CO₂) emissions linked to energy. Vapour compression refrigeration systems alone account for roughly 40% of those greenhouse gases (GHGs) emissions in comparison to the total vehicle emission, whilst the cold chain individually consumes nearly 15% of the energy generated from fossil fuels worldwide (Stellingwerf *et al.*, 2018).

Provided the unfortunate circumstances that the transport sector is still heavily dependent on fossil fuels, there is a need to explore possible alternatives (García-Olivares *et al.*, 2018). This then justifies the recent interest of different authors in the development of RE technologies such as solar panels and wind turbines (WT) (García-Olivares *et al.*, 2018; Sibanda and

Workneh, 2020a; Sibanda and Workneh, 2020b). Wind turbines have great potential to generate energy in vehicles. Unlike large WT, which have been fully developed, the working principles of small wind turbines (SWT) in developing countries have been overlooked and lack development (Papi *et al.*, 2021). Most evidently, wind energy and other RES are still underdeveloped for utility in powering cooling technologies and use in the transportation sector, thus requiring to be looked at to mitigate power and environmental challenges. The focus of this research is to design an energy technology that uses a renewable energy resource to generate electric energy that can be used to power a mobile cooling system independently from the engine. This is done to produce clean energy as well as relieve the engine of the energy load to power a cooling technology. Therefore, fighting against global warming and extreme climate change.

Several authors have been involved in research that integrates RES, such as solar energy and biomass, into electrical/ mechanical systems (Anbazhaghan *et al.*, 2005; Mansuri *et al.*, 2016; García-Olivares *et al.*, 2018; Nkolisa *et al.*, 2018a; Sharma and Kumar, 2018; Hossain, 2020b). Mansuri *et al.* (2016) and Nkolisa *et al.* (2018a) conducted studies where a solar system was used to provide power to the ECS for the storage of fruits and vegetables. The solar system has been incorporated into many other systems in the agricultural sector, like the solar borehole pumps and storage facilities, including cooling technologies (refrigerators) (Abdulateef *et al.*, 2009; Sharma and Kumar, 2018). In the study done by Nkolisa *et al.* (2018a), the Go Power solar panel was able to power the evaporative cooler. The system was able to produce satisfactory results, with the average cooling efficiency found to be 67.17%, a temperature reduction from 23.0 °C ambient temperature to 19.8% inside storage temperature and an increase in the relative humidity from 63.59% to 83.91%.

Biomass energy has also been incorporated to power mobile systems, either as an independent or hybrid system (Anbazhaghan *et al.*, 2005). Other cars even use biomass energy to run their engines. Even though biofuels may release carbon dioxide into the atmosphere, this tends to have a less environmental impact. As a result of this, biomass energy or biofuels are said to be carbon neutral, meaning that the amount of carbon dioxide emitted to the atmosphere during combustion is removed and compensated for during the growth of the energy crops. Other authors like Hossain (2020b) have investigated the possible use of small wind turbines on vehicles to replace combustion engines. Given that wind energy is abundantly available for moving vehicles, Sibanda and Workneh (2020a) have also recommended the integration of this

energy source into mobile cooling technologies. Ohlrogge *et al.* (2009) proposed the use of carbon-neutral energy sources such as solar, nuclear, wind, hydropower, and biomass for use to power vehicles. Even though wind energy integration into vehicles is picking up in order to replace fossil fuel-dependent engine, there is no literature available for the incorporation of wind energy technologies into existing mobile cooling technology as its power supply.

The case study of this research will incorporate wind energy as the power supply to an ECS (Sibanda and Workneh, 2020a; Sibanda and Workneh, 2020b). The ECS was developed to store perishable commodities for smallholder farmers (Nkolisa *et al.*, 2018a; Sibanda and Workneh, 2020a; Sibanda and Workneh, 2020b). The aim of this research project is to design and develop a small wind turbine to power any cooling technology during the transportation of FV in South Africa. This report presents a critical review of literature on the evaporative cooling system, the wind energy conversion system and wind power generation parameters. It also discusses in detail the design of a SWT prototype and modelling of a SWT on MATLAB Simulink, testing and evaluating the design and performance parameters. The SWT design parameters include the WT swept area, blade shape and material. Then the important performance evaluation parameters for the WT include the coefficient of performance and tip speed ratio. The key research questions for this research are:

- (a) Will the designed wind turbine be able to supply sufficient electric power to the ECS?
- (b) What is the effect of varying wind speed on cooling efficiency?
- (c) What is the cut-in, optimal and cut-out wind speed of the small wind turbine?
- (d) What is the effect of very low and high wind speeds on power generation?
- (e) Is the cooling system able to continuously operate when the vehicle is stationary, and the wind turbine ceases energy generation?
- (f) What is the role of the surface area and shape of the turbine blades in power generation and cooling efficiency?

This research project aims to design and develop a small wind turbine to power an evaporative cooler unit during the transportation of fruit and vegetables in KwaZulu-Natal. The objectives of this research are to:

- (a) Develop a small wind turbine that can run a portable evaporative cooler loaded on small vehicles for fruit and vegetables preservation for the smallholder farmers in KwaZulu-Natal.
- (b) Design, optimize and model the wind turbine components using the blade element momentum (BEM) theory and MATLAB Simulink with special focus on rotor blade

parameters such as airfoil shape, chord length, wind speed, tip speed ratio, pitch angle, twist angle, wind speed, and swept area

- (c) Construct, test and evaluate the performance of a small wind turbine prototype, operated individually as well as integrated on an evaporative cooler unit.

The hypothesis of this study is as follows:

- (a) The small wind turbine can adequately power a mobile evaporative cooler unit throughout a delivery trip.
- (b) The high wind speeds on the road account for the small size of the rotor and sufficient power is generated to power the evaporative cooling unit.

1.1 Outline of Dissertation Structure

This dissertation is classified into the following chapters:

- Chapter 1: Provides a general background on the study accounting for the justification of the research project.
- Chapter 2: Provides an outline of the available cooling technologies and renewable energy sources. It critically reviews the literature on the evaporative cooling system, wind energy generation and the main components of the wind turbine design, including the turbine rotor, the blades, and the generator.
- Chapter 3: Discusses the modelling and simulation of the small wind turbine design using Blade Element Momentum theory, QBlade and MATLAB Simulink.
- Chapter 4: Discusses the prototype construction and testing of the small wind turbine.
- Chapter 5: Assesses the performance of the ECS unit powered by a wind turbine.
- Chapter 6: Presents the general conclusion of the study along with the suggested recommendations that can be made to improve the design in the study.

1.2 References

- Abdulateef, J, Sopian, K, Alghoul, M and Sulaiman, M. 2009. Review on solar-driven ejector refrigeration technologies. *Renewable and Sustainable Energy Reviews* 13 (6-7): 1338-1349.
- Anbazzhaghan, N, Saravanan, R and Renganarayanan, S. 2005. Biomass based sorption cooling systems for cold storage applications. *International journal of green energy* 2 (4): 325-335.
- Benedek, J, Sebestyén, T-T and Bartók, B. 2018. Evaluation of renewable energy sources in peripheral areas and renewable energy-based rural development. *Renewable and Sustainable Energy Reviews* 90 (2018): 516-535.
- Cherono, K and Workneh, T. 2020. The Efficacy of Postharvest Biocontrol Treatments in Controlling Spoilage of Tomato Fruit in South African Commercial Supply Chains. *J. Eng. Agric. Environ* 5 19-25.
- Elik, A, Yanik, DK, Istanbulu, Y, Guzelsoy, NA, Yavuz, A and Gogus, F. 2019. Strategies to reduce post-harvest losses for fruits and vegetables. *Strategies* 5 (3): 29-39.
- Fontes, CHdO and Freires, FGM. 2018. Sustainable and renewable energy supply chain: A system dynamics overview. *Renewable and Sustainable Energy Reviews* 82 (1): 247-259.
- García-Olivares, A, Solé, J and Osychenko, O. 2018. Transportation in a 100% renewable energy system. *Energy Conversion and Management* 158 (2018): 266-285.
- Gogo, EO, Opiyo, A, Ulrichs, C and Huyskens-Keil, S. 2018. Loss of African indigenous leafy vegetables along the supply chain. *International Journal of Vegetable Science* 24 (4): 361-382.
- Hossain, MF. 2020. Application of wind energy into the transportation sector. *International Journal of Precision Engineering and Manufacturing-Green Technology* 8 (2020): 1-13.
- Kabir, E, Kumar, P, Kumar, S, Adelodun, AA and Kim, K-H. 2018. Solar energy: Potential and future prospects. *Renewable and Sustainable Energy Reviews* 82 (1): 894-900.
- Kitinoja, L, Saran, S, Roy, SK and Kader, AA. 2011. Postharvest technology for developing countries: challenges and opportunities in research, outreach and advocacy. *Journal of the Science of Food and Agriculture* 91 (4): 597-603.
- Louw, A and Jordaan, D. 2016. Supply chain risks and smallholder fresh produce farmers in the Gauteng province of South Africa. *Southern African Business Review* 20 (1): 286-312.

- Louw, A, Jordaan, D, Ndanga, L and Kirsten, JF. 2008. Alternative marketing options for small-scale farmers in the wake of changing agri-food supply chains in South Africa. *Agrekon* 47 (3): 287-308.
- Magesa, MM, Michael, K and Ko, J. 2020. Access and use of agricultural market information by smallholder farmers: Measuring informational capabilities. *The Electronic Journal of Information Systems in Developing Countries* 86 (6): e12134.
- Maja, MM and Ayano, SF. 2021. The impact of population growth on natural resources and farmers' capacity to adapt to climate change in low-income countries. *Earth Systems and Environment* 5 (2021) 271-283.
- Mansuri, SM, Sharma, P and Samuel, D. 2016. Solar powered evaporative cooled storage structure for storage of fruits and vegetables. 86 (7): 916-22.
- Mpandeli, S and Maponya, P. 2014. Constraints and challenges facing the small scale farmers in Limpopo Province, South Africa. *Journal of agricultural Science* 6 (4): 135.
- Murthy, DS, Gajanana, T, Sudha, M and Dakshinamoorthy, V. 2009. Marketing and post-harvest losses in fruits: its implications on availability and economy. *Indian Journal of Agricultural Economics* 64 (902-2016-67302).
- Njoroge, P, Ndunya, L and Kabiru, P. 2018. Hybrid Solar-Wind Power System for Truck Refrigeration. *2018 IEEE PES/IAS PowerAfrica*, 1-9. IEEE.
- Nkolisa, N, Magwaza, LS, Workneh, TS and Chimphango, A. 2018. Evaluating evaporative cooling system as an energy-free and cost-effective method for postharvest storage of tomatoes (*Solanum lycopersicum* L.) for smallholder farmers. *Scientia Horticulturae* 241 (2018): 131-143.
- Nurunnabi, M, Esquer, J, Munguia, N, Zepeda, D, Perez, R and Velazquez, L. 2020. Reaching the sustainable development goals 2030: Energy efficiency as an approach to corporate social responsibility (CSR). *GeoJournal* 85 (2): 363-374.
- Ohlrogge, J, Allen, D, Berguson, B, DellaPenna, D, Shachar-Hill, Y and Stymne, S. 2009. Driving on biomass. *Science* 324 (5930): 1019-1020.
- Papi, F, Nocentini, A, Ferrara, G and Bianchini, A. 2021. On the Use of Modern Engineering Codes for Designing a Small Wind Turbine: An Annotated Case Study. *Energies* 14 (4): 1013.
- Rai, A and Tassou, SA. 2017. Environmental impacts of vapour compression and cryogenic transport refrigeration technologies for temperature controlled food distribution. *Energy Conversion and Management* 150 (2017): 914-923.

- Raut, RD, Gardas, BB, Narwane, VS and Narkhede, BE. 2019. Improvement in the food losses in fruits and vegetable supply chain-a perspective of cold third-party logistics approach. *Operations Research Perspectives* 6 (2019): 100117.
- Sharma, P and Kumar, HA. 2018. Solar powered movable cold storage structure for perishables. *Current Science* 114 (10): 2020-2022.
- Sibanda, S and Workneh, TS. 2020a. Performance evaluation of an indirect air cooling system combined with evaporative cooling. *Heliyon* 6 (1): e03286.
- Sibanda, S and Workneh, TS. 2020b. Potential causes of postharvest losses, low-cost cooling technology for fresh produce farmers in Sub-Sahara Africa. *African Journal of Agricultural Research* 16 (5): 553-566.
- Singh, RK and Ahmed, MR. 2013. Blade design and performance testing of a small wind turbine rotor for low wind speed applications. *Renewable Energy* 50 (2013): 812-819.
- Stellingwerf, HM, Kanellopoulos, A, van der Vorst, JG and Bloemhof, JM. 2018. Reducing CO2 emissions in temperature-controlled road transportation using the LDVRP model. *Transportation Research Part D: Transport and Environment* 58 (2018): 80-93.

2. LITERATURE REVIEW ON COOLING TECHNOLOGIES AND RENEWABLE ENERGY SOURCES APPLICABLE TO THE COLD CHAIN

This chapter discusses in detail the literature review on the topic under study with a specific focus on cooling technologies, renewable energy sources, wind energy and most importantly the components of the wind turbine technology.

2.1 Cooling Technologies

Most modern cooling technologies are advanced, but each is reserved for a selected type of fresh produce. They also require a high energy supply and have expensive initial and operating costs, making them unappealing to smallholder farmers (Sibanda and Workneh, 2020a; Sibanda and Workneh, 2020b). These cooling technologies include mechanical refrigeration, hydro, vacuumIAC and forced-air cooling, which ultimately can be transformed into mobile cooling technology (Sibanda and Workneh, 2020a; Sibanda and Workneh, 2020b). Mechanical refrigeration systems use refrigerants to provide cooling. Usually, these refrigerants are expensive, have high energy requirements and are detrimental to the atmosphere. Overall, refrigerated systems' initial purchase and running costs are relatively high. Using renewable energy as an alternative power source may help decrease the running/incurred costs of the refrigeration system and consequently reduce the leasing price.

On average, the energy consumption is around 8.2 kW for a storage capacity that can accommodate 4 tons of fruits and vegetables (Zhu *et al.*, 2019). Refrigeration systems can achieve an inside storage temperature of -20°C, -10°C, 0 °C and +12 °C (Tassou *et al.*, 2012). Most times, refrigeration units operate at low temperatures, less than 10°C. Since some fruits and vegetables are sensitive to low temperatures, refrigeration is somehow less efficient for extending or improving the shelf life of these FVs. Instead, the fruit and vegetables are subjected to chilling injury, which is also a reason why smallholder farmers and farmers in general use bakkies or open-air trucks to transport their FV such as tomatoes, cabbages, and so on.

One of the cooling technologies applicable to vehicles is the evaporative cooling system. Evaporative cooling refers to a cooling method that utilizes water flowing in a cooling pad material to cool the outside air through the process of evaporation and transfer it inside the storage chamber, thereby lowering the FV's temperature and increasing the RH with the help of an exhaust mechanism (Adekanye and Babaremu, 2019) Unlike other cooling systems, the ECS uses less electric power for mainly operating the water pump and fan. It also works well in hot, arid and remote regions, and most importantly, it has low initial investment costs (Tilahun, 2010b; Sibanda and Workneh, 2020a; Sibanda and Workneh, 2020b). The energy consumption of an ECS can be approximated to 600 W for a storage capacity of 53.39 m³ (Sibanda and Workneh, 2020a; Sibanda and Workneh, 2020b). Similar to greenhouses, an evaporative cooling system is able to attain favourable environmental conditions inside the storage units.

In an ECS, cooling occurs by passing ambient air over a wetted pad and the water evaporates, removing sensible heat along. ECS cools down air using the principles of evaporation. The less the RH, the more cooled air can be achieved by the ECS. ECS are divided into three types, direct evaporative cooling (DEC), indirect evaporative cooling (IEC) and indirect/direct evaporative cooling (IDEC) (Shirmohammadi and Gilani, 2019). The DEC, also known as a swamp cooler, refers to cooling whereby air passes through a wet cooling pad, which is cooled and humidified, resulting in reduced air temperature and increased RH because of added moisture. Oppositely to IEC, a secondary heat exchanger is utilized to cool the air, which prevents humidity from being added to the airstream thus, the RH remain unchanged (Shirmohammadi and Gilani, 2019). IDEC combines IEC and DEC, where a water-soaked pad and a secondary heat exchanger are used to prevent humidity from entering the controlled-conditions space. IDEC systems use 60 – 70% less electricity than conventional refrigeration systems.

Furthermore, ECS can be categorized into natural and forced ventilation evaporative coolers. Forced ventilation evaporative coolers have a suction fan to either draw in air from the outside to the evaporative cooler or from the ECS into the storage chamber. Whilst with natural ventilation, there is free movement of air between the ECS and the storage chamber without the assistance of a fan. DEC and IEC are highly efficient in hot and arid regions, negating the need for compressors in the cooling cycle. Temperature and RH are two critical parameters that need to be controlled to reduce PHL (Nkolisa *et al.*, 2018a). Nkolisa *et al.* (2018a)

evaluated the performance of a low-cost ECS powered by a solar plate and the effect it has on the quality of FV in hot and arid regions. The ECS was able to achieve an inside temperature of 19.8°C compared to 23°C in ambient conditions, and a RH of 83.91% from 63.59% was achieved, with the average cooling efficiency at 67.17%. These results were found satisfactory given that this is a semi-humid area, the air is already saturated and based on literature, ECS performs very well in dry areas as cooling is achieved through the principles of evaporation. Overall, the system's efficiency suggests that the cooling technology can store and maintain the quality of FV for longer and improve the shelf life.

Another study by Sibanda and Workneh (2020a) evaluated the performance of indirect air-cooling combined with an evaporative cooling (IAC + EC) system. The performance of an IAC + EC system was high during the day, between 10h00 – 16h00 because of the high ambient temperature during these times which favours evaporation. An IAC + EC system can attain a temperature of around 10-15 °C inside the storage chamber and a RH of 90%, allowing for an increased shelf life of tomatoes from 3 to 15 days in hot and sub-humid regions (Sibanda and Workneh, 2020a; Sibanda and Workneh, 2020b). The study that was done by Sibanda and Workneh (2020a) shows that the system was able to achieve an inside temperature of 15.7-16.4 °C. The RH inside the IAC + EC system was found to be between 89.6 – 93.8% for hot and sub-humid regions, which was deemed satisfactory because the recommended RH for FV ranges between 85 - 95%. Lastly, the IAC + EC system achieved an almost impeccable cooling efficiency, ranging between 88.04 – 95.6%. An ECS in arid regions performs similarly to an IAC + EC in hot and sub-humid regions. The energy consumption of the IAC + EC system was found to be 2.343 kW for body volume of 53 m³ with a storage capacity of 3.8 – 4 tons.

Hydro cooling and vacuum cooling are cooling technologies mainly used as pre-cooling methods immediately after farm produce is harvested to cool it before the product is transferred into a secondary cooling technology used during transportation. Vacuum cooling is a batch processing method used for particular leafy food products such as lettuce and mushroom (Kitinoja and Thompson, 2010). During this process, the additional moisture contained by the fresh produce evaporates under vacuum, causing cooling. For example, vacuum cooling can reduce the temperature of lettuce from 25 °C to 1°C in less than 33 minutes almost tripling the shelf life of lettuce from 3-5 days to 14 days (Zhu *et al.*, 2019). The energy consumption of vacuum cooling is estimated at 0.51 kWh (Zhu *et al.*, 2019).

Hydro cooling is a pre-cooling method that uses chilled water to cool perishable commodities. It has an energy consumption ranging between 0.67 kWh to 0.78 kWh for high and low flow, respectively (Zhu *et al.*, 2019). Forced-air cooling method exposes packages of food in a cold room to high pressure on one side. The difference in pressure forces air through the packages, past the produce and in the process, removes sensible heat and offers cooling. For a body volume of 3.5 m³, storing 700kg, the energy requirement of a forced-air cooler is 2.9 – 3.5 kW (Kitinoja and Thompson, 2010). Table 2.1 shows the advantages, disadvantages, and characteristics of different cooling technologies.

Table 2.1 Summary of advantages, disadvantages and characteristics of different cooling technologies (Sibanda and Workneh, 2020b)

Cooling technology	Advantages	Disadvantages	Performance characteristics	References
Evaporative cooling	Low capital cost; high energy efficiency; environmental benign; low weight loss; low deterioration in quality; suitable for rural application, requires no special skill to operate; can be made from locally available materials; and easy to maintain.	Requires constant water supply; no humidification, and high dew point; condition decreases the cooling capability; mineral deposits leading to pad and interior damage.	Can maintain temperatures 10 – 15 °C below ambient; Can achieve relative humidity of 90%; Can increase shelf life from 3 days to 15 days. Typical cooling time is 40 – 100 h in passive cooling and 20 - 100 hours in fan-ventilated systems.	Mordi and Olurunda (2003) Anyawu (2004) Basediya et al. (2011) Chaudhari et al. (2015) Tigist et al. (2011)
Hydro-cooling	Rapid cooling; prevents loss of moisture during cooling; cools and cleans the produce at the same time; simple and effective pre-cooling method; high energy efficient.	Not uniform may leave “hot spots”; not suitable for leafy produce; not suitable for products that do not tolerate wetting; not suitable for products that can be damaged by falling water; water left on surface can lead to fungus growth or discoloration; capital cost is relatively high; the equipment is not portable	Cooling can be achieved in 20 – 30 min; water removes heat about 15 times more faster than air at typical flow rates and temperature difference; Refrigeration capacity of 1.4 kW cool 500kg produce per hour to achieve 11 °C depression	Wills et al. (2007) Brosnan and Sun (2001) Rennie et al. (2003) Prusky (2011)
Vacuum cooling	Rapid cooling achievable; distinct advantage over other cooling methods; cooling can achieve uniform cooling, gives highest energy efficiency; and hygienic since air only goes to the vacuum chamber; No potential for decay contamination; equipment is portable	Very capital cost; limited application for large growers; causes weight loss in produce; only suitable for produce with high surface to volume ratio; works best only for produce like lettuce; cabbage, mushroom	Rapid cooling; method and can achieve temperatures of 1 °C; Can increase shelf life from 3 – 5 days at ambient days to 14 days when combined with cold storage at 1 °C; For every 5.5 °C reduction in temperature there is 1 % weight loss	Turk and Celik (1993) Kim et al. (1995) Ito et al. (1998) Brosnam and Sun (2001) Rennie et al. (2003)

2.2 Renewable Energy Sources

The adoption of renewable energy resource use in the transportation sector is an excellent yet challenging transition from fossil fuel-powered vehicles (Dominković *et al.*, 2018; García-Olivares *et al.*, 2018). It is estimated that about one-third of the total energy consumption and one-fifth of the GHG emissions is due to the transport sector and its systems (Dominković *et al.*, 2018; García-Olivares *et al.*, 2018). As a result of all these negative impacts, researchers around the globe are looking for substitutes and alternative solutions to achieve a goal where fossil fuels are a thing of the past (García-Olivares *et al.*, 2018; Stellingwerf *et al.*, 2018; Hossain, 2020b). Amongst many renewable energy resources available, this study will only discuss those applicable to the transport sector, which include biomass, solar and wind energy (Benedek *et al.*, 2018; Fontes and Freires, 2018; Sibanda and Workneh, 2020a; Sibanda and Workneh, 2020b)

2.2.1 Biomass

Biomass is considered one of the main substitutes for fossil fuels to provide energy in the transport industry because it helps reduce GHG emissions, although it is not completely clean (Liu *et al.*, 2017). Biomass refers to any organic matter derived from plants or animals used as fuel to produce electricity, including manure, agricultural, forestry, and industrial matter (Fontes and Freires, 2018). Some crops, such as starch crops, switchgrass, reed canary grass, bamboo, etc., are purposefully grown for energy production (Liu *et al.*, 2017). Unfortunately, energy crops cannot be grown fast enough to replace fossil fuels and has a low energy efficiency of less than 30 % (Liu *et al.*, 2017). Growing these energy crops requires a large piece of land to match that equivalent to fossil fuels, thus resulting in high costs of production than fossil fuels. Anbazhaghan *et al.* (2005) developed and tested a biomass-powered absorption refrigeration system. They found the coefficient of performance (COP) to be around 0.2 -0.35, with the lowest temperature obtained at -5 °C. This system was able to decrease the carbon dioxide significantly thus proved to be environmentally friendly. As a result of shortage of cold storage facilities and unreliable power supply in rural areas of India, Panja and Ganguly (2019) developed a biomass and solar hybrid power system to the cold storage facilities for small-scale farmers. The system was found to be efficient, with a coefficient of performance (COP) between 0.7 – 0.82 and a chiller temperature around 8 – 10 °C.

Biomass energy can be made available for use by vehicles in two ways, biofuels or bio-electricity stored in batteries. Laser and Lynd (2014) conducted a study that concluded that both these ways are efficient in powering a vehicle. This energy type can be recovered through different processes, including direct combustion, gasification and pyrolysis, with the pyrolysis process being the most common method adopted. Biomass pyrolysis is the process used to heat organic material in the absence of oxygen and convert it into combustible gases and charcoal. Biofuels produced through pyrolysis have been found to be efficient in the transport sector to power the car as well as have near to zero carbon emission effect. Although biomass energy/biofuels are well known, and literature on the evaluation of the energy source is widely available, not much direct case studies where biofuel or bio-electricity was developed and tested in a vehicle in order to support and validate its use on vehicles can be found.

2.2.2 Solar energy

Solar energy is the most abundant, free and prominent energy source of all (Fontes and Freires, 2018; Kabir *et al.*, 2018). Solar energy is generated from the sun using technologies such as photovoltaic (PV) panels and concentrated solar power (CSP) (Kabir *et al.*, 2018; Shahsavari and Akbari, 2018). PV panels convert sunlight radiation directly into electrical energy using semiconductors, whilst CSP utilizes high magnification mirrors to first concentrate solar energy before converting it into heat energy to drive a steam turbine that finally generates electrical power (Kabir *et al.*, 2018). The African continent has the greatest potential for PV and CSP technologies' energy generation since it consists of the sunniest places on the planet. The capacity of energy generation is mainly dependent on the size of the RE technology itself, and with transportation, space is very limiting therefore, researchers have to be more innovative in working on these technologies to generate enough energy to power the vehicle's system and accommodate night travel (Hossain, 2020b).

Olosunde *et al.* (2016) designed and developed a solar power evaporative cooling storage system (SPECSS) to be utilized by rural smallholder farmers with no power supply to store fresh produce and improve its shelf life. The findings show that the 0.39 m³ storage system was able to store fruits and vegetables for a prolonged time at low power input. The SPECSS temperature varied between 7.8 – 15.4 °C, while the RH ranged between 44 – 96.8%. The tomatoes' shelf life was then extended from 6 days in ambient storage conditions storage without a cooling technology to 21 days in SPECSS chamber storage conditions. Sharma and

Kumar (2018) designed and developed a movable refrigeration storage structure powered by a system of solar photovoltaic panels for the storage of fruits and vegetables. The solar system was able to generate an average of 2.07 kWh. Then the refrigerator achieved an inside storage temperature of 9 - 11 °C and relative humidity of 73 - 92 %. They found the solar-powered refrigerator helpful to the community with little to no power supply. Kumar and Bharj (2016) designed, constructed and tested a viable solar hybrid mobile cold storage system for the storage of perishable foods including vegetables, where there is an unreliable energy supply. The system was able to achieve a storage temperature of -8 °C for 7 – 8 hours from battery-stored solar energy.

2.2.3 Wind energy

After solar energy, wind energy is known to be the fastest-growing and promising energy source in the world (Sibanda and Workneh, 2020a; Sibanda and Workneh, 2020b). Wind energy, like any RES, is a free, clean and readily available energy source, but the installation is very costly and has several challenges associated with transmission (Sumathi *et al.*, 2015; Hossain, 2020b). Wind energy is the kinetic force of moving air per unit volume (Hossain, 2020b). The wind turbine is the technology used to harness wind energy and convert it into electrical energy (Hossain, 2020b). According to the International Electrochemical Commission (IEC) 61400-2 Standard, SWTs are defined as those with a turbine rotor swept area of less than 200 m², corresponding to a blade radius of less than 8 m and a power output below 50 kW (Wood, 2011). Power generation of a wind turbine installed in a vehicle has much great potential because of high windspeed readily availability (Hossain, 2020b). Hossain (2020b) designed, developed and implemented a small wind turbine on a small car to serve as its main power supply. The findings showed that the use of wind energy in a car is very functional. From the study, it was observed that a car moving at 10 km.h⁻¹ can generate 8 kWh for an average wind speed of 2 km.h⁻¹ (0.556 m.s⁻¹). The energy generated is considered enough to run a car via battery storage since a standard car requires 20 kWh, which is provided by two hours of charging at 10 km.h⁻¹, allowing the car to move for at least 200 km with the stored power. Table 2.2 shows the summary of the wind turbine performance studies performed by other researchers. While solar energy is a fairly known and developed renewable energy source in both the agricultural sector and road transport, wind energy is still rather in the introductory phase and requires development for integration into vehicles, in this particular case the mobile cooling units (Bharj, 2018; Njoroge *et al.*, 2018; Rossetti *et al.*, 2022). Therefore, it is important

to conduct research to develop, adopt and utilise this form of energy since it is free, abundant and easily available for moving vehicles.

Table 2.2 Summary of the wind turbine performance studies by various researchers

WT no.	No. of blades	Rotor diameter (m)	Tip speed ratio	Wind speed (m.s ⁻¹)	Power (W)	Power coefficient	Authors
1	3	4	6.5	5.5	650	0.445	Muhsen <i>et al.</i> (2019)
	3	4	6.5	7	1180	0.4	Muhsen <i>et al.</i> (2019)
2	3	3	-	7.5	616	0.35	Ozgener (2006)
3	3	0.64		10	478.5	0.79	Tahir <i>et al.</i> (2019)
4	3	1.6	-	12	600		Salih <i>et al.</i> (2012)

2.2.4 Wind energy power

Similar to solar energy, computations must be performed to size the generator and associated electrical components. Therefore, this sub-section discusses the wind energy power equation, the energy conversion system and battery power storage. More focus will be placed on explaining each variable within the power equation and how each affects the power generation. These variables include air density, swept area, wind speed and most importantly, the power coefficient.

The Equation used to compute the aerodynamic wind power output produced by the wind turbine generator is given by Equation 2.1 (Schubel and Crossley, 2012; Bisoyi *et al.*, 2013):

$$P_T = \frac{1}{2} C_p(\lambda, \beta) \rho A V^3 \quad (2.1)$$

where

P_T = Aerodynamic power output (W),

C_p = Power coefficient,

λ = Tip speed ratio,

β = Pitch angle (°),

ρ = Air density (kg.m⁻³),

A = Swept area (m²), and

V_1 = Undisturbed windspeed (m.s⁻¹).

Normally, an increase in RH implies a possible increase in the air density, which could mean a potential increase in the power output. But the air density barely varies much in closed regions, thus, the air density is mostly assumed to remain constant. Unfortunately, the energy in the wind cannot be fully captured or harnessed by the wind turbine, therefore the introduction of the power coefficient concept. The power coefficient is a function of the blade pitch angle, $\beta(^{\circ})$ and the tip speed ratio, λ . Given that the swept area of the rotor and air density remain constant, the value of C_p is dependent on λ , which is determined by the blade design. The maximum value of C_p is equal to 0.593, which means the maximum power that can be extracted is 59.3% of that available in the wind (Bisoyi *et al.*, 2013). This is called the Betz limit. Even in the absence of the drag effect, a horizontal axis wind turbine (HAWT) can never reach the Betz limit. Small wind turbines generally achieve a power coefficient of 0.4, while large wind turbines can get close to the Betz limit by 0.52.

2.2.5 Energy conversion system

The energy conversion system is the systematic path which energy takes from the source to the final power output described by a chain of interacting subsystems (Hossain, 2020b). In a wind turbine, kinetic wind energy is captured through the rotation of the turbine blades which is controlled by the amount of airflow, wind speed. This mechanical energy rotates the connecting shaft coupled to the electrical generator that ultimately produces the electric energy to power the electrical components of the system (Sumathi *et al.*, 2015; Hossain, 2020b). The entire configuration of a small wind turbine is shown in Figure 2.1. In this particular case, a permanent magnet synchronous generator (PMSG) was used to convert mechanical energy into electrical energy. On this figure, the wind blew on the rotor which caused the rotation of the rotor. Then, the PMSG creates electrical energy due to this mechanical rotation which rotates the shaft of the generator. A battery is used to store the power and supply it to the loads.

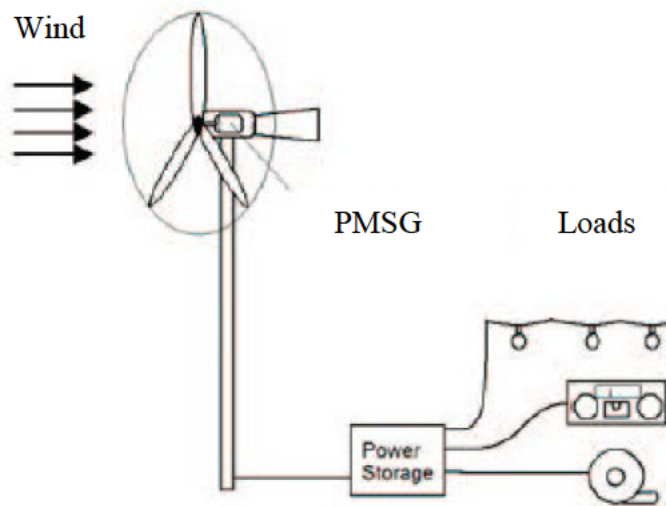


Figure 2.1 A small wind turbine configuration (Harrouz *et al.*, 2016)

The output power of the WT is dependent on parameters such as wind speed, size and shape of the WT (Ofualagba and Ubeku, 2008; Sumathi *et al.*, 2015). The subsystems of a conventional wind energy conversion mechanism are shown in Figure 2.2. Wind turbines can be classified into two modes according to wind speed, namely the constant/fixed-speed (FS) and variable-speed (VS) wind turbines. The constant-speed wind turbine has a fixed wind speed at which it rotates regardless of the changing airspeed, and the rotor aerodynamic performance is only optimal at a given wind speed, while the tip speed ratio (TSR) changes with the wind speed. Contrary to a fixed-speed wind turbine, a variable-speed wind turbine allows the rotor and generator windspeed to vary between the cut-in and rated speed range. This allows for maximum aerodynamic power extraction in the wind as it varies, which means that the TSR and aerodynamic performance remains constant. Then, above the rated speed, the rotor speed is held constant, and the generator produces constant maximum power.

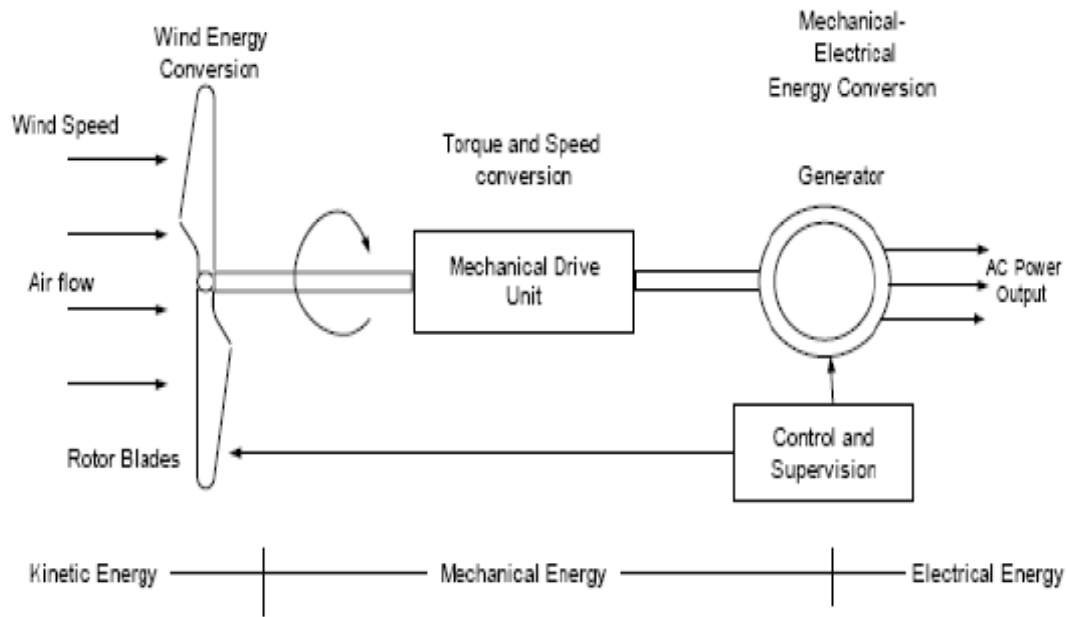


Figure 2.2 Wind energy conversion systems (Ofualagba and Ubeku, 2008)

2.2.6 Electric generator

An electric generator, also known as a dynamo, is a machine that converts mechanical energy into electrical power (Harrouz *et al.*, 2016). Its operation relies on magnetic induction in the form of voltage arranged in two ways. Either a conducting coil is in a changing magnetic field, or the coil moves around the magnetic field. Most WT use a generator where the conducting coil is in a changing magnetic field. The mechanical force of the blades drives the rotor of the generator, creating a rotating magnetic flux inside the stator of the armature coil. The main types of industrial electric generators available on the market include the Squirrel Cage Induction Generators (SCIG), Doubly-Fed Induction Generator (DFIG), Permanent Magnet Synchronous Generator (PMSG) and Switched Reluctance Generator (SRG) (Harrouz *et al.*, 2016). The interest in SCIG has decreased while that of SRG is increasing, but both the SCIG and SRG are of low cost, low energy use and low maintenance. SCIGs have a poor starting torque and operate with fixed speed, but they are also more reliable and have good speed regulation. SRG, on the other side can withstand high-speed application and temperature, although it is difficult to control.

DFIG and PMSG are the most common variable speed wind generators (Bisoyi *et al.*, 2013; Harrouz *et al.*, 2016). The PMSG is preferred for SWT since it can be connected directly to the turbine rotor without the gearbox. They can achieve a larger air-gap flux density and stator

bore diameter, and an efficiency of 97% (Harrouz *et al.*, 2016). DFIG helps to lower noise and mechanical stress, it improves power quality and makes up for torque and power pulsation (Sathiyarayanan and Senthil Kumar, 2014). When the power storage or supply is faulty, the DFIG can be blocked and then, after a while it automatically reconnects to the power network (Sathiyarayanan and Senthil Kumar, 2014). One of the most prominent limitations of using the DFIG is that it requires a gearbox, making it prone to bearings and gear faults which ultimately means high maintenance. Figure 2.3 shows the different types of electric generators.

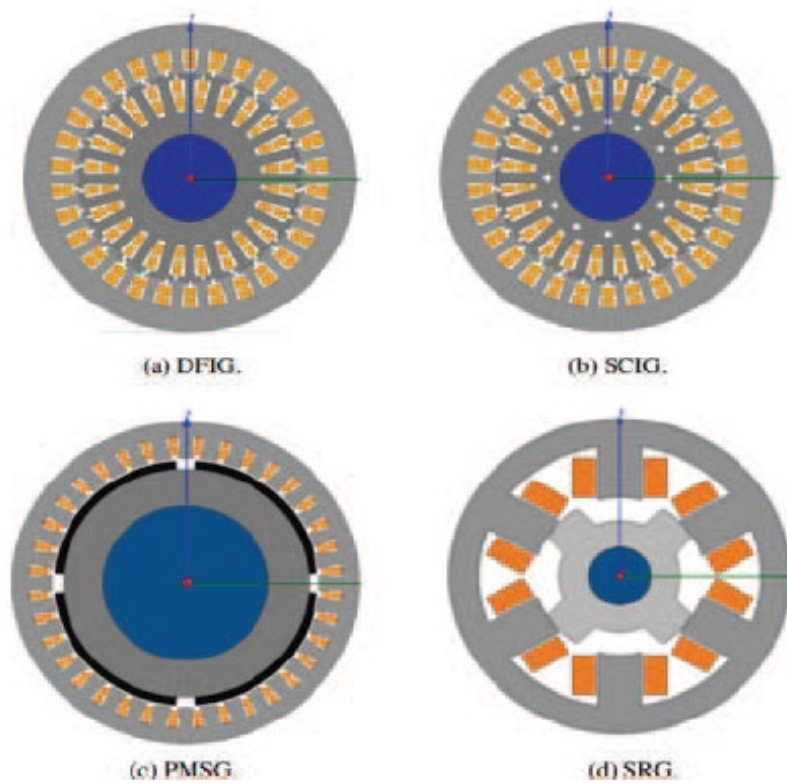


Figure 2.3 Cross-sectional view of each wind electrical power generator type (Harrouz *et al.*, 2016).

2.2.1 Bridge rectifier

A rectifier is an electrical device used to convert an oscillating two-directional alternating current (AC) power into a direct current (DC) power, which flows in only one direction (Sakui and Fujita, 1994; Lian *et al.*, 2008). A bridge rectifier typically uses four or more diodes in a bridge circuit configuration to convert AC power into DC power (Saura *et al.*, 2021). The rectifier can be either single or three-phase. Figure 2.4 shows the basic circuit of a three-phase bridge rectifier with the input being the AC power and the output being the rectified DC power.

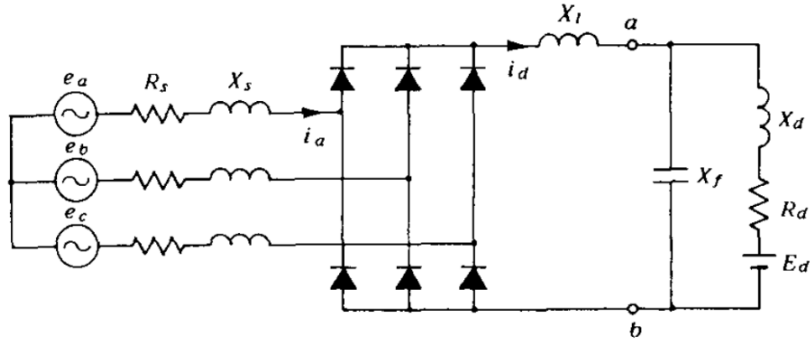


Figure 2.4 Three-phase bridge rectifier circuit (Sakui and Fujita, 1994).

2.2.2 Power inverter

An inverter is used to convert DC power into an AC power as well as step-up battery energy from lower voltage to a high, suitable voltage of 220-230 V that can be utilised by electrical appliances (Soares-Ramos *et al.*, 2021). Its function is the opposite of the rectifier. Electrical components utilise 230 VAC, therefore it is important to use the inverter when using a DC battery source in order to be able to utilise the electrical energy in it (Velasco *et al.*, 2019).

2.2.3 Battery power storage

After electricity is produced by the electric generator, it can be utilized directly from the wind turbine or indirectly via a rechargeable battery storage (Hossain, 2020b). Batteries are devices that store electric energy in an electrochemical form and deliver direct current power. The importance of the battery storage is to maintain voltage stability and consistency in energy supply regardless of fluctuating power output as a result of variable wind speed (Esmaili *et al.*, 2013; Amrouche *et al.*, 2016). The battery also allows for a readily available energy source and storage of excess energy to use at a later stage in the case of events such as start-up energy requirement, low efficiency of the WT, traffic and awaiting loading or offloading. The most common battery types utilized for energy storage include the value-regulated lead-acid (VRLA) and Lithium-ion (Li-ion) batteries (Amrouche *et al.*, 2016).

The Li-ion battery has a greater capacity per unit volume compared to the VRLA battery, although it can differ between models and manufacturers (Amrouche *et al.*, 2016). It is lightweight and has a fair lifespan. Most importantly, it has an energy efficiency of around

90%, and it is temperature tolerant, therefore possessing a high measure of safety (Dragičević *et al.*, 2014). The VRLA battery is an improved version of the lead-acid battery. It is compact, low maintenance, has an efficiency of around 60%, and 90% of the material is recyclable. The most prominent drawback of a Li-ion battery is that it's expensive and almost double the price of a lead-acid battery. The total power that the battery is required to store to cover a specific duration is presented on Equation 2.2. Ohm's law is used to determine the current rating needed to size the battery to give the required power storage as presented by Equation 2.3.

$$P_{tot} = P_A \times t \quad (2.2)$$

where

P_{tot} = Total power of the battery (Wh),
 P_A = Aerodynamic power output (W), and
 t = Travel duration (h).

$$P_{tot} = V \times I \quad (2.3)$$

where

P_{tot} = Total power of the battery (Wh),
 V = Battery voltage (V)
 I = Battery current (Ah)

2.3 Wind Turbine Power Generation

The main parts of a SWT include a turbine rotor, electric generator, tail and support (Schubel and Crossley, 2012). A SWT does not require a gearbox since the rotors rotate at a windspeed significantly larger than the utility level turbine and can be directly coupled to their electric generators. In the case of an EC unit, the electric energy produced from the wind turbine is used to power the suction fan to draw air into the storage chamber, power the water pump for water circulation and the light bulbs in the storage chamber. (Workneh, 2010; Sibanda and Workneh, 2020a; Sibanda and Workneh, 2020b). This section critical reviews the literature on the WT parts, including the WT rotor geometry, rotor blades and electrical generator.

2.3.1 Turbine rotor geometry

One of the main classifications of the wind turbine is based on the orientation of the shaft and rotational axis, namely the horizontal axis wind turbine (HAWT) and vertical axis wind turbine (VAWT) (Schubel and Crossley, 2012; Raj *et al.*, 2016). HAWT has its shaft horizontally parallel to the ground, while VAWT has its shaft normal to the ground. HAWT is the most used wind turbine, generally used in regions where the airflow is in a constant direction, and the flow is not turbulent (Johari *et al.*, 2018). Whilst VAWT can capture the wind in any direction and can operate in areas with high turbulence. Figure 2.5 shows the horizontal and vertical axis wind turbine orientation. The rest of the wind turbine geometry is based on the turbine blades (Johari *et al.*, 2018).

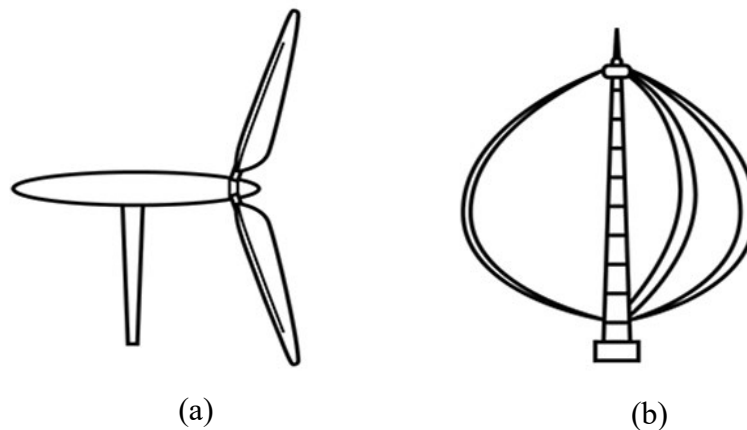


Figure 2.5 Rotor geometries (a) horizontal and (b) vertical wind turbine (Goriounov, 2013)

2.3.2 Rotor blades design through Blade Element Momentum (BEM) theory

The rotor is the most important part of the wind turbine design. Its design determines the amount of power that the wind turbine can harness from the approaching wind. The rotor is made of the hub and blades, as shown in Figure 2.6. A wind turbine rotor can be made of any number of blades depending on the manufacturer, which account for centrifugal body forces, the efficiency of electric energy generation, and aerodynamic efficiency (Schubel and Crossley, 2012). Having few blades reduces drag, but two blades are unstable in the wind. Three blades have constant angular momentum and are able to harness optimum wind energy without additional mass and costs compared to four or more blades.

Due to harsh environmental conditions, including high wind loads, blades are subjected to tear and wear. Therefore, a control mechanism must be incorporated to slow the rotor rotation and ensure a safe design with minimal damage. Two control mechanisms are available, stall and pitch regulation. Stall regulation involves fixing the blades to the hub at a constant pitch angle, β , as shown in Figure 2.7. When the blades reach a certain angle of attack (AOA), it slows down or stops rotating. It is a relatively simple blade control mechanism. Then, with pitch regulation, the blades are allowed to move according to the wind direction, thus changing pitch. Therefore, the amount of power harnessed is dependent on the pitch angle. Small wind turbines commonly use the stall regulation. The pitch regulation is used by large wind turbines since it is the most efficient regulation system and economic sound, unlike with SWTs, where it would make the design unnecessarily expensive. This sub-section discusses in detail the BEM theory for the blade design, size, material, and loads acting on the blades. The amount of electric power generated to run the system is directly dependent on the size and shaping of the wind turbine. Wider blades near the hub result in a greater torque which assists in the start of the WT, and then the narrower part of the blades at the tip allows for greater revolutions with lower torque (Raj *et al.*, 2016).

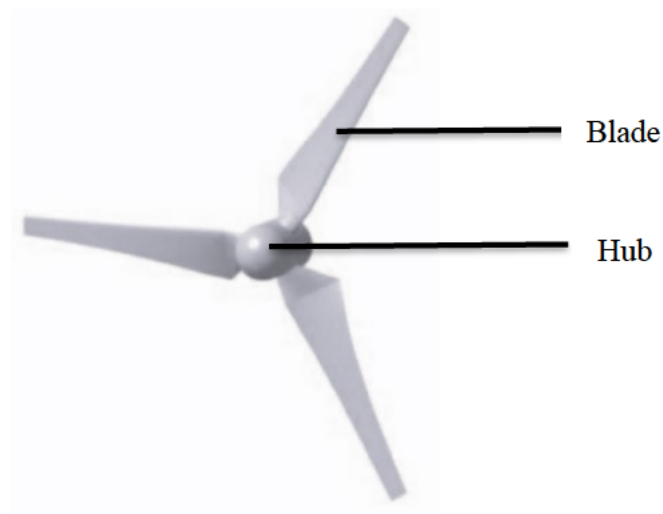


Figure 2.6 Labelled wind turbine components, hub and blades (Koç *et al.*, 2016)

Most HAWTs are designed using the Blade Element Momentum (BEM) theory. The Blade Element Momentum theory is a method which is used for the optimization of the wind turbine blade design. The BEM method is a combination of the blade element theory and the momentum theory initially used to analyse the airplane propeller performance. The blade element theory divides the blade into multiple elements, which act independently as two-

dimensional airfoils. Then the forces and moments on the blades can be computed separately and finally sum them up to attain the total forces and moments. On the other side, the second part of the BEM method, the momentum theory, presumes that wind turbines harnesses energy from incoming wind, thereby, the wind is subjected to losses in pressure and moment. The corrections on the BEM method make them applicable to wind turbines. The corrections include tip loss, hub loss, Glauert and Buhl empirical, skewed wake, and “3D” corrections.

The most important design parameter of the wind turbine blades, the power coefficient, C_p can be calculated using either of these equations presented by Equation 2.4 and 2.5.

$$C_p = \frac{P}{\frac{1}{2}\rho AV^3} \quad \text{or} \quad C_p = 4a(1-a)^2 \quad (2.4)$$

$$C_p = 0.22 \left(\frac{116}{\gamma} - 0.4\beta - 5 \right) \exp \frac{-12.5}{\gamma} \quad \text{where } \gamma = \frac{1}{\frac{1}{\lambda+0.05\beta} - \frac{0.035}{\beta^3+1}} \quad (2.5)$$

where

a = Axial induction factor, and

a' = Tangential induction factor.

The axial and tangential induction factors can be determined using Equation 2.6 and 2.7, respectively.

$$a = \frac{1}{\frac{4F\sin^2\varphi}{\sigma C_x} + 1} \quad (2.6)$$

$$a' = \frac{1}{\frac{4F\sin\varphi\cos\varphi}{\sigma C_y} - 1} \quad (2.7)$$

Where the inflow angle, φ is presented by Equation 2.8:

$$\varphi = \tan^{-1} \left(\frac{(1-a)V_1}{(1+a)\omega r} \right) \quad (2.8)$$

The solidity factor is then given by Equation 2.9:

$$\sigma = \frac{cB}{2\pi r} \quad . \quad (2.9)$$

Then, the hub-tip loss factor, F is:

$$F = \frac{2}{\pi} \cos^{-1} \left(e^{\frac{-B(R-r)}{2r \sin \varphi}} \right) \quad (2.10)$$

And finally the normal and tangential loads coefficient, C_x and C_y are given by Equation 2.11 and 2.12, respectively. Figure 2.7 shows the airfoil blade section with the angles, forces and planes clearly defined.

$$C_x = C_L \cos \varphi + C_D \sin \varphi \quad (2.11)$$

$$C_y = C_L \sin \varphi - C_D \cos \varphi \quad (2.12)$$

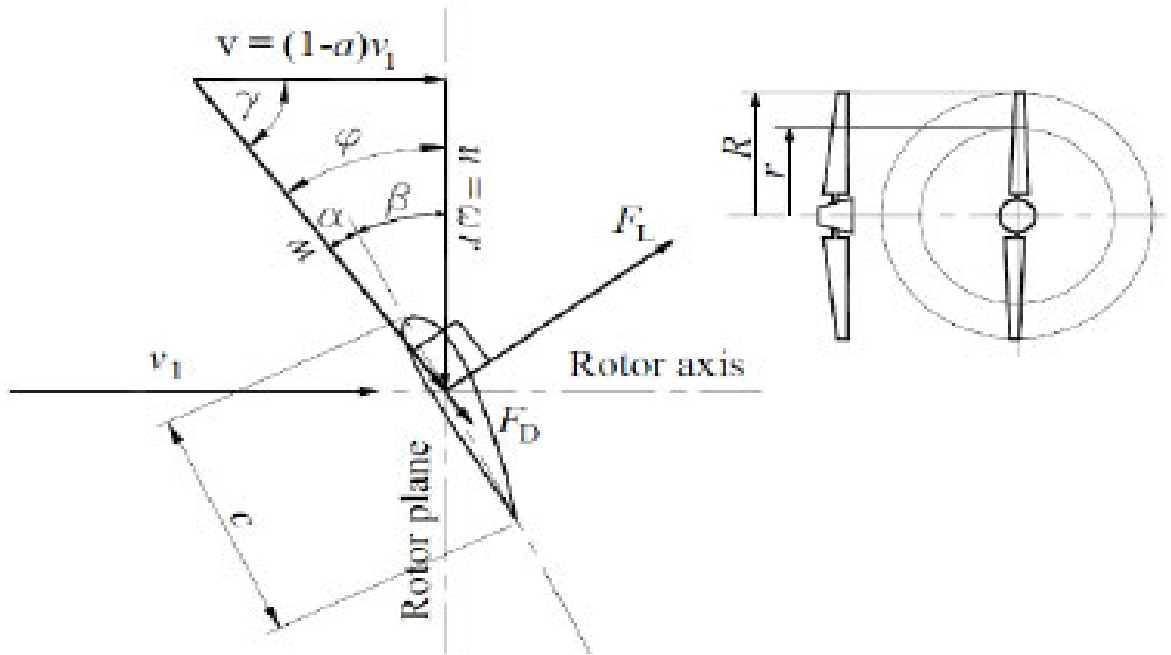


Figure 2.7 Blade element section with all angles, forces and planes on the blade element section defined (Berger and Kühn, 2015)

Axial induction factors which were found higher than 0.4 using Equation 2.6 need to be recalculated using an equation by defined by Buhl (2005) as presented by Equation 2.13.

$$\alpha = \frac{18F - 20 - 3\sqrt{C_N(50 - 36F) + 12F(3F - 4)}}{36F - 50} \quad (2.13)$$

The angle of attack, AOA is then calculated using Equation 2.14:

$$\alpha = \varphi - \beta \quad (2.14)$$

where

α = Angle of attack,

φ = Inflow angle, and

β = Pitch angle.

Generally, an SWT requires a cut-in speed of 3 - 4 m. s⁻¹ to operate, and at about 10-15 m. s⁻¹, the maximum power is generated depending on the turbine rotor size. According to Barroso Montes (2011a), the shut-down wind speed is around 25 m.s⁻¹. Table 2.3 shows the cut-in, rated and cut-out wind speed observed by different researchers.

Table 2.3 Summary of the cut-in, rated, and cut-out wind speed of small wind turbine

Cut-in wind speed	Rated wind speed	Cut-out wind speed	Author
2.8 – 3	10	15	Tahir <i>et al.</i> (2019)
5	-	25	Barroso Montes (2011b)
2.4	12	18	Ozgener (2006)
3.6	12	45	Hirahara <i>et al.</i> (2005)
4	12	25	(Salih <i>et al.</i> , 2012)

Given that the directly measured wind speed from an anemometer as the vehicle travels is different from the wind speed in front of the wind rotor, if calculations of the power coefficient are performed using the measured wind speed, it will result in large errors. Moreover, these errors will result in computing an incorrect power output at a given wind speed. Therefore, the speed/velocity of incoming flow, W is expressed as the resultant of the undisturbed airspeed, V_1 and the rotational speed, ω . The velocity of incoming flow, W , is represented by Equation 2.15:

$$W = \sqrt{[(1 - a)V_1]^2 + [(1 + a')\omega r]^2} \quad (2.15)$$

Provided that $|a_{n+1} - a_n| < 0.001$ and $|a'_{n+1} - a'_n| < 0.001$

where

- W = Velocity of incoming flow (m.s^{-1}),
- V_1 = Undisturbed air speed (m.s^{-1}),
- ω = Wind turbine rotational speed (rev.min^{-1}), and
- r = Radial distance from the hub to the blade element (m).

Even more, the undisturbed airspeed is not simple to acquire for mobile systems. This is because it is a combination of airspeed and the vehicle's travelling speed, giving resultant to the undisturbed apparent wind speed. Generally, the speed limits are 60 km.h^{-1} on a public road within an urban area, 100 km.h^{-1} on public roads outside an urban area which is not a freeway and 120 km.h^{-1} on a freeway (ArriveAlive, 2020). The undisturbed/apparent wind speed is given by Equation 2.16:

$$V_1 = \sqrt{V_c^2 + V_a^2 + 2V_c \cdot V_a \cos \alpha} \quad (2.16)$$

where

- V_1 = Apparent/ undisturbed windspeed (m.s^{-1}),
- V_c = Vehicle speed (m.s^{-1}),
- V_a = Air velocity (m.s^{-1}), and
- α = True pointing angle ($^\circ$).

The true pointing angle of the wind is taken as 0° for upwind conditions and 180° for downwind conditions. The relationship between airspeed and change in air temperature is directly proportional, while that of airspeed and relative humidity is inversely related. In dry weather where the temperature is high, and relative humidity is low, the true airspeed is high and vice versa for cold and humid areas. This is because there is less air to put up resistance against any moving object.

The chord length and twist angle of each blade element is computed using the Schmitz formula. Along with the airfoil section design, the chord lengths and twists angle define the basic shape of the rotor blades. The chord length and twist angle are given by Equation 2.17 and 2.18, respectively:

$$c(r) = \frac{16\pi r}{B(C_L)_D} \sin^2\left(\frac{1}{3} \tan^{-1}\left(\frac{R}{r\lambda_D}\right)\right) \quad (2.17)$$

$$\beta(r) = \frac{2}{3} \tan^{-1}\left(\frac{R}{r\lambda_D}\right) \quad (2.18)$$

where

B = Number of blades,

$(C_L)_D$ = Design lift coefficient,

R = Radius of the rotor/ blade length (m), and

λ_D = Design tip speed ratio.

The design tip speed ratio (TSR) is then presented by Equation 2.19.

$$\lambda_D = \frac{\omega R}{V_1} = \frac{2\pi R N}{60 V_{des}} \quad (2.19)$$

where

ω = Rotational velocity (rad.s^{-1}),

R = Radius (m), and

V_1 = Windspeed (m.s^{-1}).

Aerodynamic performance is important in the efficient design of blades. Two forces act on the WT, the lift force (F_L) and drag force (F_D). The aerodynamic lift is the force on the blades, which is responsible for the energy harnessed by the wind turbine required to maximize power generation. The drag force is the opposing force, giving rise to frictional resistance, and thus must be minimized for high energy efficiency. (Schubel and Crossley, 2012). The lift-to-drag ratio is found on the airfoil section performance catalogue dependent on the AOA.

The values of the lift coefficient (C_L), drag coefficient (C_D), and the lift to drag ratio for before stall conditions are read off the wind turbine two-dimensional (2D) airfoil performance curve, which includes C_L vs α , C_D vs α and C_L/C_D vs α . For optimal WT blades design, $C_L > C_D$ and C_D must be approximated to at least $\frac{1}{10} C_L$ (Salibindla *et al.*, 2020). The total lift force, F_L and drag force, F_D acting on the blades can be determined using Equation 2.20 and 2.21, respectively.

$$F_L = \frac{1}{2} \rho c W^2 C_L \quad \text{or} \quad F_y = B \sum_{i=1}^N (dF_y)_i \quad (2.20)$$

$$F_D = \frac{1}{2} \rho c W^2 C_D \quad \text{or} \quad F_x = B \sum_{i=1}^N (dF_x)_i \quad (2.21)$$

where

$$dF_y = \left(\frac{1}{2} \rho W^2 c \, dr \right) C_y \text{ and}$$

$$dF_x = \left(\frac{1}{2} \rho W^2 c \, dr \right) C_x.$$

According to the BEM theory, lift and drag forces are computed individually from each blade element with thickness, dr and then summed up to give the total force loads by calculating each dF_x and dF_y . The torque and power of the wind turbine can then be calculated using Equation 2.22 and 2.23, respectively.

$$dT = r \, dF \quad (2.22)$$

$$dP = \omega \, dT \quad (2.23)$$

$$P = B \sum_{i=1}^N (dP)_i \quad (2.24)$$

Finally, the power coefficient can be determined from the aerodynamic power computed and the mechanical power.

For $\alpha_{stall} < \alpha < 90^\circ$, Viterna and Corrigan proposed a post-stall model which is used to determine the lift and drag coefficient of a HAWT operating in the stall region. The Viterna and Corrigan is an extension to the BEM theory for post-stall conditions since the 2D airfoil sections do not fully accommodate all the angles where the wind turbine operates post-stall.

$$C_{D,max} = 2.01; AR > 50 \quad (2.25)$$

$$C_{D,max} = 1.11 + 0.018AR; AR \leq 50 \quad (2.26)$$

$$C_D = B_1 \sin^2(\alpha) + B_2 \cos(\alpha), \alpha_{stall} \leq \alpha \leq 90^\circ \quad (2.27)$$

$$B_1 = C_{D,max} \quad (2.28)$$

$$B_2 = \frac{1}{\cos(\alpha_{stall})} \cdot (C_{D,stall} - C_{D,max} \sin^2(\alpha_{stall})) \quad (2.29)$$

$$C_L = A_1 \sin(2\alpha) + \frac{A_2 \cos^2(\alpha)}{\sin(\alpha)} \quad (2.30)$$

$$A_1 = \frac{B_1}{2} \quad (2.31)$$

$$A_2 = [C_{L,stall} - C_{D,max} \sin(\alpha_{stall}) \cos(\alpha_{stall})] \left[\frac{\sin(\alpha_{stall})}{\cos^2(\alpha_{stall})} \right] \quad (2.32)$$

where

AR = Aspect ratio between the blade length and tip chord,

α_{stall} = inflow angle at stall onset (usually 15°),

$C_{D,stall}$ = drag coefficient at stall onset, and

$C_{L,stall}$ = lift coefficient at stall onset.

Reynolds number, Re is important for the design and analysis of rotor blades. The Reynolds no. is a dimensionless value that helps to determine the aerodynamic data such as the lift coefficient, drag coefficient and the lift-to-drag ratio for a selected airfoil design. The Reynolds number is expressed by Equation 2.33:

$$Re = \frac{Wc}{\nu} = \frac{\rho Vc}{\mu} \quad (2.33)$$

where

W = relative wind speed,

c = chord length,

ν = kinematic viscosity of air, and

μ = kinetic viscosity.

In the preliminary design, for simplicity, Re is approximated using the following formula defined by Equation 2.34. This is because the relative wind speed and tip chord length are unknown, although Equation 2.34 forces the author to make an assumption on the chord length.

$$Re = V_1 \cdot c \cdot 70000 \quad (2.34)$$

where 70000 is the constant value for air measured in $s.m^{-2}$

The material used to make rotor blades is crucial in designing a high-functioning WT since they determine the fatigue and strength of the machine (Raj *et al.*, 2016). The material used for the blades must be lightweight to reduce the aerodynamic drag force. One of the simplest and cheap material is the polyvinyl chloride (PVC) pipe. It is weather-resistant, light in weight and makes easy blade shaping, although it can be difficult to cut the right shape. The disadvantages of PVC pipes include the inability to determine the optimum twist angle, pitch angle and angle of attack. Wood, metals, glass fibre reinforced polymers (GFRP), natural fibre reinforced polymer (NFRP), carbon fibre reinforced polymers (CFRC), and nanocomposites are some of the other materials available for making rotor blades (Kale *et al.*, 2015). GFRP and CFRC are preferred to metal due to their properties, but their dependency on petroleum-based resources is a drawback since they are rapidly depleting (Kale *et al.*, 2015). NFRP is a good substitute to address this challenge, given that they are plant-based fibres reinforced with thermoplastic epoxy (Kale *et al.*, 2015). CSP and GFRP are strong materials, but their brittle nature and the fact that they are expensive materials is a downside to their utility. The properties of three materials, CFRP, GFRP, PVC, epoxy and polyester are presented in Table 2.4. These properties include the modulus elasticity, tensile strength, yield strength, strength to weight ratio and other properties that are helpful in the selection of the material for optimum blade design. CFRP and GFRP have high strength to weight ratio and tensile strength. Table 2.5 shows the strengths, weaknesses, opportunities and threats (SWOT) analysis for blades material.

Table 2.4 Material properties of CFRP, GFRP and PVC

Property	CFRP	GFRP	PVC	Epoxy	Polyester
Elastic modulus (N.mm ⁻²)	228000	39300	3-4830	3810-5810	2068-4412
Poisson's ratio	0.32	0.39-0.41	0.4	0.29-0.34	0.65-0.75
Tensile strength (N.mm ⁻²)	1500-3500	480-1600	0.00123-60.8	23-85	42
Yield strength (N.mm ⁻²)	2500	2750-2875	28.0-57.4	91.33	85
Thermal expansion coefficient	2.99 x10 ⁻⁵	20-30 x10 ⁻⁶	28.0x10 ⁻⁶	10-13 x10 ⁻¹	123.5
Mass density (kg.m ⁻³)	1500-2000	1490-1540	1130-1850	1100	1100

Table 2.5 SWOT Analysis of materials for rotor blades (Kale *et al.*, 2015)

Materials	Strengths	Weaknesses	Opportunities	Threats
NFRP	<ul style="list-style-type: none"> • Environmental friendly • Compatible specific strength and specific stiffness • Can be formed into intricate shape • Suitable manufacturing process • Low cost of raw material and manufacturing 	<ul style="list-style-type: none"> • Hygroscopic in nature • Require coating material • Low range of working temperature • Less developed manufacturing process of raw material 	<ul style="list-style-type: none"> • Life and performance can be improved after lamination • Can also be as reinforcement in the NFRP • Recyclable • Increased interest and awareness towards clean energy & environmental issues 	<ul style="list-style-type: none"> • High crack growth rate will cause sudden failure • Change in length due to temperature, humidity and load, varies the stress concentration and load distribution at the interface
Nano-composites	<ul style="list-style-type: none"> • Variability in properties as per type of material choice • Good dimensional stability • Can be formed into intricate shape • High range of working temperature • High specific stiffness and specific strength 	<ul style="list-style-type: none"> • High cost of raw material • It's not readily available • Time consuming manufacturing process • Not eco-friendly • High energy consumption in the fabrication of material • Skilled workers required • Prone to coagulation and segregation of nano-powder during fabrication of the nanocomposites 	<ul style="list-style-type: none"> • Can be used as coating material to reduce the effect of the impact of the dust particles • Can be used with NFRP to reduce the effect of the temperature, humidity and radiation 	<ul style="list-style-type: none"> • Recycling and sustainability is difficult • Repair cost after damage will be high • Failure analysis is difficult • Stress distribution is non-uniform • Life prediction is difficult • High thermal and electrical conductivity

2.4 Integration of Renewable Energy on Cooling Technologies and Vehicles

The wind-solar energy hybrid has been researched for use in transportation but has not yet been fully developed (Merabti *et al.*, 2019). Most of the previously performed wind turbine modelling has been either through MATLAB Simulink or Computational Fluid Dynamics (CFD). Hossain (2020b) performed an experiment in a small vehicle whereby the diesel power supply was replaced by the wind power supply to run the vehicle. The experiment was a success, and the vehicle was able to run efficiently using a wind turbine model from MATLAB Simulink, whereby one can adjust the power coefficient value according to the wind speed (Hossain, 2020b). A study was performed by Abdulateef *et al.* (2009), where it was concluded that a solar-powered ejector-driven refrigeration technology is not only suitable for providing energy to the cooling technology in remote areas for food preservation and medical storage, but it also mitigates energy and climate change crisis.

2.5 Theoretical Framework

This section discusses the wind turbine and evaporative cooling system performance parameters.

2.5.1 Wind turbine performance parameters

The performance parameters used to evaluate wind turbines include the power coefficient and tip speed ratio, which gives the performance curve (Bisoyi *et al.*, 2013). The tip speed ratio (λ) defines the relationship between the rotor blade velocity and the relative wind velocity (Schubel and Crossley, 2012). It is an important design parameter from which other rotor dimensions are determined (Schubel and Crossley, 2012). Aside from the TSR, the power coefficient is the most important parameter used to measure the efficiency of the design and evaluate its performance.

The most important design parameters that are considered for the wind turbine design include the surface area, blade pitch angle, angle of attack, material, weight, and environmental conditions such as wind speed and air density (Bisoyi *et al.*, 2013; Raj *et al.*, 2016). Figure 2.8 provides a summary of the parameters for the wind turbine design.

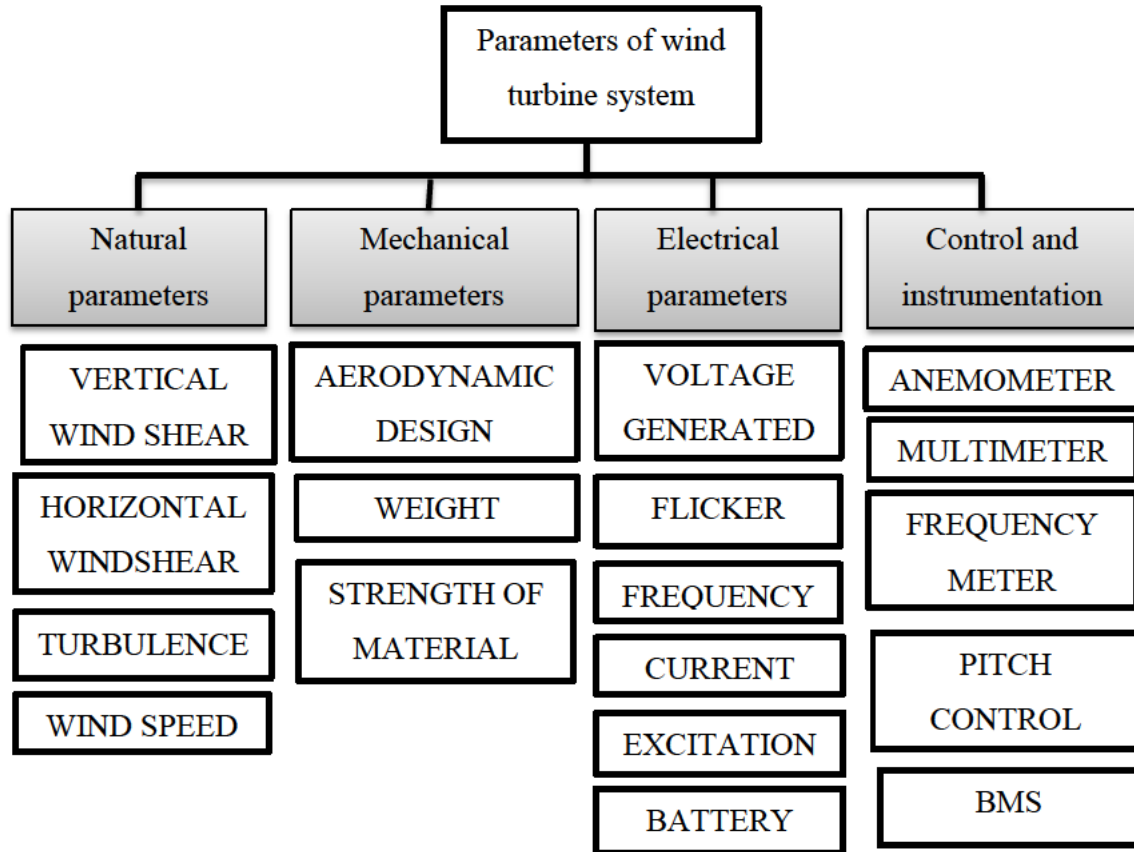


Figure 2.8 Parameters for wind turbine design (Raj *et al.*, 2016)

2.5.2 Evaporative cooling system performance parameters

The performance parameters considered for the ECS include the wet-bulb temperature, relative humidity and shelf-life (Mogaji and Fapetu, 2011). The shelf life can be assessed by measuring the flavour, colour, texture, microbial growth, physical damage, and nutritive value of the fresh produce from start, during and after storage on a cooling technology (Tilahun, 2010b). As soon as fruits and vegetables are detached from their mother plants, they deteriorate because they continue to respire at a faster rate because of high temperature and dry conditions (Nkolisa *et al.*, 2018a). Cooling technologies help to slow down the respiration rate by lowering the outside ambient temperature and increasing the RH (Sibanda and Workneh, 2020a; Sibanda and Workneh, 2020b). Therefore, the performance of an ECS is measured using the difference in temperature and RH change.

2.6 Discussion and Conclusion

The main drive for the great interest in the RES substitutes for utility in the agricultural sector is the growing energy needs for powering agricultural systems, in this particular case, the cooling technologies. Cooling technologies help to maintain the quality of agricultural produce long after they are harvested and increase its shelf-life three times more than in ambient storage conditions. This means the end consumers get quality products, and farmers do not experience high post-harvest losses than could potentially cause high loss of profit. Climate challenges brought by the use of fossil fuels in both the agricultural and industrial sectors have also played a great role in the urgency to review alternative energy sources. Wind energy, along with biomass and solar energy, are the major RES applicable to transportation. Although small wind turbines are still in the developmental phase for incorporation into small vehicles, their working principles are very similar to large wind turbines, meaning the same design concepts can be adopted by SWT. More advantageous is the fact that SWTs do not require complex control such as pitch control, yaw behaviour and the incorporation of a gearbox, instead the rotor and generator are directly coupled. The technology has proven to be efficient and reliable for use in transportation according to the recent research articles done by different authors to power and drive small vehicles and replace diesel/ petrol engine systems.

The swept area and blade geometry design are crucial in obtaining the optimal and highest power supply from the wind turbine. Wind turbines can either have a fixed pitch (stall-regulated) or an adjustable pitch (pitch-regulated). The stall control is the most used control for SWT and is relatively the simplest wind turbine control mechanism against damage. The BEM theory is the common method used for the design and optimization of the blade shape using 2D airfoil. In addition to the BEM theory, the Viterna and Corrigan model can be used to determine the post-stall lift and drag coefficients provided that the angle of attack at which stall occurs is correctly defined. With lightweight materials, the drag force is reduced, and the WT can capture more energy, close to the Betz limit, 59.3%. The materials used for making rotor blades include wood, metals, glass fibre-reinforced polymers (GFRP), natural fibre-reinforced polymer (NFRP), and carbon fibre-reinforced composites (CFRC). Out of these, GFRP, CFRC and NFRP possess the great properties to withstand design wind load and are made to have less deformation. Doubly-Fed Induction Generator (DFIG) and Permanent Magnet Synchronous Generator (PMSG) are the best variable-wind speed electric generators available for energy generation. Then, when it comes to energy storage, Li-ion and VRLA batteries are the most

commonly used battery type because of their high energy efficiency, especially the Li-ion battery type. Although Li-ion batteries have a great capacity per unit volume, have a longer lifespan and are temperature tolerant compared to VRLA batteries, they are relatively expensive, and VRLA is highly recyclable and low maintenance, although it can differ between models and manufacturers (Amrouche *et al.*, 2016).

An evaporative cooling system is preferred to other cooling technologies because it has low installation and maintenance costs, is environmentally friendly, and most importantly, consumes a small amount of energy to power its subsystems. Compared to a refrigeration system, the EC system has less energy consumption. The ECS has a great performance in hot and sub-humid regions with low energy consumption that is around 0.6 kWh for 53 m³ storage. While a refrigeration system requires approximately 8.2 kWh energy supply to run a system of the same carrying capacity. Therefore, the ECS is a good cooling technology for implementation by smallholder farmers. Moreover, the refrigeration system uses refrigerants and compressors, which are harmful to the environment, and mostly, the refrigerated trucks are relatively of large size in relation to the perishable commodities transported by individual smallholder farmers. Vacuum and hydro cooling are just pre-cooling methods that require a secondary system for FV in transit for long distances. Vacuum cooling is specific to food produce, and thus, smallholder farmers who produce a variety of FV cannot utilise it.

Tip speed ratio and power coefficient are the parameters used to measure the performance of SWT. Whilst the performance parameters considered for the ECS are the wet-bulb temperature and relative humidity, the design parameters of the wind turbine include the surface area, blade pitch angle, angle of attack, wind speed and air density. Although solar energy technologies have gained momentum in powering refrigeration systems in the transportation industry, not much literature has been done on the use of wind turbines to directly power cooling technologies used to transport fruits and vegetables in the cold chain. Therefore, the purpose of this literature review was to gather information on renewable energy sources, especially small wind turbines and the BEM theory which can be used to design and develop a small wind turbine prototype to supply power to a mobile cooling technology for smallholder farmers in order to reduce the running costs of purchasing or hiring a cooling technology. Through reducing the running costs, that is petrol and diesel costs used to run the cooling technology, farmers can be able to afford to hire mobile cooling technologies, which will reduce post-

harvest losses. In this way farmers will be able to make profit from selling as well as from saving on fuel costs.

2.7 References

- Abdulateef, J, Sopian, K, Alghoul, M and Sulaiman, M. 2009. Review on solar-driven ejector refrigeration technologies. *Renewable and Sustainable Energy Reviews* 13 (6-7): 1338-1349.
- Adekanye, TA and Babaremu, KO. 2019. Evaluation of an active evaporative cooling device for storage of fruits and vegetables. *Agricultural Engineering International: CIGR Journal* 21 (1): 203-208.
- Amrouche, SO, Rekioua, D, Rekioua, T and Bacha, S. 2016. Overview of energy storage in renewable energy systems. *International Journal of Hydrogen Energy* 41 (45): 20914-20927.
- Anbazhaghan, N, Saravanan, R and Renganarayanan, S. 2005. Biomass based sorption cooling systems for cold storage applications. *International journal of green energy* 2 (4): 325-335.
- ArriveAlive. 2020. Speed limits and the law [Internet]. Google. Available from: <https://www.arrivealive.co.za/Speed-Limits-And-The-Law>. [Accessed: May 2021].
- Barroso Montes, M. 2011a. Optimal control of wind turbines in strong wind conditions. Unpublished Masters thesis, Mechanical Engineering, Technical University of Denmark, Copenhagen, Denmark.
- Barroso Montes, M. 2011b. Optimal control of wind turbines in strong wind conditions. Unpublished thesis, Mechanical Engineering, Technical University of Denmark, Kongens Lyngby, Denmark.
- Benedek, J, Sebestyén, T-T and Bartók, B. 2018. Evaluation of renewable energy sources in peripheral areas and renewable energy-based rural development. *Renewable and Sustainable Energy Reviews* 90 (2018): 516-535.
- Berger, F and Kühn, M. 2015. Investigating the aerodynamic implications of slender wind turbine blade design. *WE KnOW WInD* 130.
- Bharj, R. 2018. Energy consumption of solar hybrid 48V operated mini mobile cold storage. *IOP Conference Series: Materials Science and Engineering*, 012049. IOP Publishing.

- Bisoyi, SK, Jarial, R and Gupta, R. 2013. Modeling and control of variable speed wind turbine equipped with PMSG. *International Journal of Emerging Technologies in Computational and Applied Sciences* 6 (1): 56-62.
- Dominković, DF, Bačeković, I, Pedersen, AS and Krajačić, G. 2018. The future of transportation in sustainable energy systems: Opportunities and barriers in a clean energy transition. *Renewable and Sustainable Energy Reviews* 82 (2): 1823-1838.
- Dragičević, T, Pandžić, H, Škrlec, D, Kuzle, I, Guerrero, JM and Kirschen, DS. 2014. Capacity optimization of renewable energy sources and battery storage in an autonomous telecommunication facility. *IEEE Transactions on Sustainable Energy* 5 (4): 1367-1378.
- Esmaili, A, Novakovic, B, Nasiri, A and Abdel-Baqi, O. 2013. A hybrid system of li-ion capacitors and flow battery for dynamic wind energy support. *IEEE Transactions on industry applications* 49 (4): 1649-1657.
- Fontes, CHdO and Freires, FGM. 2018. Sustainable and renewable energy supply chain: A system dynamics overview. *Renewable and Sustainable Energy Reviews* 82 (1): 247-259.
- García-Olivares, A, Solé, J and Osychenko, O. 2018. Transportation in a 100% renewable energy system. *Energy Conversion and Management* 158 (2018): 266-285.
- Harrouz, A, Colak, I and Kayisli, K. 2016. Control of a small wind turbine system application. *2016 IEEE International Conference on Renewable Energy Research and Applications (ICRERA)*, 1128-1133. IEEE, Birmingham, UK.
- Hirahara, H, Hossain, MZ, Kawahashi, M and Nonomura, Y. 2005. Testing basic performance of a very small wind turbine designed for multi-purposes. *Renewable energy* 30 (8): 1279-1297.
- Hossain, MF. 2020. Application of wind energy into the transportation sector. *International Journal of Precision Engineering and Manufacturing-Green Technology* 8 (2020): 1-13.
- Johari, M, Jalil, M and Shariff, MFM. 2018. Comparison of horizontal axis wind turbine (HAWT) and vertical axis wind turbine (VAWT). *International Journal of Engineering and Technology* 7 (4.13): 74-80.
- Kabir, E, Kumar, P, Kumar, S, Adelodun, AA and Kim, K-H. 2018. Solar energy: Potential and future prospects. *Renewable and Sustainable Energy Reviews* 82 (1): 894-900.
- Kale, SA, Kulkarni, SR, Shravagi, SD and Bharambe, GP. 2015. Materials for small wind turbine blades. In: *Chapter 3*, Pune, India.

- Kitinoja, L and Thompson, JF. 2010. Pre-cooling systems for small-scale producers. *Stewart Postharvest Review* 6 (2): 1-14.
- Koç, E, Günel, O and Yavuz, T. 2016. Comparison of Qblade and CFD results for small-scaled horizontal axis wind turbine analysis. *2016 IEEE International Conference on Renewable Energy Research and Applications (ICRERA)*, 204-209. IEEE.
- Kumar, S and Bharj, DR. 2016. Design for Solar Hybrid Mobile Multipurpose Cold Storage system. *International Journal of Technical Research & Science* 1 (9): 289 - 294.
- Lian, K, Perkins, BK and Lehn, P. 2008. Harmonic analysis of a three-phase diode bridge rectifier based on sampled-data model. *IEEE Transactions on power delivery* 23 (2): 1088-1096.
- Liu, W, Wang, J, Richard, TL, Hartley, DS, Spataro, S and Volk, TA. 2017. Economic and life cycle assessments of biomass utilization for bioenergy products. *Biofuels, Bioproducts and Biorefining* 11 (4): 633-647.
- Merabti, L, Abbas, M and Taane, W. 2019. Applicability of Solar Evaporative Cooling in Greenhouses productivity Improvement. *2019 7th International Renewable and Sustainable Energy Conference (IRSEC)*, 1-4. IEEE.
- Mogaji, TS and Fapetu, OP. 2011. Development of an evaporative cooling system for the preservation of fresh vegetables. *African Journal of Food Science* 5 (4): 255-266.
- Muhsen, H, Al-Kouz, W and Khan, W. 2019. Small wind turbine blade design and optimization. *Symmetry* 12 (1): 18.
- Njoroge, P, Ndunya, L and Kabiru, P. 2018. Hybrid Solar-Wind Power System for Truck Refrigeration. *2018 IEEE PES/IAS PowerAfrica*, 1-9. IEEE.
- Nkolisa, N, Magwaza, LS, Workneh, TS and Chimphango, A. 2018. Evaluating evaporative cooling system as an energy-free and cost-effective method for postharvest storage of tomatoes (*Solanum lycopersicum* L.) for smallholder farmers. *Scientia Horticulturae* 241 (2018): 131-143.
- Ofualagba, G and Ubeku, E. 2008. Wind energy conversion system-wind turbine modeling. *2008 IEEE Power and Energy Society General Meeting-Conversion and Delivery of Electrical Energy in the 21st Century*, 1-8. IEEE, Pittsburgh, PA, USA.
- Olosunde, WA, Aremu, AK and Onwude, DI. 2016. Development of a solar powered evaporative cooling storage system for tropical fruits and vegetables. *Journal of Food Processing and Preservation* 40 (2): 279-290.
- Ozgener, O. 2006. A small wind turbine system (SWTS) application and its performance analysis. *Energy conversion and Management* 47 (11-12): 1326-1337.

- Panja, P and Ganguly, A.2019. Modelling and analysis of a hybrid solar thermal and biomass driven vapor absorption refrigeration system for cold storage purpose. *Proceedings of fifth international congress on engineering and technology (ICET2019), Pune, India.*
- Raj, A, Gurav, R, Sankpal, J, Chavan, DS and Karandikar, P.2016. Study of output parameters of horizontal axis wind turbines using experimental test setup. *2016 IEEE 1st International Conference on Power Electronics, Intelligent Control and Energy Systems (ICPEICES)*, 1-6. IEEE, Delhi, India.
- Rossetti, A, Marinetti, S, Artuso, P, Fabris, F and Minetto, S. 2022. Implementation of a solar aided refrigeration unit for refrigerated trucks employing photovoltaic generators. *Energy Reports* 8 7789-7799.
- Sakui, M and Fujita, H. 1994. An analytical method for calculating harmonic currents of a three-phase diode-bridge rectifier with DC filter. *IEEE transactions on Power Electronics* 9 (6): 631-637.
- Salibindla, AK, Masuk, AUM, Tan, S and Ni, R. 2020. Lift and drag coefficients of deformable bubbles in intense turbulence determined from bubble rise velocity. *Journal of Fluid Mechanics* 894 (2020): 1-15.
- Salih, SM, Taha, MQ and Alawsaj, MK. 2012. Performance analysis of wind turbine systems under different parameters effect. *International Journal of Energy and Environment* 3 (6): 895-904.
- Sathiyarayanan, J and Senthil Kumar, A. 2014. Doubly fed induction generator wind turbines with fuzzy controller: a survey. *The Scientific World Journal* 2014 1-8.
- Saura, J, Mesas, JJ and Sainz, L. 2021. Average value of the DC-link output voltage in multi-phase uncontrolled bridge rectifiers under supply voltage balance and unbalance conditions. *Electrical Engineering* 103 (6): 3097-3109.
- Schubel, PJ and Crossley, RJ. 2012. Wind turbine blade design. *Energies* 5 (9): 3425-3449.
- Shahsavari, A and Akbari, M. 2018. Potential of solar energy in developing countries for reducing energy-related emissions. *Renewable and Sustainable Energy Reviews* 90 (2018): 275-291.
- Sharma, P and Kumar, HA. 2018. Solar powered movable cold storage structure for perishables. *Current Science* 114 (10): 2020-2022.
- Shirmohammadi, R and Gilani, N. 2019. Effectiveness enhancement and performance evaluation of indirect-direct evaporative cooling system for a wide variety of climates. *Environmental Progress & Sustainable Energy* 38 (3): 1-11.

- Sibanda, S and Workneh, TS. 2020a. Performance evaluation of an indirect air cooling system combined with evaporative cooling. *Heliyon* 6 (1): e03286.
- Sibanda, S and Workneh, TS. 2020b. Potential causes of postharvest losses, low-cost cooling technology for fresh produce farmers in Sub-Sahara Africa. *African Journal of Agricultural Research* 16 (5): 553-566.
- Soares-Ramos, EP, De Oliveira-Assís, L, Sarrias-Mena, R, García-Triviño, P, García-Vázquez, CA and Fernández-Ramírez, LM. 2021. Averaged Dynamic Modeling and Control of a Quasi-Z-Source Inverter for Wind Power Applications. *IEEE Access* 9 114348-114358.
- Stellingwerf, HM, Kanellopoulos, A, van der Vorst, JG and Bloemhof, JM. 2018. Reducing CO₂ emissions in temperature-controlled road transportation using the LDVRP model. *Transportation Research Part D: Transport and Environment* 58 (2018): 80-93.
- Sumathi, S, Kumar, LA and Surekha, P. 2015. Wind energy conversion systems. In: *Solar PV and Wind Energy Conversion Systems*. Springer, Switzerland.
- Tahir, MH, Malik, A, Saeed, MA, Zaffar, N, Adeel, HM and Amjad, HMS. 2019. Experimental Performance Evaluation of 600 W Small Wind Turbine to Overcome Energy Crisis in Pakistan.
- Tassou, S, De-Lille, G and Lewis, J. 2012. Food transport refrigeration. *Centre for Energy and Built Environment Research, Brunel University, UK*.
- Tilahun, S. 2010. Feasibility and economic evaluation of low-cost evaporative cooling system in fruit and vegetables storage. *African Journal of Food, Agriculture, Nutrition and Development* 10 (8): 2984 - 2997.
- Velasco, FEH, Velasco, CIH and Candelo-Becerra, JE. 2019. DC-AC power inverter controlled analogically with zero hysteresis. *International Journal of Electrical and Computer Engineering* 9 (6): 4767.
- Wood, D. 2011. Small wind turbines. In: *Advances in wind energy conversion technology*. Springer.
- Workneh, S. 2010. Feasibility and economic evaluation of low-cost evaporative cooling system in fruit and vegetables storage. *African Journal of Food, Agriculture, Nutrition and Development* 10 (8): 2984-2997.
- Zhu, Z, Geng, Y and Sun, D-W. 2019. Effects of operation processes and conditions on enhancing performances of vacuum cooling of foods: A review. *Trends in Food Science & Technology* 85 (2019): 67-77.

3. WIND TURBINE MODELLING USING BLADE ELEMENT MOMENTUM THEORY, QBLADE AND MATLAB-SIMULINK

Abstract

This study aimed to design and optimise the blades of a 600 W wind turbine by using the blade element momentum (BEM) theory and QBlade modelling software. MATLAB Simulink was also used to model the entire wind turbine, including all the associated electrical components. QBlade and MATLAB Simulink are two of the commonly used software for the analysis of wind turbines. The blade element momentum theory is employed mainly for the optimization of the chord length, twist angle and overall shape of the blade. Initially, the BEM method was used to perform the computations of the wind turbine design. Then, QBlade was used to model the small wind turbine with a power output rated around 600 W and the SG6043 airfoil section used for the design of the blades. This study was conducted using a small horizontal-axis wind turbine (HAWT) driven by a permanent magnet synchronous generator (PMSG). The important parameters considered for the design include air density, wind speed, rotor diameter, pitch, and twist angle. According to the BEM method, the required power output of 600 W for a design wind speed of 16.8 m.s^{-1} , a design TSR value of 6 and a pitch

angle of 7° is found at a rotor rotational speed of $3200 \text{ rev.min}^{-1}$. The QBlade model showed that a SWT with a rotor diameter of 600 mm, a design tip speed ratio of 6 running at 19 m.s^{-1} can generate electrical energy of 0.6 kW at a rotor rotational speed of $3200 \text{ rev.min}^{-1}$, and the power coefficient was found at 0.45. Both the BEM theory and QBlade obtained similar results, showing that a rotational speed of $3200 \text{ rev.min}^{-1}$ is required to produce 600 W of electrical energy with a diameter of 0.6 m. A power output of 611.8 W was produced using the model on MATLAB Simulink, with the wind speed at 16.8 m.s^{-1} and a pitch angle of 7° . The BEM theory and QBlade software help create a blade that harnesses the maximum amount of wind energy to generate the maximum electrical energy. The chord length, twist angle, pitch angle, design wind speed and rotor rotational speed obtained in these models are essential in developing a fully functional wind turbine prototype.

3.1 Introduction

Specific modelling and simulation tools are used for the design of wind turbines. Amongst the many modelling tools available, the blade element momentum theory, QBlade, and MATLAB Simulink are some of the common tools used to model wind turbines (Alaskari *et al.*, 2019; Noronha and Krishna, 2020). The blade element momentum theory is a mathematical model used to compute the basic parameters of the wind turbine design (Alaskari *et al.*, 2019). QBlade and MATLAB Simulink are models used to design, simulate, and analyse the wind turbine performance. QBlade is a simple, easy-to-use open-source software that was specifically designed for wind turbine analysis (Koç *et al.*, 2016). It is used for the design and real-time simulation of SWT, and it provides a performance curve for the power output, power coefficient, torque, thrust, the bending moment, measured against the wind speed, tip speed ratio and rotational speed (Alaskari *et al.*, 2019; Bracco and Razzetti, 2022). The functionality of QBlade include airfoil design and analysis, lift and drag polar extrapolation, blade design and optimisation, and lastly turbine definition and simulation (Noronha and Krishna, 2020). On QBlade, the NACA foils data can be used or the airfoil data can be imported from the specially designed website even though it is limited experimental data (AirfoilTools, 2022). Based on the airfoil data, the software can produce the lift-to-drag ratio, lift coefficient, and drag coefficient versus the angle of attack curves (Bracco and Razzetti, 2022).

Extrapolation of the imported airfoil data for post-stall operation in order to include the 360 range angle of attack can be done using either the Montgomerise or Viterna method (Hassanzadeh *et al.*, 2016). QBlade is able to design a blade with different airfoil sections and shapes for optimum blade design (Bracco and Razzetti, 2022). With the blade design and optimization part, the chord length can be optimised using the Schmitz, Betz, or linear method. Then the twist angle can be optimised using the optimum lift-to-drag coefficient, stall, and linear method for each blade element. QBlade uses the blade element momentum method for simulation of wind turbines and provision of real-time data (Alaskari *et al.*, 2019; Suresh and Rajakumar, 2020). On the other side, MATLAB Simulink is part of the MathWorks package. It can be used to model and simulate the electric connections of a fully functional wind turbine system using mainly built-in blocks and programming with a customizable set of blocks. MATLAB Simulink is a relatively complex programming software that requires a bit of learning and understanding of the connections and electric systems. MATLAB Simulink permits one to specific set up or code each of the electrical components of the wind turbine

electrical circuit (Quintal-Palomo and Dybkowski, 2019). MATLAB Simulink is able to produce the power output, rotational speed, voltage and current measurements as well as the power coefficient curves among many parameters it can generate. This study aimed to design and optimise a 600 W wind turbine using different modelling methods for the development of a fully functional wind turbine prototype.

3.2 Wind Turbine Blade Design Using the Blade Element Momentum (BEM) Theory

This section discusses the mathematical computations involved in the design of the small wind turbine using the BEM theory and Viterna and Corrigan model for the optimization of the blade design for the best possible performance. The International Electrotechnical Commission (IEC) 61400-2 standard: Design requirements of a small wind turbine was used in the design of the structure to make it a safe and compatible design. This section discusses in detail the theoretical design of the wind turbine blades using the BEM theory, which outputs the total electric power generated by the wind turbine along with the power coefficients, which measures the efficiency of the design. The initial design parameters and assumptions of the calculations are presented on Table 3.1.

An iterative procedure is required to compute the axial and tangential induction factor and eventually the power output and power coefficient. The steps are as follows:

- (a) Initially, set the values of a and a' to zero,
- (b) Compute φ and AOA using Equation 2.8 and 2.14, respectively,
- (c) Obtain C_L , C_D and C_L/C_D using the computed AOA from standardised plots specific to the airfoil section and Reynold's number,
- (d) Determine the tip-hub loss factor, chord length and solidity factor, assuming the twist angle to be zero,
- (e) Calculate the normal and tangential coefficient, C_x and C_y ,
- (f) Reassign a and a' values using Equation 2.6 and 2.7,
- (g) If $a > 0.4$, use Equation 2.13,
- (h) Once the a and a' values are determined, calculate the axial and tangential forces acting on each blade element, and
- (i) Lastly, compute the torque and power output for each blade element.

Table 3.1 Initial design parameters of the small wind turbine

Design parameters	Value	Units
Wind turbine rated power output, P	600	W
Design/rated design wind speed, V_{design}	12	m.s^{-1}
Number of blades, B	3	-
Design tip speed ratio, λ	6	-
Air density, ρ	1.24	kg.m^{-3}
Rotor radius, R	0.3	M
Design rotational speed, ω	3200	rev.min^{-1}
Design Reynolds number, Re	200 000	-

The apparent wind speed for a moving vehicle on the road ranges between 12 - 29 m.s^{-1} and possibly higher. Considering these high wind speeds, a movable louvre mechanism structure is used to reduce the undisturbed/apparent wind speed to a lower value that is suitable for wind turbine operation as seen from the range presented in Figure 3.1. This is because high wind speeds can potentially cause wear and tear on the blade surface, making the wind turbine fail in its original purpose or potentially be a safety hazard. From Figure 3.1, it is clear that the wind turbine reaches its highest performance between 10 – 15 m.s^{-1} , and the cut-off speed is 25 m.s^{-1} . Outside of this range, the wind turbine ceases operating. Taking this into account, the convenient design wind speed is between 10 - 25 m.s^{-1} . For the preliminary design, the wind speed is taken as 16.8 m.s^{-1} , from an average wind speed of 12 m.s^{-1} as defined from the IEC 61400-2 standard calculated using Equation 3.1:

$$\begin{aligned}
 V_{\text{design}} &= 1.4 V_{\text{ave}} \dots\dots\dots (3.1) \\
 &= 1.4 (12) \\
 &= 16.8 \text{ m.s}^{-1}
 \end{aligned}$$

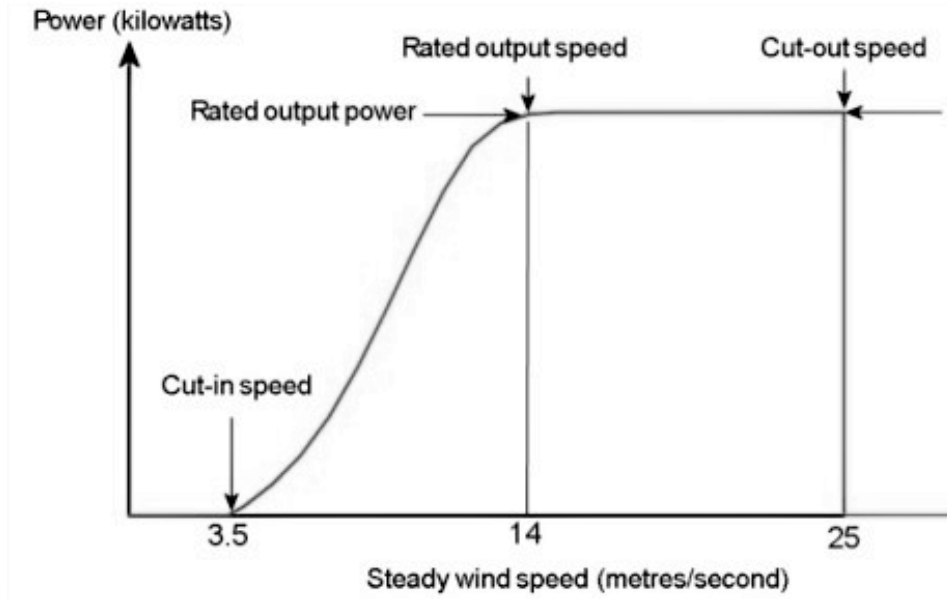


Figure 3.1 Power curve of a wind turbine (Cole, 2022)

For the wind turbine blade design, the tip speed ratio, TSR, is taken as 6 since most small wind turbines have high performance at the TSR around 5-7. Then, the rotor diameter is fixed at 600 mm. These are basic assumptions which are important in the wind turbine design. The first computation done after determining the design wind speed is determining the rotor/generator rotational speed and angular velocity. Using the assumptions and a design wind speed of 16.8 m.s^{-1} , the rotor rotational speed was calculated and found to be $3208.564 \text{ rev.min}^{-1}$, while the angular speed, ω was found to be 336 rad.s^{-1} as shown by Equation 3.2 and 3.3, respectively.

$$\lambda = \frac{\omega R}{V_1} = \frac{\frac{2\pi R.N}{60}}{V_{des}} \quad (3.2)$$

$$6 = \frac{\frac{2\pi(0.3).N}{60}}{16.8}$$

$$N = \frac{6 \cdot 16.8 \cdot 60}{2\pi(0.3)}$$

$$= 3208.564 \text{ rev.min}^{-1}$$

$$\omega = \frac{2\pi N}{60} \dots\dots\dots (3.3)$$

$$= \frac{2\pi(3208.564)}{60}$$

$$= 336 \text{ rad.s}^{-1}$$

With a and a' initially taken as zero, the design wind speed, V_1 at 16.8 m.s^{-1} and the computed angular velocity, ω at 336 rad.s^{-1} , the inflow angle, φ of the incoming airflow is calculated for different elements/segments along the blade using Equation 3.4. The sample calculations were done for the middle element at the radial distance, r equal to 0.15 m . The inflow angle was calculated and found to be 18.4° as shown by Equation 3.4. The inflow angle of each blade element is presented in Table 3.2. Then, with the inflow angle calculated at 18.4° from a radial distance of 0.15 m and the pitch angle at 7° , the angle of attack for the third blade element was calculated using Equation 3.5 and found to be 11.4° . The angle of attack of the incoming flow for each of the blade elements is also presented in Table 3.2 for the entire blade length.

$$\begin{aligned}\varphi &= \tan^{-1}\left(\frac{(1-a)V_1}{(1+a)\omega r}\right) \dots\dots\dots (3.4) \\ &= \tan^{-1}\left(\frac{(1-0)16.8}{(1+0)336*0.15}\right) \\ &= 18.4^\circ\end{aligned}$$

$$\begin{aligned}\alpha &= \varphi - \beta \dots\dots\dots (3.5) \\ &= 18.435 - 7 \\ &= 11.4^\circ\end{aligned}$$

Table 3.2 Inflow angle and angle of attack at different blade elements

Element number	r (m)	φ (°)	α (°)
1	0.05	45.0	38.0
2	0.1	26.565	19.6
3	0.15	18.435	11.4
4	0.2	14.036	7.0
5	0.25	11.310	4.3
6	0.3	9.462	2.5

Assuming that the chord length is between 0.05 m and 0.1 m and knowing the design wind speed to be 16.8 m.s^{-1} , the Reynolds number was calculated using Equation 3.6. The Reynolds number for a chord length of 0.05 m and 0.1 m was found to be $58\,880$ and $117\,600$, respectively, as shown by Equation 3.6 and 3.7. In order to account for safety and extreme turbulence conditions on the road and ensure that the blades can withstand higher winds

imposed on the wind turbine structure, the Reynolds number is taken as 200 000 since from the preliminary design, the Reynolds number was calculated above 100 000 and the next curve at which the airfoil section data is available is for Re at 200 000.

$$\begin{aligned}
 Re &= V_1 \cdot c \cdot 70000 \dots\dots\dots (3.6) \\
 &= 16.8 \cdot 0.05 \cdot 70000 \\
 &= 58888
 \end{aligned}$$

$$\begin{aligned}
 Re &= V_1 \cdot c \cdot 70000 \dots\dots\dots (3.7) \\
 &= 16.8 \cdot 0.1 \cdot 70000 \\
 &= 117\,600
 \end{aligned}$$

The next parameters which need to be determined are the axial and tangential induction factors, but firstly, some unknowns such as the tip-hub loss factor, solidity factor, lift coefficient, drag coefficient, and the normal and tangential loads coefficients must be calculated. The lift and drag coefficients were read off the C_L vs α and C_D vs α plots provided from the selected airfoil section catalogue (AirfoilTools, 2020). The airfoil section chosen for the wind turbine blades was the SG6043 airfoil section. The SG6043 section was specifically created for small wind turbines operating at a low Reynolds number with a 10% thickness. It has a high lift to drag coefficients which is good for small wind turbine and obtains high performance compared to the other airfoil section. Figure 3.2 shows the design and shape of the SG6043 airfoil section. Using Re at 200 000 and the inflow angle for each of the six elements, the C_L , C_D and C_L/C_D values were read from Figure 3.3, 3.4 and 3.5 for the SG6043 airfoil section. The C_L , C_D and C_L/C_D values are presented in Table 3.3 for each blade element along the blade length from the pre-determined angles of attack. Table 3.4 shows the legends used to define the plots in Figure 3.3, 3.4 and 3.5

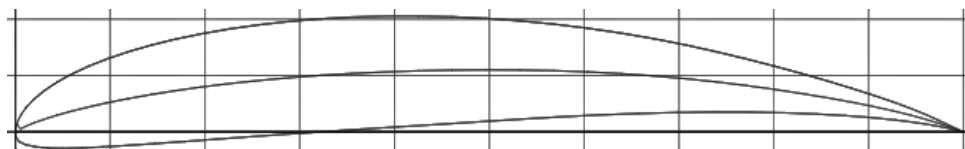






Figure 3.2 SG6043 airfoil section design

Table 3.3 C_L , C_D and C_L/C_D values for Re at 200 000 for each angle of attack at different blade elements operating post-stall and during stall conditions.

	α (°)					
	38.0	19.6	11.4	7.0	4.3	2.5
C_L	2.204	1.588	1.5	1.38	1.17	1
C_D	1.384	0.162	0.036	0.016	0.014	0.014
C_L/C_D	1.592	9.802	44	87	94	73

Table 3.4 SG6043 airfoil section data, including curve plots according to Reynolds number, Ncrit and max C_L/C_D with the corresponding

Plot	Airfoil	Reynolds no.	Ncrit	Max C_L/C_D
	SG6043	50 000	9	39.7 at $\alpha = 8.75^\circ$
	SG6043	100 000	9	66.5 at $\alpha = 7^\circ$
	SG6043	200 000	9	98 at $\alpha = 5.5^\circ$
	SG6043	500 000	9	143 at $\alpha = 3.5^\circ$

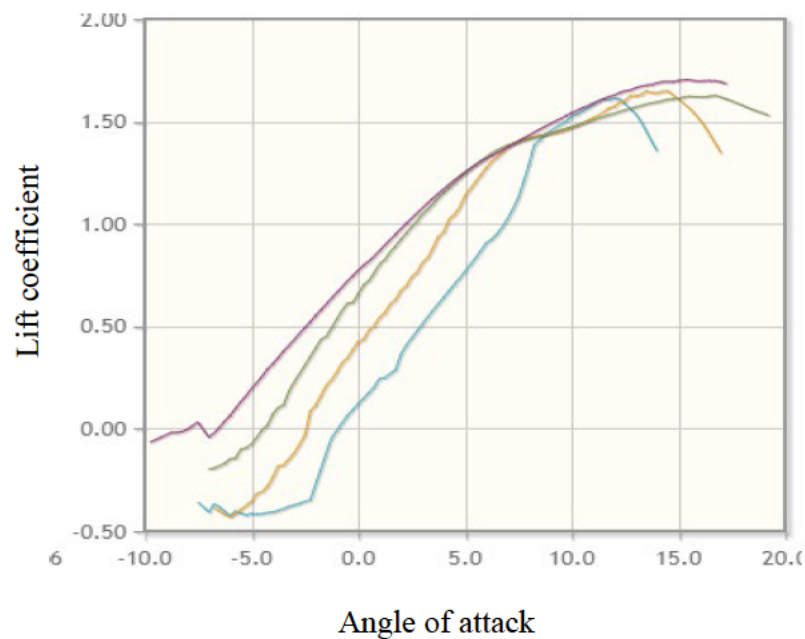


Figure 3.3 Lift coefficient (C_L) vs angle of attack (α) for SG6043 airfoil section at different Reynolds number (Re)

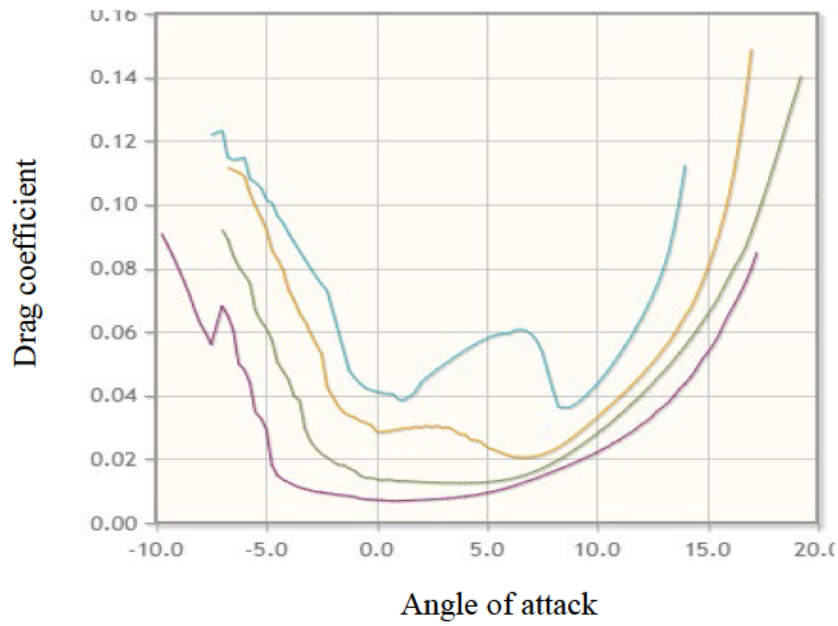


Figure 3.4 Drag coefficient (C_D) vs angle of attack (α) for SG6043 airfoil section at different Reynolds number (Re)

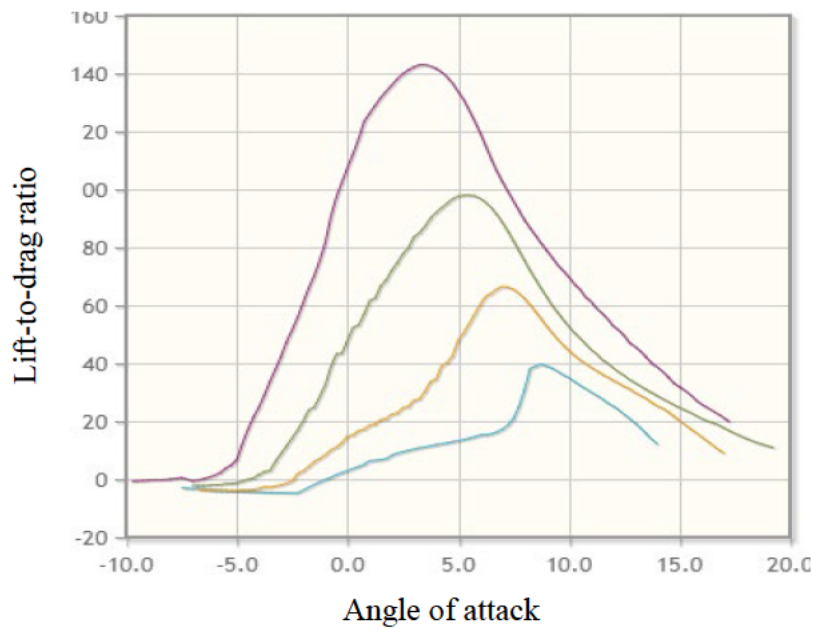


Figure 3.5 Lift to drag ratio (C_L / C_D) vs angle of attack (α) for SG6043 airfoil section at different Reynolds number (Re)

For $\alpha_{stall} < \alpha < 90^\circ$ where α_{stall} is established at 19° from the chosen Reynolds number, the C_L , C_D and C_L/C_D values were determined using the Viterna and Corrigan model. This is for the blade sections operating at stall condition since the available tested airfoil section design data is limited to the lower angles of attacks. Given the rotor radius at 0.3 m, the angle of attack

at stall found at 19°, the tip chord length at 0.0165 m, the lift coefficient at stall at 1.56 and the drag coefficient at stall at 0.14, the C_L , C_D and C_L/C_D values at AOA at 38.0° and 19.6° are determined using the Viterna and Corrigan model as Table 3.3.

From the literature review, it was noted that the three blades wind turbine has high performance and stability without additional mass and costs to the design, therefore, the number of blades, N is taken as 3. Equation 3.8 was used to determine the tip-hub loss factor with the rotor radius taken as 0.3 m. For three blades, a rotor radius of 0.3 m, an inflow angle of 45° and a radial distance of 0.05 m from the hub, the tip-hub loss factor was found to be 57.295. The values of F are presented in Table 3.5.

$$\begin{aligned}
 F &= \frac{2}{\pi} \cos^{-1} \left(e^{\frac{-B(R-r)}{2r \sin \phi}} \right) \dots \dots \dots (3.8) \\
 &= \frac{2}{\pi} \cos^{-1} \left(e^{\frac{-3(0.3-0.05)}{2(0.05) \sin(45)}} \right) \\
 &= 57.295
 \end{aligned}$$

Table 3.5 Tip-hub loss factor, F

ϕ (°)	r (m)					
	0.05	0.1	0.15	0.2	0.25	0.3
45.0	57.295	56.771	52.913	44.4	31.282	0
26.565	57.296	57.251	56.021	50.437	37.72	0
18.435	57.296	57.293	56.978	53.887	42.791	0
14.036	57.296	57.296	57.221	55.639	46.553	0
11.310	57.296	57.296	57.278	56.499	49.332	0
9.462	57.296	57.296	57.291	56.914	51.388	0

To compute the solidity factor, the chord length must be first determined. The chord length is computed using Equation 3.9 for each element. With the number of the blades taken as three, the TSR taken as 6, and the design lift coefficient taken as 1.17, corresponding to the maximum C_L/C_D , the chord length can be determined. Then the solidity factor is determined using Equation 3.10. The airfoil section design together with the pitch angle, chord length and twist angle give the overall shape of the wind turbine structure. In order to not complicate the design, the twist angle is assumed to be zero. The chord length for a radial distance of 0.15 m, a radius

of 0.3 m, and a design TSR of 6 was found to be 0.0246 m, while the solidity factor was found to be 0.0783. The chord length and corresponding solidity factors for the entire blade length are presented in Table 3.6.

$$\begin{aligned}
 c &= \frac{16\pi r}{B(C_L)_D} \sin^2\left(\frac{1}{3} \tan^{-1}\left(\frac{R}{r\lambda_D}\right)\right) \dots\dots\dots (3.9) \\
 &= \frac{16\pi(0.15)}{3(1.17)} \sin^2\left(\frac{1}{3} \tan^{-1}\left(\frac{0.3}{0.15(6)}\right)\right) \\
 &= 0.0246 \text{ m}
 \end{aligned}$$

$$\begin{aligned}
 \sigma &= \frac{cB}{2\pi r} \dots\dots\dots (3.10) \\
 &= \frac{0.15(3)}{2\pi(0.15)} \\
 &= 0.0783
 \end{aligned}$$

Table 3.6 Chord length and solidity factor for different elements along the blade length

Element no.	r (m)	c (m)	σ
1	0.05	0.0480	0.4580
2	0.1	0.0339	0.1620
3	0.15	0.0246	0.0783
4	0.2	0.0191	0.0455
5	0.25	0.0155	0.0296
6	0.3	0.0130	0.0207

The normal and tangential loads coefficient, C_x and C_y are computed using Equation 3.11 and 3.12, respectively. Table 3.7 shows the normal and tangential loads coefficient along the blade length. Then finally, the axial and tangential induction factors are calculated using Equation 3.13 and 3.14 and reassigned values as shown in Table 3.7.

$$\begin{aligned}
 C_x &= C_L \cos\varphi + C_D \sin\varphi \dots\dots\dots (3.11) \\
 &= 1.5\cos(18.435) + 0.036\sin(18.435) \\
 &= 1.434
 \end{aligned}$$

$$C_y = C_L \sin\varphi - C_D \cos\varphi \dots\dots\dots (3.12)$$

$$= 1.5\sin(18.435) - 0.036\cos(18.435)$$

$$= 0.440$$

$$a = \frac{1}{\frac{4F\sin^2\varphi}{\sigma C_x} + 1} \dots\dots\dots (3.13)$$

$$= \frac{1}{\frac{4(57.978)\sin^2(18.435)}{0.0783(1.434)} + 1}$$

$$= 0.004906856$$

$$a' = \frac{1}{\frac{4F\sin\varphi\cos\varphi}{\sigma C_y} - 1} \dots\dots\dots (3.14)$$

$$= \frac{1}{\frac{4(57.978)\sin(18.435)\cos(18.435)}{0.0783(0.440)} - 1}$$

$$= 0.00050457$$

Table 3.7 Normal loads coefficient, tangential loads coefficient, axial and tangential induction factor along the blade length

Element no.	F	φ (°)	C_x (C_n)	C_y (C_t)	A	a'
1	57.296	0.458	2.537	0.580	00010039152	0.00232299
2	57.293	0.162	1.493	0.565	0.005249289	0.00100012
3	56.978	0.078	1.434	0.440	0.004906856	0.00050457
4	53.887	0.045	1.343	0.319	0.004794476	0.00028639
5	42.791	0.030	1.150	0.216	0.005137362	0.00019377
6	0	0.021	0.989	0.151	1	-1

The relative wind speed can now be determined. Given the design wind speed at 16.8 m.s^{-1} , and the angular velocity at 336 rad.s^{-1} , and the radial distance, the axial and tangential induction factors defined for each blade element are used to compute the relative wind speed of the incoming flow as shown by Equation 3.15.

$$W = \sqrt{[(1 - a)V_1]^2 + [(1 + a')\omega r]^2} \dots\dots\dots (3.15)$$

$$= \sqrt{[(1 - 0.004906856)(16.8)]^2 + [(1 + 0.00050457)(336)(0.15)]^2}$$

$$= 53.124$$

The axial and tangential forces of the incoming flow on a blade element which essentially make up the lift and drag forces on the rotor blade, are calculated using Equation 3.16 and 3.17, respectively. Taking the air density as 1.2041 kg.m^{-3} , the blade element thickness as 0.05 m and other variables defined for each blade element, the axial and tangential force is calculated. Table 3.8 shows the computed axial and tangential force for each blade element.

$$dF_x = \left(\frac{1}{2}\rho W^2 c dr\right)C_x \dots\dots\dots(3.16)$$

$$= \left(\frac{1}{2}(1.2041)(53.124)^2(0.0246)(0.05)\right)(1.434)$$

$$= 2.999 \text{ N}$$

$$dF_y = \left(\frac{1}{2}\rho W^2 c dr\right)C_y \dots\dots\dots(3.17)$$

$$= \left(\frac{1}{2}(1.2041)(53.124)^2(0.0246)(0.05)\right)(0.440)$$

$$= 0.920 \text{ N}$$

Table 3.8 Relative wind speed, axial force, tangential force, torque and power output for each blade element.

Element no.	r (m)	W (m.s ⁻¹)	dF _x	dF _y	dT (= rdF _y)	dP (=ωdT)
1	0.05	23.668	2.052	0.469	0.023	7.878
2	0.1	37.557	2.151	0.814	0.081	27.366
3	0.15	53.124	2.999	0.920	0.138	46.392
4	0.2	69.267	3.695	0.878	0.176	59.033
5	0.25	85.663	3.931	0.738	0.184	61.955
6	0.3	0	0	0	0	0
Total			14.829	3.820	0.609	202.625

From the tangential force, the torque that is required to move the generator shaft is calculated using Equation 3.18 for each blade element. Then the power output is calculated from the angular velocity and torque for each blade element using Equation 3.19. The power harnessed by each blade was found to be 202.625 W, then the total power output of the wind turbine generator for the design of three blades at a fixed pitch angle of 7° was calculated and found to be 607.877 W. This power output is enough to run an evaporative cooler unit with 53 m^3 volume.

$$\begin{aligned}
dT &= r dFy & (3.18) \\
&= 0.15 (0.920) \\
&= 0.138 \text{ N.m}
\end{aligned}$$

$$\begin{aligned}
dP &= \omega dT & (3.19) \\
&= 336 (0.138) \\
&= 46.392 \text{ W}
\end{aligned}$$

$$\begin{aligned}
P &= \sum_{i=1}^N (dP)_i & \dots\dots\dots (3.20) \\
&= 202.625 \text{ W}
\end{aligned}$$

3.3 Modelling the Wind Turbine Blades using QBlade

For this wind turbine design, QBlade was used to model and simulate the design of the small wind turbine adopting the BEM theory. QBlade is a software specifically designed for modelling and analysing wind turbines. The initial proceeding in QBlade modelling includes the selection of the type of wind turbine, which in this case is a horizontal axis wind turbine (HAWT). Then, the blade airfoil section, which is the SG6043 airfoil design was selected and imported from the airfoil catalogue into QBlade. The SG6043 airfoil section is displayed in Figure 3.6.

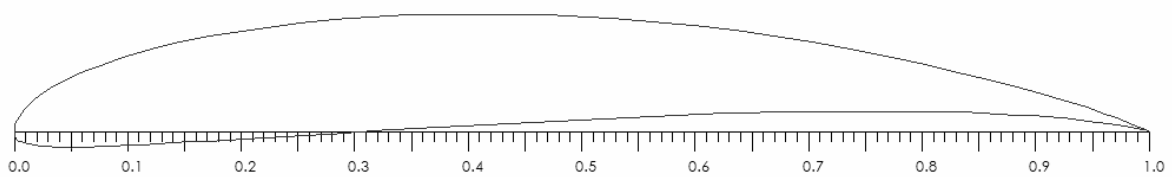


Figure 3.6 SG6043 airfoil section design created on QBlade

3.3.1 Modelling on QBlade

After choosing the type of wind turbine, the most important thing to do was to define the analysis. The Reynolds number was set to 200 000, and then the mach number and Ncrit value were set to 0 and 9, respectively. The Ncrit value was set to 9 to represent the wind tunnel experiments that make data validation possible. Then the mach number was set to zero since there is no need to compare the speed of wind to that of sound.

After defining the analysis, the 360° polar is created. On this setting, the Viterna model was selected which was used to extrapolate the 2D airfoil data and make it available for a wide range of angles of attack, rather than limited to the angle of attack which is less than 20°. Table 3.9 shows the HAWT blade design with a rotor made of three blades and a hub radius of 25 mm. The position measured in metres represents the radial distance from the hub to the blade element. In total, there are eight blade elements that make up the blade length. The chord lengths developed theoretical using the BEM method were used to generate the blade design along with a pitch angle of 7°. For the first 25 mm, the circular foil was used which is joined to the hub. The rest of the blade design is the SG6043 airfoil. Figure 3.7 shows the blade elements along the blade length, clearly displaying the blade design.

Table 3.9 Horizontal axis wind turbine blade design on QBlade

Element no.	Position (m)	Chord length (m)	Twist angle (°)	Foil	Polar
1	0.000	0.020	0	Circular foil	CD = 12 360 Polar
2	0.025	0.020	0	Circular foil	CD = 12 360 Polar
3	0.050	0.048	15.09	SG6043	T1_Re0.200_M0.00_N9.0 360V
4	0.100	0.034	5.28	SG6043	T1_Re0.200_M0.00_N9.0 360V
5	0.150	0.025	0.91	SG6043	T1_Re0.200_M0.00_N9.0 360V
6	0.200	0.019	-1.53	SG6043	T1_Re0.200_M0.00_N9.0 360V
7	0.250	0.015	-3.08	SG6043	T1_Re0.200_M0.00_N9.0 360V
8	0.300	0.013	-3.66	SG6043	T1_Re0.200_M0.00_N9.0 360V



Figure 3.7 Blade length design showing the airfoil section of each blade element

From all the preceding settings, the maximum lift-to-drag ratio was easy to acquire and read off the C_L/C_D plot generated by QBlade, as presented in Figure 3.8. The maximum C_L/C_D value was found to be 97.21 at the angle of attack of 5° , which was then used to optimise the blade design.

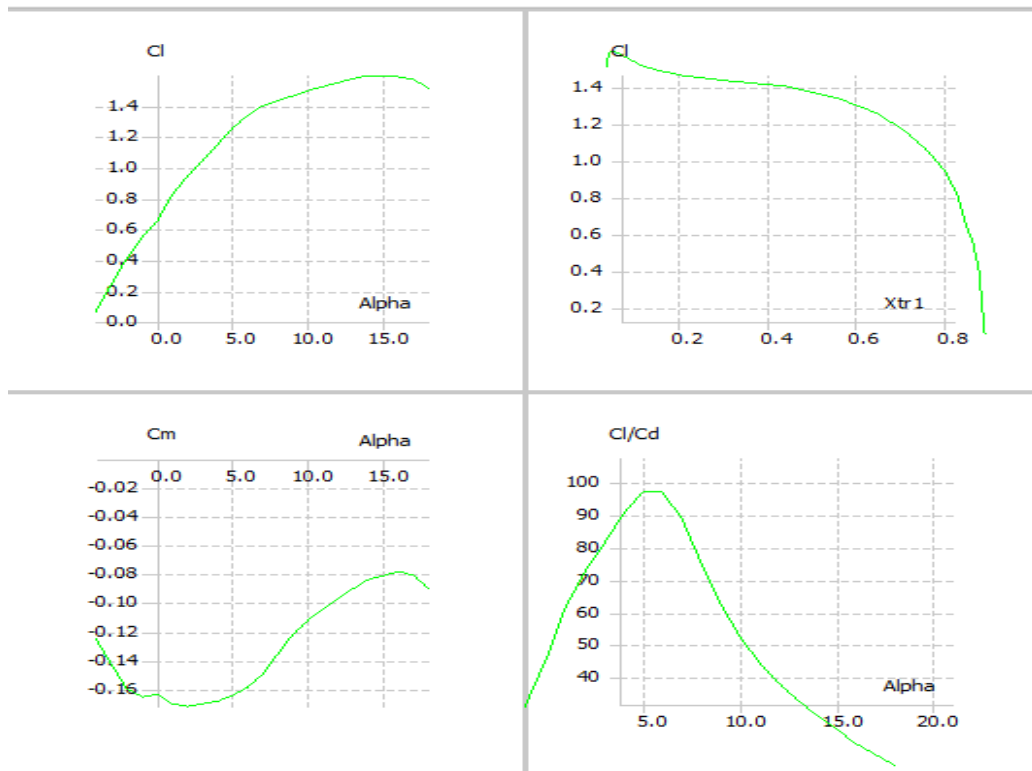


Figure 3.8 Lift coefficient, C_L and lift to drag ratio, C_L/C_D versus angle of attack, α curves

After defining the blade parameters, the HAWT blade geometry is optimised for the TSR of 6. QBlade then optimises the twist angle using the maximum lift-to-drag ratio found at the AOA equal to 5° . Then the chord length is optimised using the Betz limit. After modelling, the rotor simulation can then be performed, but first, the BEM parameters for the rotor simulation must be defined. The corrections considered for the blade design include the Prandtl tip loss, Prandtl root loss, 3D correction, Reynold drag correction and foil interpolation. The 3D correction is important for extrapolation since the SG6043 airfoil section is a 2D airfoil with a limited range of angle of attack operating in post-stall conditions taken from wind tunnel experiments. The air density, ρ was set to 1.2041 kg.m^{-3} while the viscosity was set to 0.00001647. The results

from the rotor simulation are presented and discussed in the next section. Figure 3.9 shows the rotor designed using QBlade.

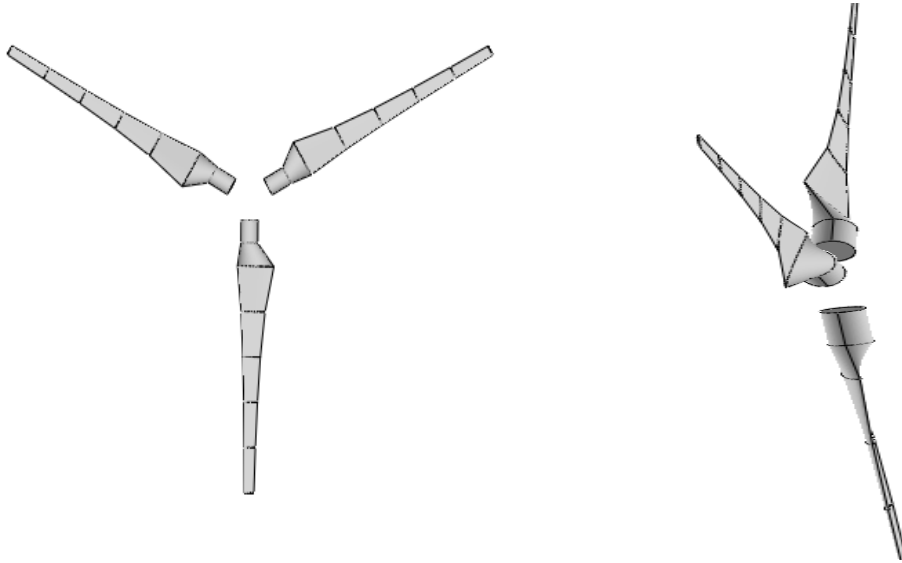


Figure 3.9 Rotor blade design on QBlade

3.3.2 Results and discussion

This sub-section discusses the results obtained from the modelling and simulation of the wind rotor performed on QBlade. It reviews the relationship between wind speed, rotor rotational speed, the power coefficient, and power output.

Figure 3.10 shows the power output estimated for each design wind speed using QBlade. The rotor simulation was done for the following design wind speeds including 12, 16.8, 19 and 25 m.s^{-1} . According to previous studies, the wind speed of 25 m.s^{-1} is the maximum value at which the wind turbine can operate without fail (Barroso Montes, 2011b; Salih *et al.*, 2012). Considering the outcomes expected from this study, the results from Figure 3.10 show that the required power output of 600 W is achieved at a design wind speed of 19.0 m.s^{-1} . This is greater than the design wind speed of 16.8 m.s^{-1} which was considered adequate during the power output computation using the BEM theory for the preliminary design. These results from QBlade modelling may imply that the BEM method overestimates the power output at a given design wind speed, although previous studies suggest that QBlade is a good modelling software.

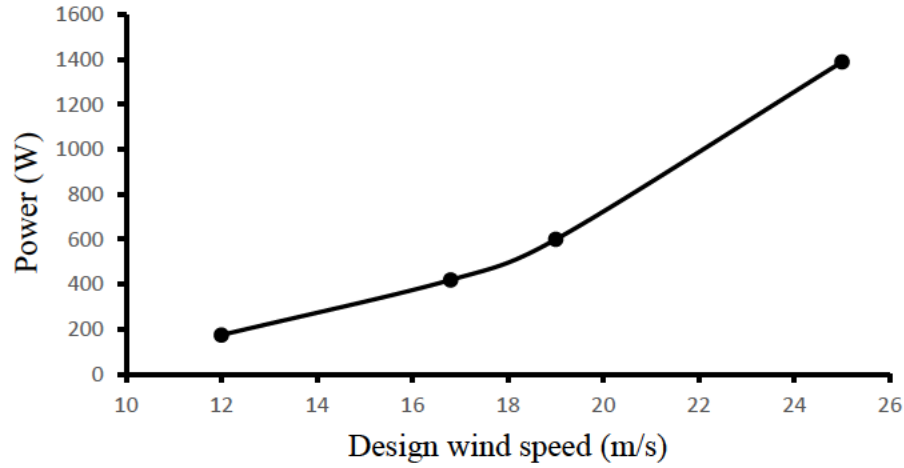


Figure 3.10 Power output versus design wind speed

As presented in Figure 3.11, the power coefficient was found at 0.44 for almost all the design wind speeds. The power coefficient of 0.44 is satisfactory because it does not exceed the Betz limit at the value of 0.593. It is within the typical power coefficient values achieved by small wind turbines from studies done by other researchers. Figure 3.12 displays that the desired power of 600 W is found around the rotor rotational speed of 3000-3300 rev.min^{-1} . These results match the calculation done using the BEM theory. Since the wind turbine rotor is directly coupled to the generator, this implies that the required design generator rotational speed is around 3000 rev.min^{-1} .

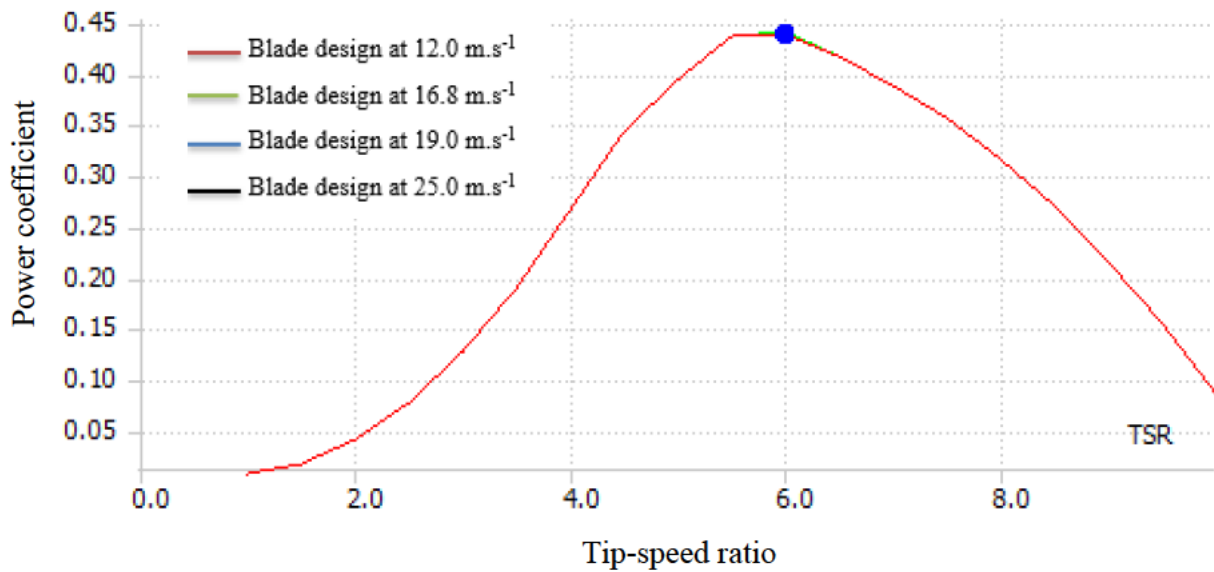


Figure 3.11 Power coefficient, C_p variation with TSR for different wind speeds

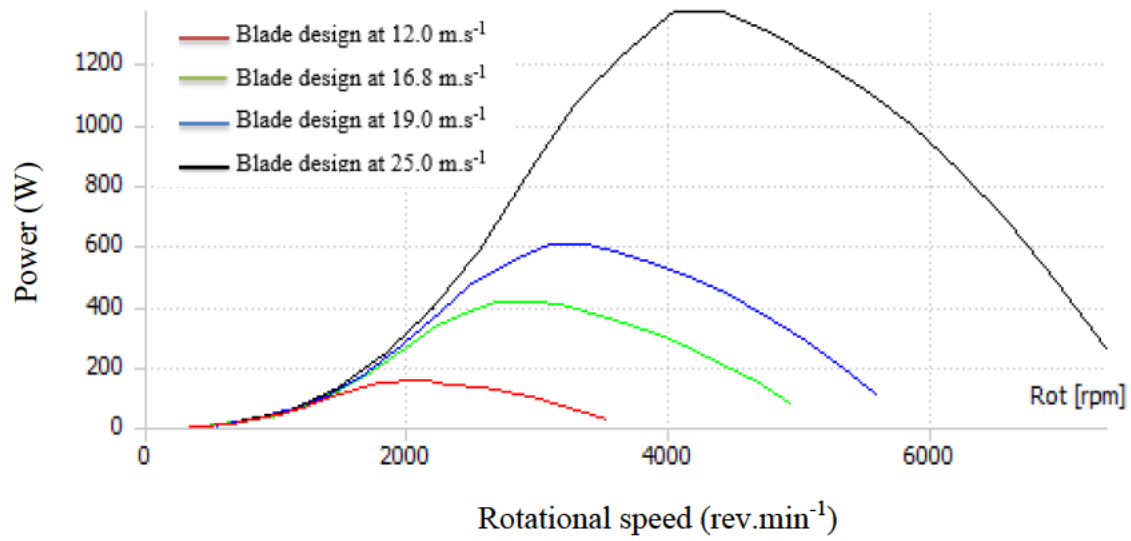


Figure 3.12 Mechanical power output variation with rotor rotational speed for different wind speeds

3.4 Modelling the Wind Turbine using MATLAB Simulink

Table 3.10 Input parameters for modelling the wind turbine on MATLAB Simulink

Input parameters	Units
Rotor diameter (m)	0.6
Initial design wind speed (m.s^{-1})	16.8
Air density (kg.m^{-3})	1.2041
ECS Load (Ω)	0.273

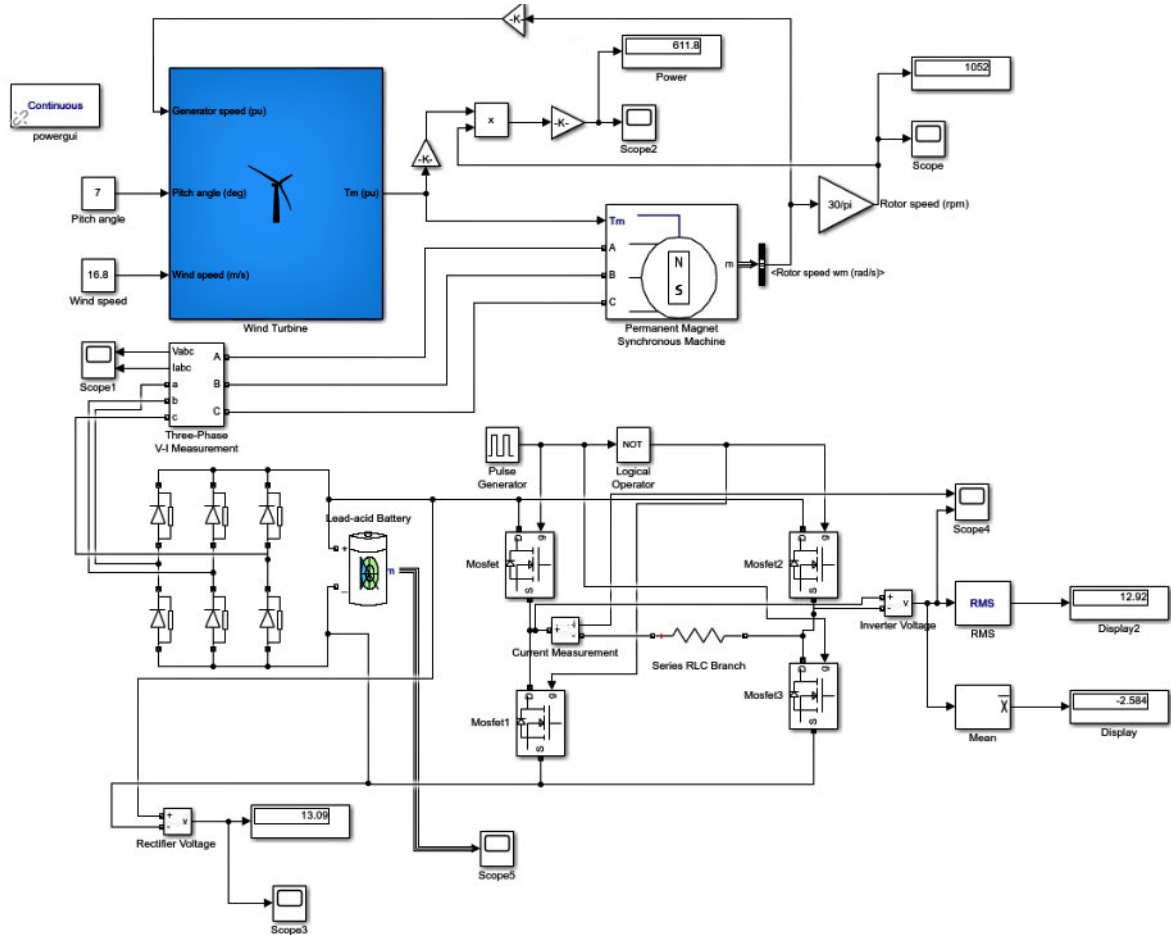


Figure 3.13 Modelling of the wind turbine using MATLAB Simulink

Figure 3.13 shows the wind turbine conversion system modelled using MATLAB Simulink. The main components of the model are the wind turbine, permanent magnet synchronous generator, rectifier, battery and inverter. The built-in wind turbine block accepts the pitch angle, wind speed and generator speed in per unit (pu) of the base wind speed as input parameters. Then the output is the torque in pu, which is fed into the permanent magnet synchronous machine/generator (PMSG). The wind turbine is a small horizontal axis wind turbine which is stall-regulated with a fixed pitch angle of 7° . The electric power output of the PMSG is set to be the rotational speed which is fed back or used as an input on the wind turbine block since the wind turbine rotor, and PMSG are directly coupled, meaning they move at relatively the same rotational speed. The base rotational speed in pu is 1.2, while the base wind speed is set at 12 m.s^{-1} . A three-phase measurement block is used to measure the current and voltage flowing from the PMSG into the three-phase rectifier system which converts AC power output into DC power output which is then stored into a battery and used by the ECS unit. From Figure 3.13, it can be seen that the rectifier is made up of the three pairs of diodes connected in series

for the three-phase power supply and has an inductance that smoothes out the rapidly pulsating voltage and current measurements for DC power storage. The overall input parameters include the generator speed, pitch angle and wind speed. Then, the output parameter is the electric power, rotational speed, current and voltage. Table 3.11 shows the electrical generator specification while Table 3.12 shows the input parameters in the MATLAB Simulink built-in wind turbine model.

Table 3.11 Electrical generator specifications

Parameter	Units	Value
Rated power	600	W
Max power	636	W
Rated rotational speed	600	rev.min ⁻¹
Rated voltage	12	V
Output current	AC	-
Generator type	Three-phase permanent magnet synchronous	-
Efficiency	>75	%
Service life	More than 20 years	-

Table 3.12 Input parameters in MATLAB Simulink wind turbine model

Input parameter	Value	Unit
Mechanical power	600	W
Wind speed	16.8	m.s ⁻¹
Pitch angle	7	°

3.4.1 Results and discussion

Figure 3.14 shows the wind turbine power characteristic curve obtained from modelling the wind turbine block at a pitch angle of 7° on MATLAB Simulink. This curve shows the power output of the wind turbine that is produced at different wind speeds which is in pu of the nominal mechanical power of 600 W, while the turbine speed is in pu of the nominal generator speed. A power output of 611.8 W was produced using the model on MATLAB Simulink, as can be seen in Figure 3.13. The power output of 611.8 W was obtained at a design wind speed

of 16.8 m.s^{-1} and a pitch angle of 7° . These findings are comparable to the study done by Noronha and Krishna (2020) who used QBlade to model a 3 m diameter wind turbine and obtained a power output of 300 W at a wind speed of 5 m.s^{-1} .

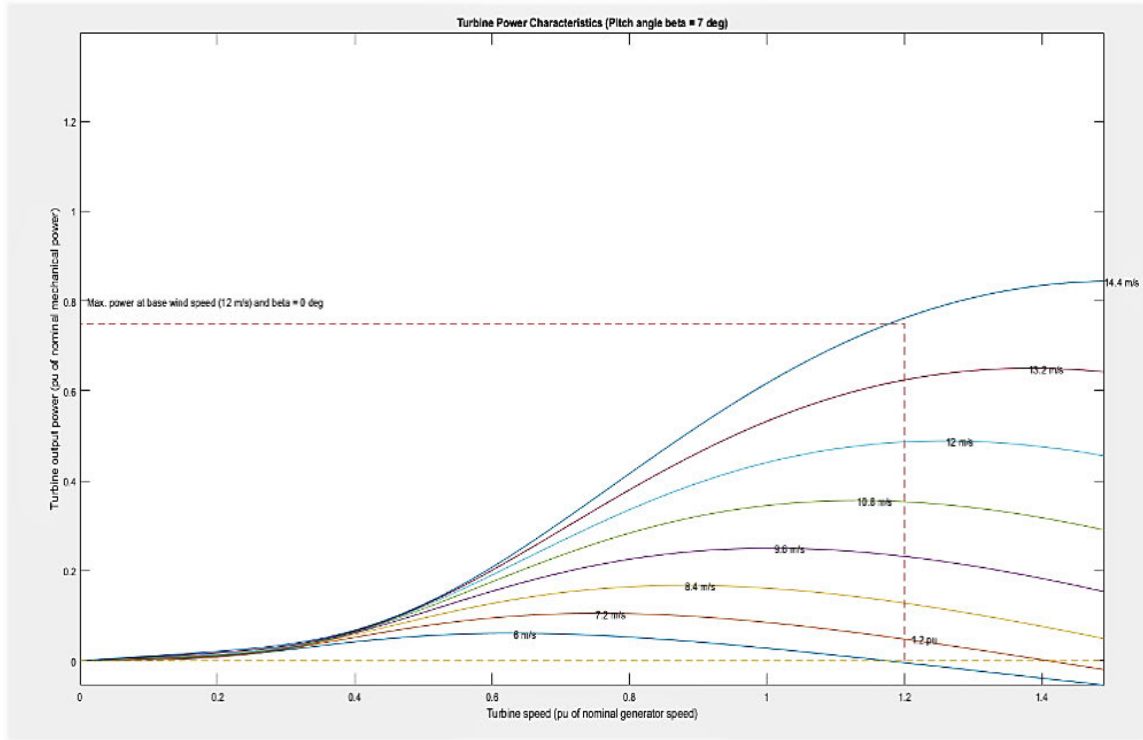


Figure 3.14 Wind turbine power characteristic curve (pitch angle = 7°)

From the simulation, both the rectifier and battery have a voltage which ranges between 13.0903 - 13.0913 V. This finding indicates that there is no known voltage losses occurring between the rectifier and the battery. While the rectifier and battery rating is 13.09 V, voltage losses occur after passing the three-phase power inverter, and the voltage is reduced to 12.92 V. This indicates that the voltage is lost (0.17 V) as it moves through electrical wires and the inverter with possibly additional losses from the PMSG. The recommendation is to make the wires as short as possible to reduce any voltage loss and provide the load with the required voltage

3.5 Conclusion

This study aimed to design, model and simulate the components of a 600 mm diameter small wind turbine using the BEM theory, QBlade, and MATLAB Simulink. The BEM theory was

mainly used to determine the chord lengths of the entire blade and determine the required rotational speed to meet the power requirement of 600 W. QBlade software was used to optimise the blade design by modelling the optimum wind speed, rotor rotational speed, and twist angle at which the power output of 600 W is obtained. The power coefficient was also observed with maximum power coefficient of 0.44. The QBlade model indicated a slightly higher wind speed of 19.0 m.s^{-1} compared to the initial design wind speed of 16.8 m.s^{-1} used for the BEM theory. Both the BEM theory and QBlade model indicated that a rotational speed of $3200 \text{ rev.min}^{-1}$ was required to get 600 W. A $3200 \text{ rev.min}^{-1}$, 600 W PMSG is not available on the market, therefore a trade-off for a 600 rev.min^{-1} , 600 W PMSG is made. Therefore, a 600 rev.min^{-1} , 600W permanent magnet synchronous generator can be used for the wind turbine prototype instead of a generator with $3200 \text{ rev.min}^{-1}$ rotational speed. MATLAB Simulink modelled and simulated the electrical components more accurate and indicated voltage losses along the energy conversion system which are not identified on QBlade but are evident through the high design speed which is needed to produce 600 W compared to the initial design wind speed of 16.8 m.s^{-1} . It is recommended to use the findings obtained for the chord lengths, twist angle and design wind speed to create a blade design and consequently develop a physical prototype of the wind turbine used to power any mobile cooling technology according to the power requirement.

3.6 References

- Alaskari, M, Abdullah, O and Majeed, MH.2019. Analysis of wind turbine using QBlade software. IOP conference series: materials science and engineering, 032020. IOP Publishing.
- Barroso Montes, M. 2011. Optimal control of wind turbines in strong wind conditions. Unpublished thesis, Mechanical Engineering, Technical University of Denmark, Kongens Lyngby, Denmark.
- Bracco, G and Razzetti, D. 2022. Aerodynamic design of a micro wind turbine and performance analysis with QBlade. Unpublished thesis, Mechanical Engineering, Polytechnic University of Turin, Turin, Italy.
- Cole, S. 2022. Wind turbine power curve. [Internet]. TheRoundup.org. Available from: <https://theroundup.org/wind-turbine-power-curve/>. [Accessed: 5/12/2022].

- Hassanzadeh, A, Hassanabad, AH and Dadvand, A. 2016. Aerodynamic shape optimization and analysis of small wind turbine blades employing the Viterna approach for post-stall region. *Alexandria Engineering Journal* 55 (3): 2035-2043.
- Koç, E, Günel, O and Yavuz, T. 2016. Comparison of Qblade and CFD results for small-scaled horizontal axis wind turbine analysis. 2016 IEEE International Conference on Renewable Energy Research and Applications (ICRERA), 204-209. IEEE.
- Noronha, NP and Krishna, M. 2020. Design and analysis of micro horizontal axis wind turbine using MATLAB and QBlade. *International Journal of Advanced Science and Technology* 9 (10S): 8877-8885.
- Quintal-Palomo, R and Dybkowski, M. 2019. Modelling and co-simulation of small wind turbine with permanent magnet synchronous generator. *Przegląd Elektrotechniczny* 1 (10): 210-215.
- Salih, SM, Taha, MQ and Alawsaj, MK. 2012. Performance analysis of wind turbine systems under different parameters effect. *International Journal of Energy and Environment* 3 (6): 895-904.
- Suresh, A and Rajakumar, S. 2020. Design of small horizontal axis wind turbine for low wind speed rural applications. *Materials Today: Proceedings* 23 16-22.

4. DEVELOPMENT AND EVALUATION OF A PORTABLE SMALL WIND TURBINE

Abstract

This study aimed to develop and evaluate the performance of a portable, low-cost small wind turbine prototype with a 600 W permanent magnet synchronous generator (PMSG) designed to power a mobile cooling technology (evaporative cooler unit). The performance of the wind turbine was analysed through the power output and power coefficient it can attain as influenced by the vehicle speed and louvre opening level. The 600 mm rotor diameter wind turbine is made of three PVC pipe material blades connected by a 60 mm \varnothing mild steel plate hub, and protected by a 800 x 800 x 500 mm mild steel protective casing. The treatment of the study are the three vehicle speeds which were set to 60, 80, and 100 km.h⁻¹, and the two opening levels, level 1 at 45° and level 2 at 80° relative to the louvre mechanism frame. The data was analysed using Genstat 18.2.1 software for three replications which were collected over three weeks. The results showed that the power output is significantly influenced ($p < 0.001$) by both the vehicle speed and louvre opening level. The power output of 113.4, 159.6 and 210.0 W per hour was observed for vehicle speed of 60, 80 and 100 km.h⁻¹, respectively, for louvre opening level 1. However, the power output of 142.8, 268.8 and 294.0 W per hour was observed for a wind speed of 60, 80, and 100 km.h⁻¹, respectively on louvre opening level 2. This shows that higher wind speeds (vehicle speeds) obtain higher power output which account for the small size of the wind turbine rotor. With the assistance of a 600 W, 230 VAC power inverter, this wind turbine is fully capable and sufficient to support a 600 W load (ECS unit). The maximum power coefficient obtained for this study was 0.49. The wind speed data obtained from direct measurement using the anemometer matched with the theoretical wind speed obtained using the apparent wind speed equation. It is recommended to integrate this small wind turbine into an evaporative cooler unit with a power requirement of 600 W to confirm the functionality of the entire system together.

4.1 Introduction

It has been identified that smallholder farmers are still experiencing trouble when it comes to affordable mobile cooling technologies or reefer units (Elik *et al.*, 2019). This is because they

require high energy input for the transportation of fresh produce to the distribution or final selling point which increases the general transport costs (Van Duin *et al.*, 2018; Telle *et al.*, 2022). Though an efficient mobile cooling technology like the refrigerator exist, it is almost out of reach by smallholder farmers who mostly stay in rural remote areas or areas far away from where they can access this type of technology for hire (Louw and Jordaan, 2016; Elik *et al.*, 2019). For mobile cooling technologies, wind energy is one of the viable options for energy generation and power supply since there is an abundance of high wind speed created while the vehicle is in motion (Hossain, 2020a). Generally, because wind turbines have large rotor areas and a gearbox, they can accept and operate with low wind speeds (Ozgener, 2006; Muhsen *et al.*, 2019). In this case where there is limited space that the wind turbine can occupy on the vehicle, the rotor size is also limited, therefore the wind speed has to be optimised as much as possible to obtain the required power output.

Second to solar energy, wind energy is the fastest growing renewable energy (Akbari *et al.*, 2022). This is because it is a free, and abundant energy source with reasonable investment costs (Hirahara *et al.*, 2005). Small wind turbines generate electricity from the wind energy. Small wind turbines are turbines that produce less than 50 kW associated with a rotor diameter of 8 m (Wood, 2011; Evans *et al.*, 2018). The wind turbine captures the wind energy using the rotor blades (Shoaib *et al.*, 2019). The rotation of the rotor causes the mechanical movement of the generator shaft which feeds the electrical generator and produces electrical energy (Chong *et al.*, 2021). The electrical generator outputs AC power which is converted into DC power by the rectifier to be kept in a battery storage (Shoaib *et al.*, 2019). An inverter is then used to change the DC power to AC power (Chong *et al.*, 2021).

The material used to make the blades is important because it affects the power output (Garmode *et al.*, 2022). Ideal materials for wind turbine blades are lightweight, heat resistant and have high tensile strength. Usually, glass and carbon fibre materials are used to make the rotor blades, but these are expensive and raises the selling price of a wind turbine in addition to the electrical generator costs (Garmode *et al.*, 2022). In an attempt to lower the costs of the wind turbine, an alternative was sought, and a PVC pipe material solution was found. Common PVC pipe used for water circulation can be cut and used for wind turbine blades (Wahyudi *et al.*, 2022). PVC pipe material is a relatively cheap, lightweight and durable material to use for small wind turbines even though its performance is less than that of conventional blade materials such as epoxy, polyester, carbon and glass fibre reinforced polymer (Ceruti, 2019;

Garmode *et al.*, 2022). Recent studies have shifted the focus of electrical generators from fixed wind speed generators to variable wind speed generators (Chong *et al.*, 2021; Bracco and Razzetti, 2022). This is favourable since the wind speed in the atmosphere varies greatly and the power can be harnessed from different wind speed, meaning there will be continuous power supply.

The doubly-fed induction generator (DFIG) and permanent magnet synchronous generator (PMSG) are both variable wind speed electrical generators (Saidi *et al.*, 2018; Chong *et al.*, 2021). Unlike the DFIG, the PMSG is a direct drive generator, which eliminates the need of a gearbox for small wind turbines (Zhang *et al.*, 2021). The PMSG outputs three-phase alternating current (Zhang *et al.*, 2021). Literature shows little to no evidence of small wind turbines being used to harvest wind energy to power mobile cooling technologies while in transit. Even though research on small wind turbines being implemented on small vehicles to replace combustion engines is starting to gain momentum, no research can be found on cooling technologies using wind turbines.

An evaporative cooler unit is available at Ukulinga Research farm that can be converted into a mobile cooling unit. The small wind turbine is to be integrated into it and assessed whether it can provide the electric energy input required. Sibanda and Workneh (2020a), designed and developed this affordable evaporative cooler for smallholder farmers. This unit requires less energy input than the one required by refrigerated units, which is used only to power the water pump, suction fan and lights, consuming approximately less than 600 W of energy per hour excluding the heat exchanger. It also has relatively low initial capital investment than other cooling technologies. This chapter discusses the airflow control and the methodology used in the design of the HAWT. It also includes a detailed description of the wind turbine design, the experimental tests and the discussion of the findings.

4.2 Material and Methods

This section details the design and development of the small wind turbine used to supply electric power to a mobile evaporative cooling system unit for the storage fruit and vegetables along the supply chain.

4.2.1 Study site and climatic data

The study was conducted at Ukulinga Research farm at the University of KwaZulu-Natal (UKZN), Pietermaritzburg (PMB), KwaZulu-Natal, South Africa ($-29^{\circ}63'S$ and $30^{\circ}40'E$ at an altitude of 673 m above sea level). PMB is a town characterised by dry and sub-humid conditions at 52% relative humidity, an ultraviolet index of 5, an average temperature of $26^{\circ}C$ in January, $19^{\circ}C$ in June, and 33 mm of rain in a year. Pietermaritzburg has a minimum wind speed of $0.30\text{ km}\cdot\text{h}^{-1}$ in the month of April, a maximum wind speed of $26.60\text{ km}\cdot\text{h}^{-1}$ in the month of October and an average wind speed of $8.12\text{ km}\cdot\text{h}^{-1}$ throughout the year. The wind turbine experimentation was conducted at Ukulinga research farm and on the road between Pietermaritzburg and Estcourt with the wind turbine mounted on a bakkie travelling at car speed ranging between $60\text{--}100\text{ km}\cdot\text{h}^{-1}$. The part of the experiment performed on the road entails the small wind turbine being mounted on the bakkie top to test the real-time power output of the wind turbine.

4.2.2 Design considerations and specifications

This sub-section lists the design considerations which are looked at to ensure an efficient and functional design, as well as the design specifications that must be followed when designing the structure of the wind turbine. The design considerations are as follows:

- (a) The wind turbine must be able to continuously power the EC unit throughout the journey,
- (b) The design must be of low-cost and affordable for smallholder farmers,
- (c) The blade material should be lightweight and have high strength to withstand extreme wind loads conditions,
- (d) The wind turbine must be able to work with variable wind speeds,
- (e) The structure should have a safety protective casing for animals' safety,
- (f) The structure must also have a wind speed control mechanism to lower the extreme wind speeds experienced on the road,
- (g) The material must be non-corrosive and heat resistant, and
- (h) The wind turbine should be zero to minimum maintenance.

Then, the design specifications include that:

- (a) The power coefficient must be 0.40,
- (b) The rotor diameter must be less than 0.6 m,

- (c) The cut-in wind speed must be around 3 m.s^{-1} ,
- (d) The rated wind speed must be between $10 - 15 \text{ m.s}^{-1}$, and
- (e) The cut-out wind speed must be around 30 m.s^{-1} .

4.2.3 Description of the wind turbine

The small wind turbine design consists of an outer protective casing, a movable louvre mechanism, a rotor, a supporting tower, a permanent magnet synchronous generator, a bridge-rectifier, a power inverter and the lead-acid battery. Figure 4.1 shows the overall and annotated design of the wind turbine. The yaw or furling mechanism is excluded in this wind turbine design since the airflow for a moving vehicle travels in one direction. The front, right, top and isometric view of the wind turbine design is shown on Figure 4.2. The protective casing is a $800 \times 800 \times 500 \text{ mm}$ square angle steel box with an opening at the back for free airflow and an adjustable pine wood louvre mechanism for airflow control at the front to reduce incoming wind speed as required. The louvre mechanism is presented in Figure 4.3. A three layer varnish coating was used to protect the wood against swelling.

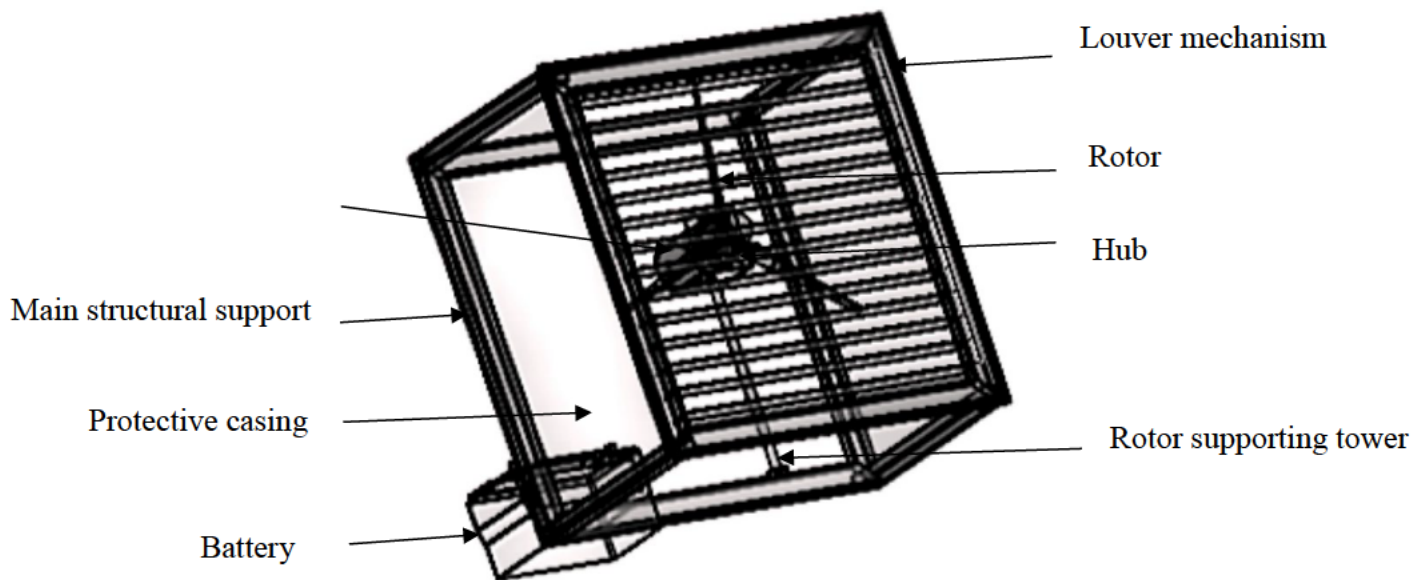


Figure 4.1 Annotated small wind turbine design

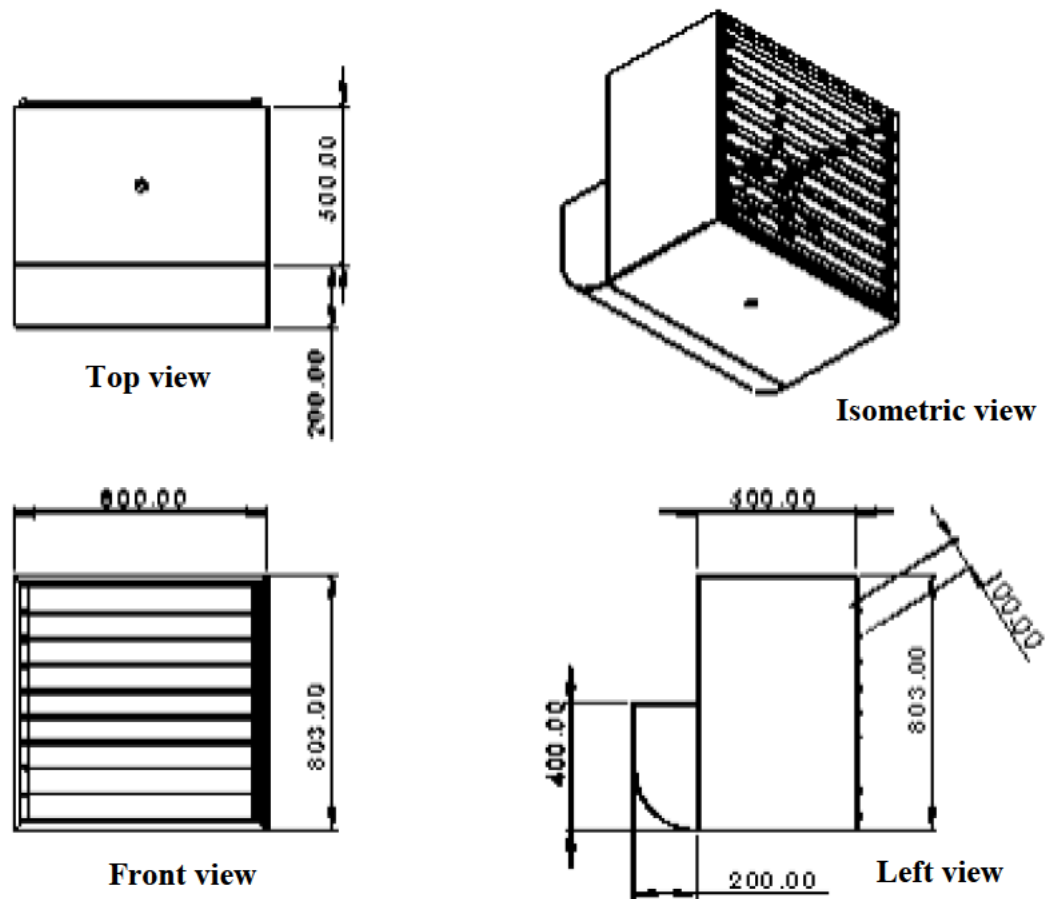


Figure 4.2 Top, front, left, and isometric view of the wind turbine design



Figure 4.3 Louver mechanism to control airflow into the wind turbine.

The wind turbine design is a 600 mm rotor with three 0.3 m long blades made of PVC pipe material connected by a 15 x 50 mm steel metal both welded and bolted to a 60 mm diameter circular steel metal. The ideal PVC blades used were heated, flattened, and shaped on one side

at an angle of 7° to be receptive to the incoming wind. Table 4.1 shows the chord lengths for each section of the PVC pipe blades. These blades are lightweight, have high strength and can withstand heat deformation on its own but it is also well protected by the protective outer structure. The rotor is then coupled directly to the PMSG via a small stainless-steel shaft of the electric generator. The wind blows on the louvre mechanism, which can control the wind speed to a tolerable wind speed range of choice. The louvre mechanism has two opening levels. Opening level 1 and 2 have their slats positioned at 45° and 80° angles, respectively, relative to the main support of the louvre mechanism. When the wind hits the rotor, it causes the mechanical rotation of the blades and, consequently, the coupled generator shaft. Figure 4.4 shows the wind turbine rotor and hub design. The PMSG then converts the mechanical energy into a three-phase alternating current (AC) electrical power. The three-phase AC power is then converted into a single-phase direct current (DC) power through the bridge-rectifier. This power is stored and used via the battery. The power inverter is used to convert DC to AC power after the battery and most importantly step up the voltage from 12 V TO 230 V that can be utilised by ECS unit. The rectifier and power inverter are connected via the battery terminals. A 12 V 105 Ah lead-acid battery is used to store and supply power for the evaporative cooler unit. This battery size can store and supply twice as much electrical power as needed by the ECS unit and, therefore, can cover two-hours travel even with setbacks along the trip. Figure 4.5 shows the overall wind energy conversion system of the small wind turbine from the wind to electrical energy. Figure 4.6 and 4.7 show the design of a portable evaporative cooler unit powered by a small wind turbine that can be loaded on the back of a bakkie or made into a trailer.

Table 4.1 Chord length for different sections of the PVC pipe blade length

Section no.	r (m)	c (m)
1	0.05	0.1440
2	0.1	0.1017
3	0.15	0.0738
4	0.2	0.0573
5	0.25	0.0465
6	0.275	0.0390

$$P = V \times I. \quad (3.1)$$

$$1200 = 12 \times I$$

$$I = \frac{1200}{12}$$

$$I = 100 \text{ Ah}$$

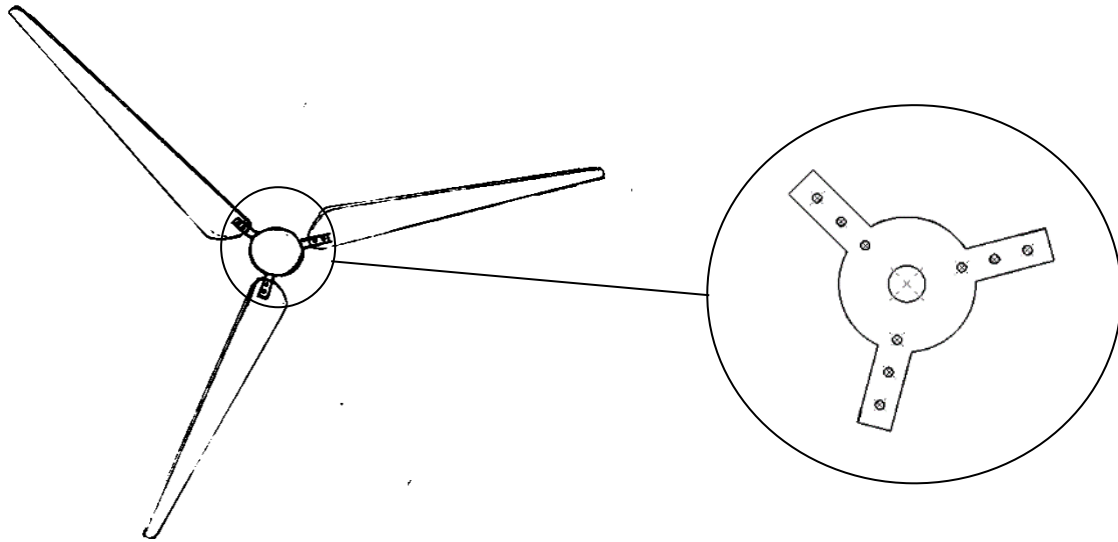


Figure 4.4 Wind turbine blades made of PVC material with magnified hub design

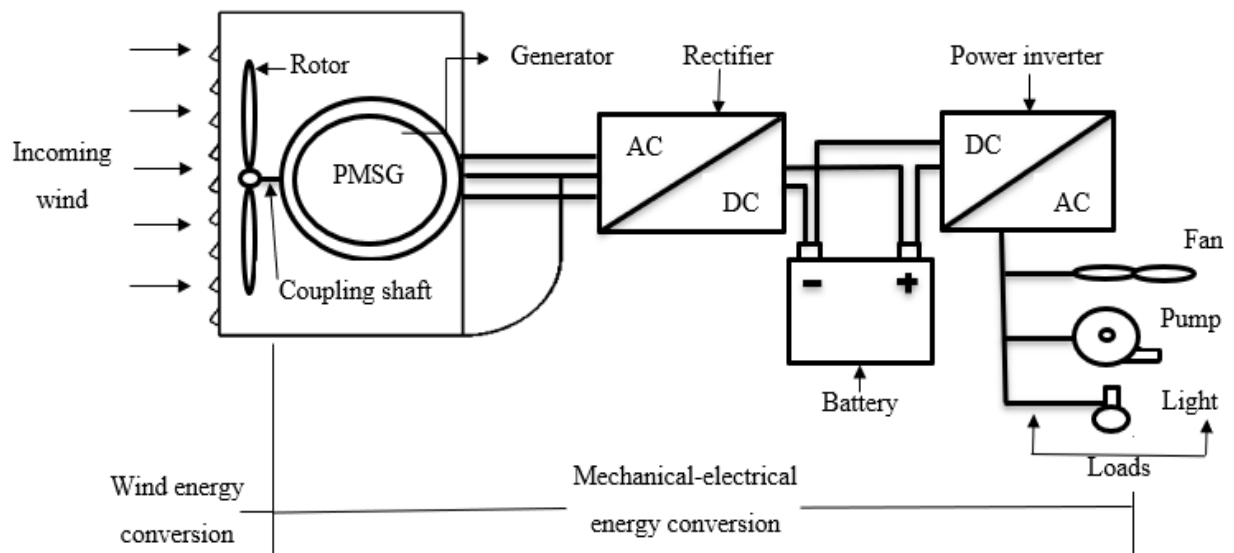


Figure 4.5 Energy conversion system of the small wind turbine

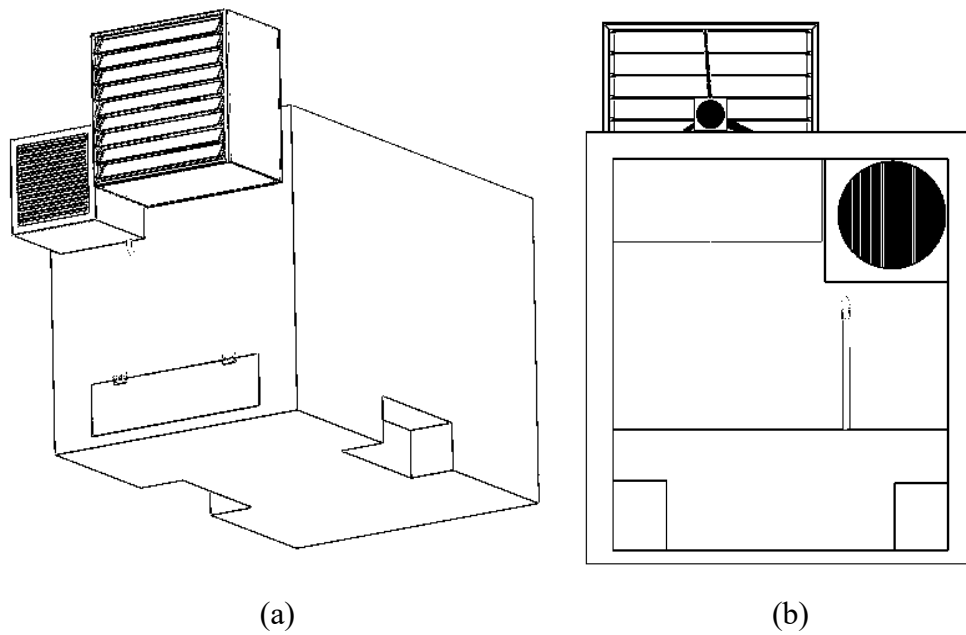


Figure 4.6 (a) Isometric view and (b) inside of a designed portable evaporative cooler unit powered by a small wind turbine

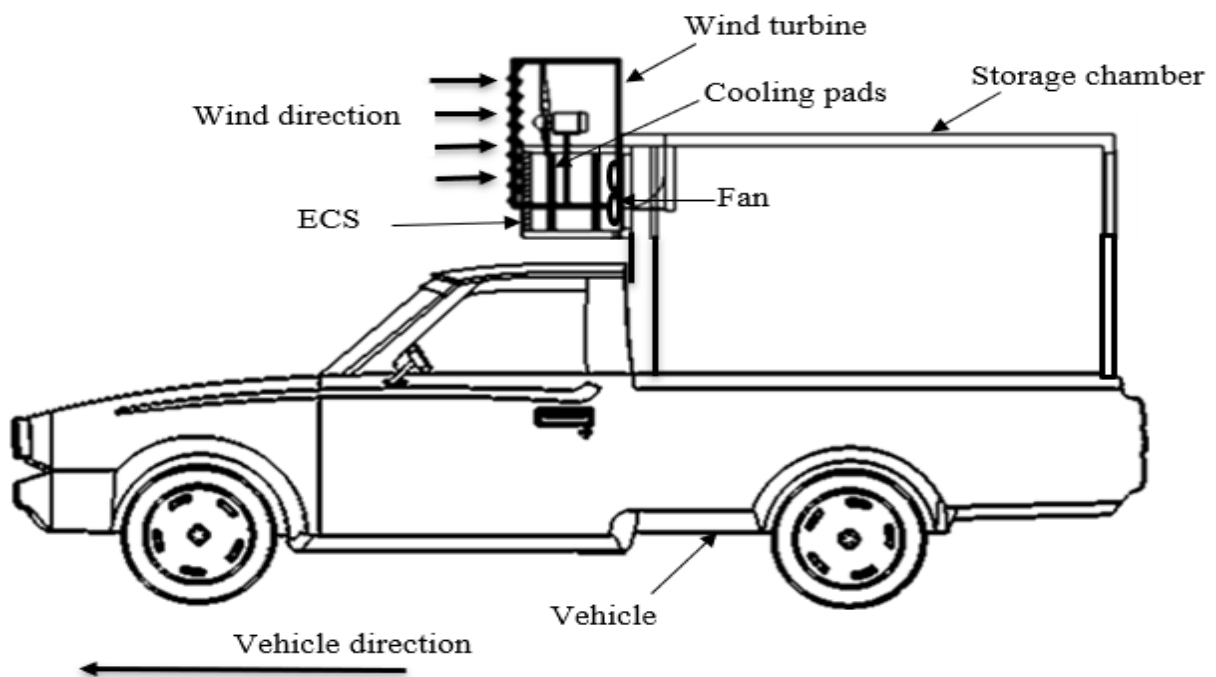


Figure 4.7 Side view of an ECS unit powered by a wind turbine mounted on a bakkie

4.2.4 Wind turbine experimental design

The wind turbine experimental design had two treatments, the opening level of the louvre mechanism and the vehicle travelling speed as shown in Figure 4.8. The purpose of this design

was to explore and investigate which opening level and wind speed achieves the optimum and maximum power supply required by the system. This is because the incoming wind speed on the road may be relatively too high for the operation of the rotor and may need to be reduced for the optimum wind speed range. The testing was done for three weeks with three replications. For testing purposes, the wind turbine was mounted on the vehicle through a steel support stand as shown in Figure 4.9.

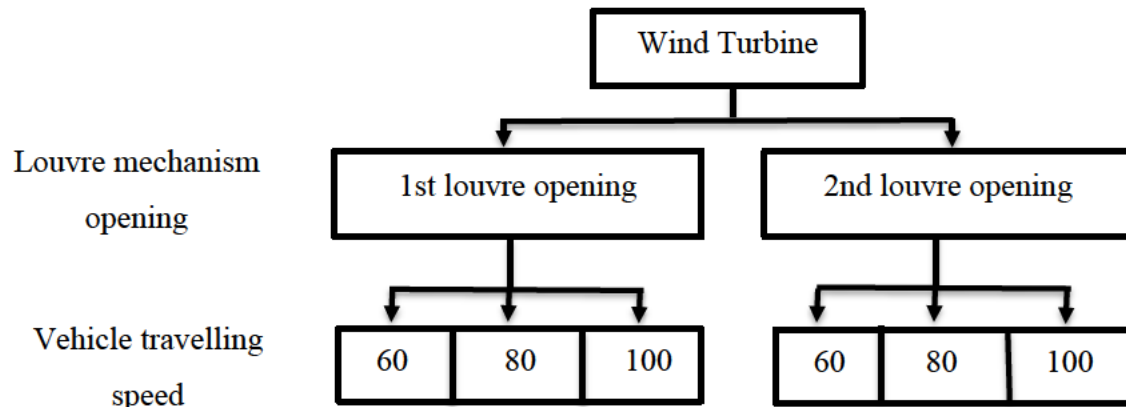
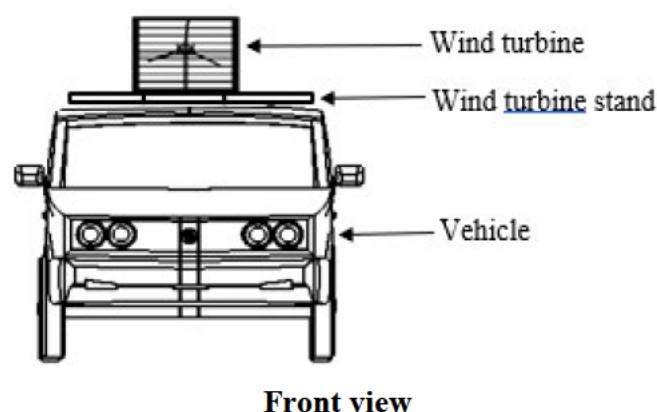
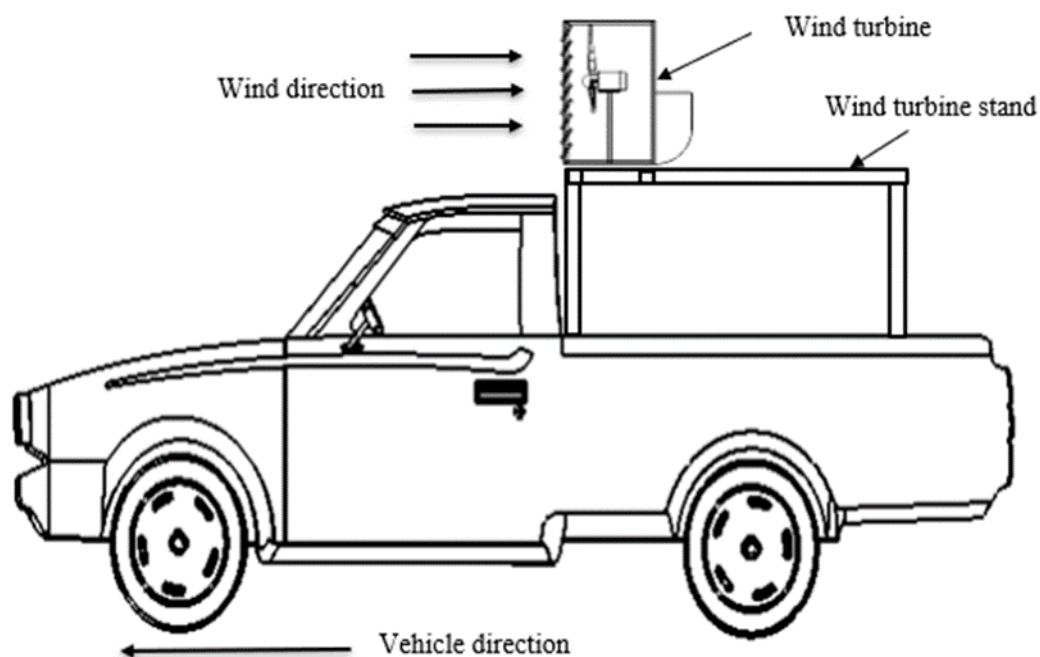


Figure 4.8 Experimental design to determine the accumulated power output of a wind turbine

The independent variable in the design is wind speed, and the dependent variable is the power output. The pitch angle, rotor diameter, air density and TSR are the fixed variables. The power coefficient and power output from the wind turbine will be used to assess the performance of the wind turbine. Figure 4.9 shows the small wind turbine prototype mounted on a bakkie for testing purposes. Tables 4.2, 4.3 and 4.4 show the generator specifications, the rotor specifications, and the technical specifications of the wind turbine.





Side view

Figure 4.9 Small wind turbine prototype mounted on a bakkie

Table 4.2 Generator specifications

Parameter	Value	Units
Rated power (W)	600 W	W
Max power (W)	636 W	W
Rated voltage	12	V
Rated current	AC	-
Rated rotational speed (rpm)	600	rev.min ⁻¹
Top net weight	9.0	Kg
Generator type	Three-phase permanent magnet synchronous generator	-
Shaft material	Stainless steel	-
Shell material	Cast iron	-
Protective grade	IP54	-
Working temperature	-40 – 80	°C

Table 4.3 Rotor specifications

Parameter	Value	Units
Rotor diameter	0.6	M

Rotor radius	0.275	M
Hub	60	M
Pitch angle	7	°
Design wind speed	16.8	m.s ⁻¹
Tip speed ratio (TSR)	6	-

Table 4.4 Technical specification of the turbine

Parameter	Value	Units
Nominal power output	600	W
Start-up wind speed	4	m.s ⁻¹
Rated wind speed	17.5	m.s ⁻¹
Survival wind speed	33	m.s ⁻¹
Rotor diameter	0.6	m
Rotor rotational speed	600	rev.min ⁻¹
No. of blades	3	-
Generator type	3-phase permanent magnet synchronous generator	
Transmission	Gearless direct drive	
Output type	230 VAC	V

4.2.5 Determination of the power output

A multi-meter was used to measure the DC voltage and current of the wind turbine through the battery. The power output is then determined through the voltage and charge capacity of the lead acid battery as shown in Equation 4.1.

$$P_A = CC \times E \quad (4.2)$$

where

P_A = Accumulated/ aerodynamic power (Wh),

CC = Capacity charge (%), and

E = Electrical energy of the battery (Wh).

4.2.6 Determination of the power coefficient

The power coefficient is determined from the accumulated power obtained from the wind turbine testing. The mechanical/rated power output of the wind turbine and the power coefficient are used to assess the performance of the wind turbine as shown in Equation 4.2.

$$C_p = \frac{P_A}{P_T} \quad (4.3)$$

where

C_p = Power coefficient,

P_A = Accumulated/ aerodynamic power (Wh), and

P_T = Total power rating of the wind turbine (Wh).

4.3 Data Collection and Analysis

The wind speed data was collected using an anemometer while the DC voltage was measured through the battery after the rectifier. Genstat software was used for the statistical analysis of the data with a 95% confidence level. The graphs used to analyse the results were generated by Microsoft Office Excel spreadsheet (2016). The data collected include the wind speed at different louvre opening levels and the voltage generated by the wind turbine on the battery. The voltage was then used to calculate the power generated by the wind turbine through capacity charge estimation. The testing was done for three weeks with three replications.

4.4 Results and Discussion

This sub-section discusses the findings of the apparent wind speed testing along with the power output and power coefficient of wind turbine prototype.

4.4.1 Relationship between vehicle speed and incoming wind speed

This sub-section discusses the initial wind speed data collection and verification of the incoming wind speed through direct measurement and theory-based equations for determining the wind speed fed into the wind turbine rotor swept area. In this study the incoming wind speed is sometimes referred to as the apparent or undisturbed wind speed.

4.4.1.1 Direct wind speed measurement

The wind speed data was recorded for the incoming airflow on the road at three different travelling vehicle speeds which are 60, 80 and 100 m.s⁻¹. This wind speed serves as the undisturbed wind speed from which the wind energy is harnessed. The wind speed data is presented in Table 4.5. The wind speed varies along the road for a constant travelling speed, therefore, a range of values is presented instead of a single value for each vehicle travelling speed. The apparent wind speed ranges between 12 – 14 m.s⁻¹ for a vehicle speed of 60 km.h⁻¹, 18 – 27 m.s⁻¹ for a vehicle speed of 80 km.h⁻¹ and 24 – 29 m.s⁻¹ for a vehicle speed of 100 km.h⁻¹. This shows that the apparent wind speed is directly and closely related to the vehicle travelling speed. This may be due to wind fluctuations associated with the change in topography and terrain which act as obstructions along the road. A downward slope will cause an increase in airflow downhill, while going uphill will reduce the airflow. The airflow is high in low-lying terrains and elevated regions while it is low in high-rising terrains and depressed regions. The wind speed data collection was performed in Pietermaritzburg which is an in-land region of the province, thus if the data is collected in coastal areas it is inclined to record high wind speeds as the wind speed for that region is already high. As a result of the high wind speed that can be experienced by a travelling vehicle, a need for a mechanism to control the airflow is realised which is because a wind turbine generally has a cut-out wind speed of 25 m.s⁻¹

Table 4.5 Wind speed data collection from a moving car at different vehicle travelling speeds

Wind speed (m.s ⁻¹)	Vehicle travelling speed (km.h ⁻¹)	Vehicle travelling speed (m.s ⁻¹)	Undisturbed/apparent wind speed (m.s ⁻¹)
0.8	60	16.67	12 – 14
0.8	80	22.22	18 – 27
0.8	100	27.78	24 – 29

4.4.1.2 Theoretical wind speed

The undisturbed wind speed was determined using the apparent wind speed equation, which is dependent on the airspeed, vehicle travelling speed and the true pointing angle. Table 4.6 shows the computed wind speed at different vehicle travelling speed and an air speed which is assumed to remain constant at 1.944 m.s^{-1} .

Table 4.6 Theoretic apparent wind speed

Vehicle travelling speed (km.h^{-1})	Vehicle travelling speed (m.s^{-1})	Apparent wind speed (m.s^{-1})
60	16.667	18.611
80	22.222	24.166
100	27.778	29.722

The outcomes from both sub-section 4.4.1.1 and 4.4.1.2 are in agreement with one another and either method can be used to attain the apparent/undisturbed wind speed. In this study the incoming wind speed is replaced by the vehicle speed since the apparent wind speed is highly influenced by the vehicle speed. In transportation it is easy to relate to vehicle speed and use it to determine the wind speed required by the wind turbine.

Table 4.7 shows the external and internal wind speed at three louvre opening level including the close louvre setting. These opening levels of the louvre mechanism were determined using the vacuum blower to calibrate the internal wind speed from the external wind that can then be feed into the wind turbine rotor. This was done to control the high incoming wind speed and ensure that the turbine blades do not break. It is also not easy for the PVC pipe blades to just bend because they are a small size. At opening level 0, the internal wind speed recorded was $0.2 - 0.3 \text{ m.s}^{-1}$ for every wind speed range. This is because the louvre slats were totally closed and did not permit airflow which is good when the wind turbine does not need to generate any more power. At opening level 1, the highest internal wind speed that can be obtained is $17.5 - 27.0 \text{ m.s}^{-1}$ from an external wind speed range of $27.0 - 35.1 \text{ m.s}^{-1}$, corresponding to the wind speed measured for a vehicle travelling between $80 - 100 \text{ km.h}^{-1}$ ($22 - 27.78 \text{ m.s}^{-1}$). On average it can be found that at opening level 1, the louvre mechanism can reduce the external wind speed by 5 m.s^{-1} to obtain the required internal wind speed. At the opening level 2, the highest

recorded internal wind speed was $21.5 - 35.1 \text{ m.s}^{-1}$ from an external wind speed of $27.0 - 35.1 \text{ m.s}^{-1}$. Opening level 2 can obtain an average reduction of wind speed by 2.4 m.s^{-1} . This means there is less airflow control at opening level 1. Opening level 2 is great when there is a need to drastically reduce the incoming wind speed and opening level 2 is good for a small reduction of the incoming wind speed.

Table 4.7 External and internal wind speed at different louvre opening level

Louvre opening level	External wind speed (m.s^{-1})	Internal wind speed (m.s^{-1})
0 (closed)	7.2 - 14.2	0.2 - 0.3
	15.0 - 26.5	0.2 - 0.3
	27.0 - 35.1	0.2 - 0.3
1	7.2 - 14.2	2.9 - 9.4
	15.0 - 26.5	13.9 - 19.9
	27.0 - 35.1	17.5 - 27.0
2 (fully open)	7.2 - 14.2	6.5 - 11.3
	15.0 - 26.5	14.4 - 25.9
	27.0 - 35.1	21.5 - 35.1

4.4.2 Power output of the wind turbine

Figure 4.10 shows the effect of vehicle speed, different louvre opening level, and time on the average accumulated power generated by a small wind turbine with a rotor diameter of 0.6 m. The power output of the 600 W PMSG ranged between $8.4 - 294 \text{ W}$ per hour for a vehicle speed of 60 and 100 km.h^{-1} (16.67 and 27.78 m.s^{-1}), respectively. The findings obtained in this study are comparable to the results obtained by Ozgener (2006) who reported a power output of 616 W for a 1.5 kW wind turbine generator at 7.5 m.s^{-1} with a rotor diameter of 3 m and Tahir *et al.* (2019) who obtained 478.5 W for a 600W permanent magnet generator operating at 10 m.s^{-1} and a rotor diameter of 0.65 m. The difference in the findings may be due to the small size of the rotor diameter, the material used for the blade design (PVC) and the changing topography of surrounding areas along the road during testing. Another important factor that possibly affects the performance of the wind turbine is the torque or ease of rotation of the generator shaft which moved well but felt heavy. Although given these constraints, the generated power output can still meet the power requirement of a 600 W or less load through

the incorporation of a step-up power inverter. The battery power is supplied by the wind turbine which is measured through the voltage state of charge. The inverter then steps up the voltage in the battery from 12 V to 230 V, which then allows the wind turbine to provide the current that is required to meet the power requirement of a 33 W fan, a 290 W fan and a 180 W water pump. At a vehicle speed of 100 km.h⁻¹ and louvre opening level 2, the power output of 294 W can cover relatively 9 hours with the assistance of the 230 V inverter which reduces the current required from the battery by increasing the voltage, thus allowing the power supply from the wind turbine to meet the power requirements of the ECS. Therefore, this power is more than capable of covering the estimated two-hour travel and even more.

Figure 4.10 (a) shows the power output at different vehicle speeds. From the graph it can be seen that vehicle speed has a significant effect ($p < 0.001$) on the power output of the wind turbine. The average power output ranged from 71.4, 105 to 129.4 W for a vehicle speed of 60, 80 and 100 km.h⁻¹, respectively averaged for both louvre opening level 1 and 2. The power output values obtained from the vehicle speeds of 80 and 100 km.h⁻¹ are close. This proves that high wind speed account from the low swept area (0.283 m²) of the wind turbine rotor to give more power output. The wide range of the incoming wind speed values that affect the wind turbine energy generation are represented by the vehicle travelling speed since the apparent wind speed harnessed and used for power generation is highly dependent on the travelling speed.

The cut-in wind speed was observed at 4 m.s⁻¹ while the rated wind speed was observed at 17.5 m.s⁻¹. No cut-out wind speed was observed although the highest wind speed observed was at 33 m.s⁻¹. These observations are comparable to the study done by Barroso Montes (2011b) who observed a cut-in and cut-out wind speed of 5 and 25 m.s⁻¹ respectively and Hirahara *et al.* (2005) who observed a cut-in wind speed of 3.6 m.s⁻¹, a rated wind speed of 12 m.s⁻¹ and a survival wind speed of 45 m.s⁻¹. Also, the findings on this study are relatable to the results found by Salih *et al.* (2012) who observed a cut-in wind speed of 4 m.s⁻¹, a rated wind speed of 12 m.s⁻¹ and a cut-out wind speed of 25 m.s⁻¹. No damage was observed on the overall wind turbine and the blades even though the wind turbine also operated at high wind speeds of more than 25 m.s⁻¹ which is the common cut-out wind speed value for most research studies.

Figure 4.10 (b) shows the effect of controlling the airflow into the wind turbine through the louvre mechanism. The average power output is 73.9 and 129.9 W for louvre opening level 1

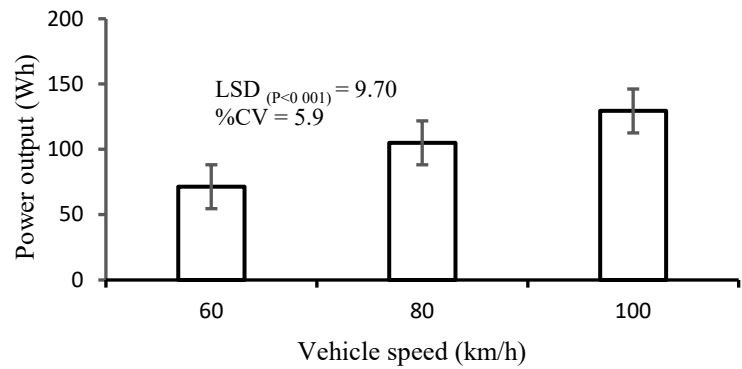
and 2, respectively. This clearly shows that the opening level of the louvre mechanism has significant effect ($p < 0.001$) on the power output of the wind turbine. The power output achieved from this study using different wind speed is far greater than depicted in this graph. This is because each of these values is an average for all vehicle travelling speeds. According to the author, the airflow in did not need interference because high wind speeds were required to generate high power output. But this design may be helpful in extreme wind conditions to control the incoming wind speed as well as protect the rotor and generator. This mechanism will help to reduce the wind speed and still be able to generate electrical energy in strong wind conditions. The louvre mechanism also helps lower the noise levels inside the wind turbine structure (Wahab *et al.*, 2020).

Figure 4.10 (c) shows the accumulated power observed at different durations for an hour. It can be seen that the accumulated power is directly related to time. There is a definite increase of the accumulated power output with growing time ($p < 0.001$) although this can be affected by the change in topography and terrains as previously discussed on section 4.4.1.1. This simply shows that the amount of power generated by the wind turbine continuously increase with time as it accumulates. Figure 4.10 (d) illustrates the accumulated power output subjected to different louvre opening level and vehicle speeds. The accumulated power of 113.4, 159.6 and 210.0 W per hour were observed for 60, 80 and 100 km.h⁻¹, respectively, on louvre opening level 1. On louvre opening level 2, the power output observed in an hour was 142.8, 268.8 and 294.0 W for a wind speed of 60, 80, 100 km.h⁻¹, respectively. The graph depicted show that the vehicle speed of 100 km.h⁻¹ achieves a high-power output compared to the other vehicle speed of 60 and 80 km.h⁻¹. An increase in vehicle speed implies an increase in the wind speed.

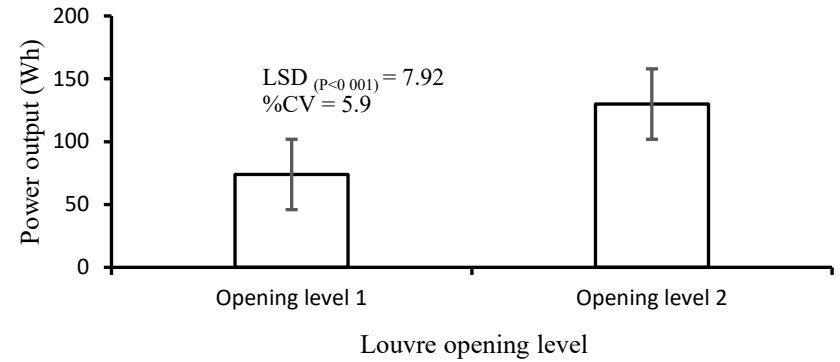
The findings of this study are comparable to the study done by Ozgener (2006) who obtained a power output of 616 W from a 1.5 kW wind turbine generator with a 3 m rotor diameter and a design wind speed of 7.5 m.s⁻¹. Based on the results it can be seen that a substitute is made between the wind speed and the rotor diameter. Many authors such as Ozgener (2006), Salih *et al.* (2012) and Tahir *et al.* (2019) performed studies which analysed wind turbines with low wind speeds and large rotor sizes. Salih *et al.* (2012) designed a 700 W wind turbine with a rotor diameter of 1.6 m which produced a 600 W electrical power at 12 m.s⁻¹. In this study the 600 W wind turbine was designed with a high design wind speed (16.8 -19.0 m.s⁻¹) and small rotor diameter (0.6 m). This proves the initial prediction that the wind speed accounts for the small nature of the rotor. A clear decline can be seen in the power output generated between

45 – 60 min for louvre opening level 1. This is attributed to the slow-moving traffic that was by the tollgate which means the rotor was turning slow and stationary at some point. During the time that the generator is not generating electrical energy, the battery steps in and continues to supply power to the load (cooling technology).

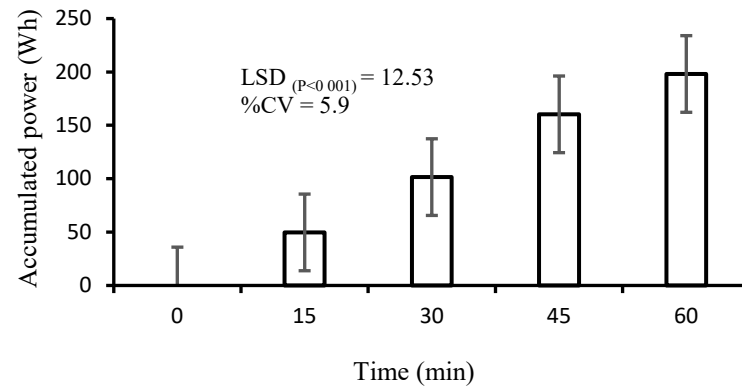
During the testing it was observed that the apparent wind turbine had no physical impact on the stability of the moving vehicle, although the wind turbine may have some slightly negative impact on the fuel efficiency and result in some aerodynamic drag because of the added weight. There is no need to prime or kickstart the generator. The wind turbine only needs less than 10 seconds to start operating if the vehicle was stationary.



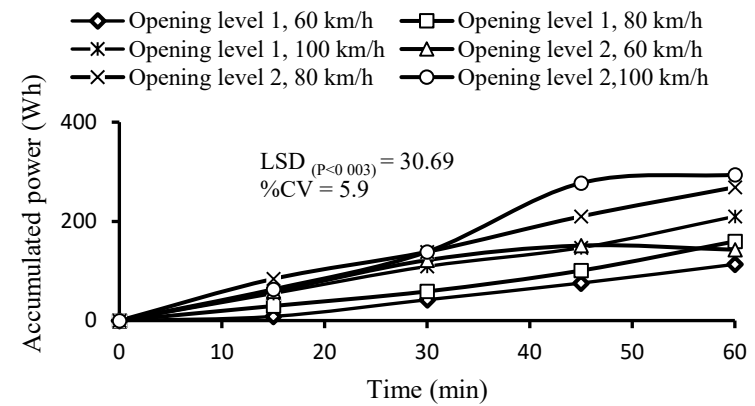
(a)



(b)



(c)



(d)

Figure 4.10 (a) Effect of vehicle speed on accumulated power, (b) Effect of louvre opening level on accumulated power, (c) Accumulated power over one-hour duration, (d) Accumulated power over time for different vehicle speeds and louvre opening level

4.4.3 Power coefficient of the wind turbine

Figure 4.11 shows the power coefficient determined for the different power output subjected to different louvre opening level and vehicle speed for a duration of one hour. The power coefficient ranged between 0.19 – 0.35 for louvre opening level 1 and 0.24 - 0.49 for louvre opening level 2. From Figure 4.11, it can be seen that the maximum power coefficient of 0.49 is achieved at a vehicle speed of 100 km.h⁻¹ and louvre opening level 2. These results are satisfactory since the maximum power coefficient achieved in this study is close but does not exceed the Betz limit at 0.59. The findings are comparable to the studies performed by authors such as Ozgener (2006) (0.35), and Muhsen *et al.* (2019) (0.4 – 0.445). This power coefficient of 0.49 is comparable to the maximum power coefficient of 0.44 obtained by QBlade.

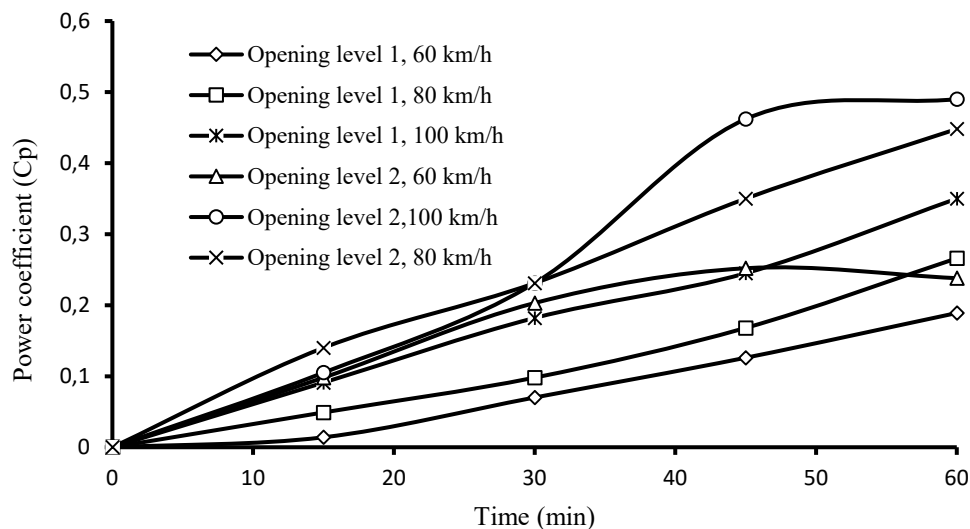


Figure 4.11 Power coefficient for different vehicle speeds

Figure 4.12 shows the power coefficient as affected by the vehicle speed. The power coefficient improves with increasing vehicle speed. In this particular case louvre opening level 2 also had an effect on the power. The maximum power coefficient obtained in this study is 0.49. Salih *et al.* (2012) evaluated the power output of a 600 W wind turbine against the wind speed and found that the power output increases with an increasing speed up until the rated wind speed where it stabilises and produce the same amount of power until the cut-out wind speed. It is recommended to use to vehicle speed of 80 – 100 km.h⁻¹ when transporting fresh produce with this wind turbine. Furthermore, it is suggested to lower the louvre opening level when there are

strong wind condition to prevent blades from breaking and still be able to generate electrical energy which is much needed by the cooling technology.

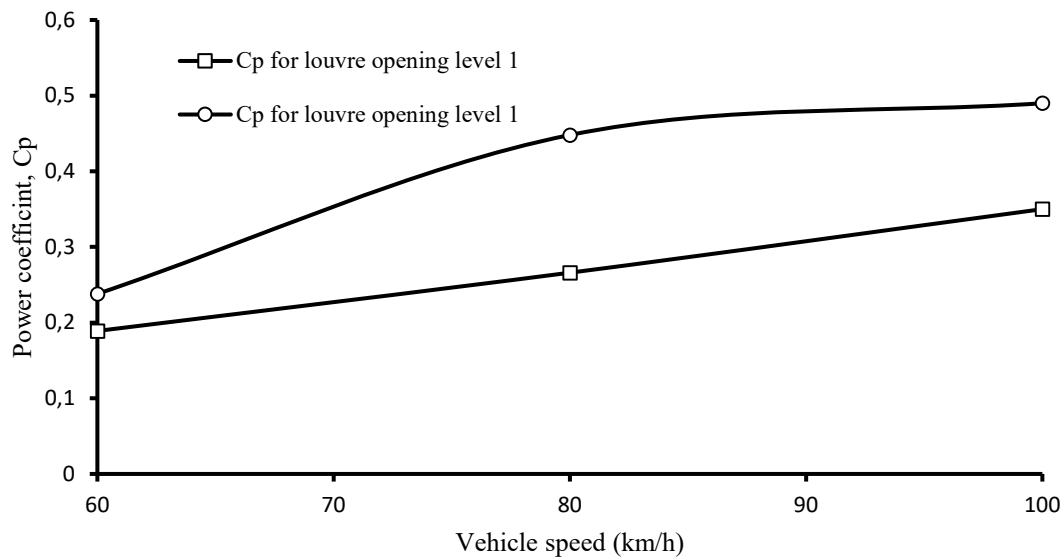


Figure 4.12 Power coefficient for different vehicle speeds

4.5 Wind Turbine Prototype Costs

The total costs of the wind turbine is R11 412.88 including freight charges and R9056.57 excluding freight charges, both with the exception of labour costs. This wind turbine is relatively cheap compared the 600 W wind turbines available on the market, therefore recommended for employment, especially for vehicle use since it considers road airflow conditions.

4.6 Conclusion

This study aimed to design and develop a low-cost, portable, small wind turbine prototype that can be used to power mobile cooling technology, particularly an ECS unit. The prototype component sizing was based on calculations performed using the BEM theory, QBlade and MATLAB Simulink. The small wind turbine incorporated a louvre mechanism to assist in controlling the wind speed at the front of the rotor. The outcome of this study revealed that the power output of the small wind turbine (0.6 m Ø) is highly influenced by vehicle speed and the louvre opening level which make up for the small size of the rotor. The highest average power

output achieved was 294.0 W at 100 km.h⁻¹ for louvre opening level 2. With the use of a 230 VAC step-up power inverter, the wind turbine prototype was a success since it was concluded to be able to continuously power a 600 W load. The maximum power coefficient obtained from this study was 0.49 which is a good indication that the system functions efficiently since the maximum power coefficient that can be achieved is 0.59 (Betz limit). As the final step of this study, it is recommended to integrate the wind turbine with a 600 W evaporative cooler unit to test the functionality of the entire system.

4.7 References

- Akbari, V, Naghashzadegan, M, Kouhikamali, R, Afsharpanah, F and Yaïci, W. 2022. Multi-Objective Optimization and Optimal Airfoil Blade Selection for a Small Horizontal-Axis Wind Turbine (HAWT) for Application in Regions with Various Wind Potential. *Machines* 10 (8): 687.
- Barroso Montes, M. 2011. Optimal control of wind turbines in strong wind conditions. Unpublished thesis, Mechanical Engineering, Technical University of Denmark, Kongens Lyngby, Denmark.
- Bracco, G and Razzetti, D. 2022. Aerodynamic design of a micro wind turbine and performance analysis with QBlade. Unpublished thesis, Mechanical Engineering, Polytechnic University of Turin, Turin, Italy.
- Ceruti, A. 2019. Meta-heuristic multidisciplinary design optimization of wind turbine blades obtained from circular pipes. *Engineering with Computers* 35 (2): 363-379.
- Chong, C, Rigit, A and Ali, I. 2021. Wind turbine modelling and simulation using Matlab/SIMULINK. *IOP Conference Series: Materials Science and Engineering*, 012034. IOP Publishing, Kuching, Malaysia.
- Elik, A, Yanik, DK, Istanbulu, Y, Guzelsoy, NA, Yavuz, A and Gogus, F. 2019. Strategies to reduce post-harvest losses for fruits and vegetables. *Strategies* 5 (3): 29-39.
- Evans, S, Bradney, D and Clausen, P. 2018. Development and experimental verification of a 5 kW small wind turbine aeroelastic model. *Journal of Wind Engineering and Industrial Aerodynamics* 181 104-111.
- Garmode, RK, Gaval, VR, Kale, SA and Nikhade, SD. 2022. Comprehensive evaluation of materials for small wind turbine blades using various MCDM techniques. *International Journal of Renewable Energy Research* 12 (2): 981-992.

- Hirahara, H, Hossain, MZ, Kawahashi, M and Nonomura, Y. 2005. Testing basic performance of a very small wind turbine designed for multi-purposes. *Renewable energy* 30 (8): 1279-1297.
- Hossain, MF. 2020. Application of wind energy into the transportation sector. *International Journal of Precision Engineering and Manufacturing-Green Technology* 1-13.
- Louw, A and Jordaan, D. 2016. Supply chain risks and smallholder fresh produce farmers in the Gauteng province of South Africa. *Southern African Business Review* 20 (1): 286-312.
- Muhsen, H, Al-Kouz, W and Khan, W. 2019. Small wind turbine blade design and optimization. *Symmetry* 12 (1): 18.
- Ozgener, O. 2006. A small wind turbine system (SWTS) application and its performance analysis. *Energy conversion and Management* 47 (11-12): 1326-1337.
- Saidi, Y, Mezouar, A, Miloud, Y and Benmahdjoub, MA. 2018. A robust control strategy for three phase voltage source PWM rectifier connected to a PMSG wind energy conversion system. *2018 International Conference on Electrical Sciences and Technologies in Maghreb (CISTEM)*, 1-6. IEEE.
- Salih, SM, Taha, MQ and Alawsaj, MK. 2012. Performance analysis of wind turbine systems under different parameters effect. *International Journal of Energy and Environment* 3 (6): 895-904.
- Shoaib, M, Siddiqui, I, Rehman, S, Khan, S and Alhems, LM. 2019. Assessment of wind energy potential using wind energy conversion system. *Journal of cleaner production* 216 346-360.
- Sibanda, S and Workneh, TS. 2020. Performance evaluation of an indirect air cooling system combined with evaporative cooling. *Heliyon* 6 (1): e03286.
- Tahir, MH, Malik, A, Saeed, MA, Zaffar, N, Adeel, HM and Amjad, HMS. 2019. Experimental Performance Evaluation of 600 W Small Wind Turbine to Overcome Energy Crisis in Pakistan.
- Telle, J-S, Schlüters, S, Schönfeldt, P, Hanke, B, von Maydell, K and Agert, C. 2022. The optimized integration of temperature-controlled transports into distributed sector-integrated energy systems. *Energy Conversion and Management* 269 116148.
- Van Duin, JR, Geerlings, HH, Verbraeck, AA and Nafde, TT. 2018. Cooling down: A simulation approach to reduce energy peaks of reefers at terminals. *Journal of Cleaner Production* 193 72-86.

- Wahab, I, Azman, AN, Abd Aziz, H, Hamberi, MJM and Ismail, LH. 2020. Adjustable Folding Aluminium Louvres Application on ‘Hop (B): Nob Marina Quay’. *Recent Trends in Civil Engineering and Built Environment* 1 (1): 88-94.
- Wahyudi, B, Faizin, A, Setiawan, A, Susilo, SH and Wicaksono, H. 2022. Simulation study of horizontal axis wind turbine using PVC pipe propeller with elbow tip. *EUREKA: Physics and Engineering* (5): 67-76.
- Wood, D. 2011. Small wind turbines. In: *Advances in wind energy conversion technology*. Springer.
- Zhang, Q, He, J, Xu, Y, Hong, Z, Chen, Y and Strunz, K. 2021. Average-value modeling of direct-driven PMSG-based wind energy conversion systems. *IEEE Transactions on Energy Conversion* 37 (1): 264-273.

5. PERFORMANCE ANALYSIS OF AN EVAPORATIVE COOLER UNIT POWERED BY A WIND TURBINE

Abstract

The purpose of this study was to assess the capability of the wind turbine to continuously supply electrical power to operate a 600 W evaporative cooler unit, with the grid electricity used as a control. The 53 m³ ECS unit located at Ukulinga Research farm, Pietermaritzburg (-29°63'S" and 30°40'E) was used to store a 5 kg tomato fruit sample. The temperature and relative humidity were measured using the HOBOWare data loggers positioned at different points around the ECS unit. The amount of power produced by the wind turbine to operate the ECS unit was evaluated based on the temperature drop, the relative humidity increase as well as the cooling efficiency that the evaporative cooler can achieve compared to the grid-power that was used to run the same ECS unit. The temperature inside the ECS unit varied between 24.65 – 31.87 °C with a temperature drop range of 2.85 °C to 10.59 °C from the ambient temperature while using the wind turbine as the power source. The relative humidity of the wind turbine-powered ECS unit ranged between 57.8 – 88.77 % with a relative humidity increase range varying between 21.66 – 29.04 %. For the grid-powered ECS unit, the temperature inside the cooling unit fluctuated between 23.71 and 25.23 °C. Then the temperature drop was found to be 3.91 – 15.75 °C. While the power supply was provided by the grid, the inside relative humidity increase of the ECS varied between 28.52 – 47.66 %. The cooling efficiency varied between 12.62 – 59.78 % and 14.26 – 55.93 % for the wind turbine and grid electricity power source, respectively. Similar results were observed between the wind turbine and grid electricity power source. This proves that the wind turbine can be used as a primary or an alternate source of electricity to power cooling technologies provided that the wind turbine is appropriately scaled and designed to meet the required power input, from the blade design and optimisation to the selection of a generator and driving at a suitable vehicle speed to achieve the required power input.

5.1 Introduction

Fresh farm commodities are highly susceptible to spoilage if not stored under appropriate environmental conditions after being plucked from the mother stem (Sibanda and Workneh,

2020b). The loss of fruits and vegetables after harvest due to external or internal interference is termed post-harvest losses (PHL) (Mothapo, 2022). High post-harvest losses are a threat to food security and the livelihood of society (Porat *et al.*, 2018). Most smallholder farmers who struggle with post-harvest losses are resource-poor and cannot afford a refrigerated truck. Authors such as Jain (2007), Olosunde *et al.* (2016), Nkolisa *et al.* (2018b), and Sibanda and Workneh (2020a) have adopted the principle of room cooling using an evaporative cooling system to offer an affordable storage facility for fruit and vegetable storage. These authors designed, developed, and tested the performance of different evaporative coolers and reported them to be able to reduce post-harvest losses in addition to being affordable. Some of these fixed evaporative coolers use grid electricity or solar energy. This study is focused on incorporating a wind turbine as the power source of a mobile evaporative cooler unit. Tomatoes (*Solanum lycopersicum* L.) are used as the test sample. Tomato fruit is an ideal test sample since it is one of the commonly grown, and highly perishable fruit worldwide, with a relatively short lifespan ranging around 2-3 weeks which can be reduced if the tomatoes are not stored appropriately and are exposed to unfavourable environmental conditions during transportation (Haile and Safawo, 2018).

According to Mothapo (2022), smallholder farmers in KwaZulu-Natal experience about 76% PHL of their tomato harvest. The tomato fruit's highly perishable nature causes it to have high postharvest losses. According to Cherono and Workneh (2020) and Sibanda and Workneh (2020a), the tomato fruit is also one of the most popular FV world-degenerativewide, coming second to potatoes because of its wide range of culinary uses and a worldwide appeal for meal preparation either as a salad, paste or processed into juice. Tomato is an important fruit because it helps improve the human immune system, prevents the development of regressive health conditions (Dorais *et al.*, 2008; Ioannidi *et al.*, 2009). The demand for the tomato fruit has increased as a result of these benefits, and the broad application of the tomato fruit. The general perishable nature of fresh produce is attributed to the fast metabolic rate it has after harvest. According to Cherono and Workneh (2020), fruits stored under ambient conditions deteriorate fast. Cooling is one conventional way used to preserve the quality of fresh produce while elongating its shelf-life (Munoz *et al.*, 2017).

In this study, the tomatoes were stored in an evaporative cooler unit to assess the quality after being powered by either the wind turbine or the grid and thus, ultimately assess the ability of the wind turbine to support the ECS power load. Wind energy is a free renewable energy,

therefore it is important to incorporate it into the ECS unit design to reduce the incurring costs and make it affordable to smallholder farmers. Most smallholder farmers are aware of the effects of not using cooling storages but the high purchase or hire costs they encounter cause them to prefer to transport their fruits and vegetable without any cooling unit (Raut and Gardas, 2018). This exposes them to unfavourable conditions along the road such as exposure to high temperature and low relative humidity. Temperature and relative humidity are important parameters to consider when handling perishable commodities (Zhang *et al.*, 2022). The ECS unit can store fresh produce at low temperature and increased relative humidity, therefore being able to maintain the quality of the produce as well as elongate the shelf-life of fresh produce (Tilahun, 2010a). Controlling the temperature and relative humidity during transportation may or may not have an immediate effect on the quality of fruits and vegetables. But it helps reduce the metabolic rate which may have a potentially detrimental impact afterwards in the future along the supply chain (Tongbram *et al.*, 2020). Therefore, fresh produce cooling units are important during transportation (Kan *et al.*, 2019; Tongbram *et al.*, 2020).

The main objective of the study is to test the functionality of the wind turbine coupled with the evaporative cooler unit and measure the wind turbine efficiency through temperature and relative humidity control inside the storage chamber of the evaporative cooler unit. The study specifications include that:

- (a) The reduction in storage temperature must be 10 – 17 °C, and
- (b) The storage relative humidity must be between 85 - 95%.

5.2 Material and Methods

This section describes the make-up of the evaporative cooler unit integrated with the wind turbine energy conversion system along with the sample preparation.

5.2.1 Study site and climatic data

This study was conducted at the University of KwaZulu-Natal (UKZN), Ukulinga Research Farm in Pietermaritzburg (PMB), KwaZulu-Natal, South Africa (-29°63'S" and 30°40'E at an altitude of 673 m above sea level). PMB is a town characterised by dry and sub-humid conditions at 52% relative humidity, an ultraviolet index of 5, an average temperature of 26 °C in January, 19 °C in June, and 33 mm of rain in a year. Pietermaritzburg has a minimum wind

speed of 0.30 km.h^{-1} in the month of April, a maximum wind speed of 26.60 km.h^{-1} in the month of October and an average wind speed of 8.12 km.h^{-1} throughout the year. The testing at the Ukulinga research farm was conducted using a 53 m^3 evaporative cooler unit erected on site which has power provided by the wind turbine and grid electricity.

5.2.2 Description of an evaporative cooler unit powered by a wind turbine

The evaporative cooler unit which is the selected cooling technology for testing has a 53 m^3 storage capacity that can store up to 3.8 tons of the test sample. It consists of a 33 W constant speed positive pressure fan, a 290 W fan used to for air transmission, and a 180 W water pump is used for water circulation. In total, the power requirement of the system is 503 W without accounting for the system losses. The design of the evaporative cooling unit is as described by Sibanda and Workneh (2019). Figure 5.1 shows the top view of the wind turbine connected to the evaporative cooler unit. The electrical energy moves from the electrical generator to the rectifier, then the battery and lastly to the power inverter before it goes to the evaporative cooler unit. The wind turbine and ECS are connected via the power inverter and the electric socket which provides the water pump and fans with electrical energy.

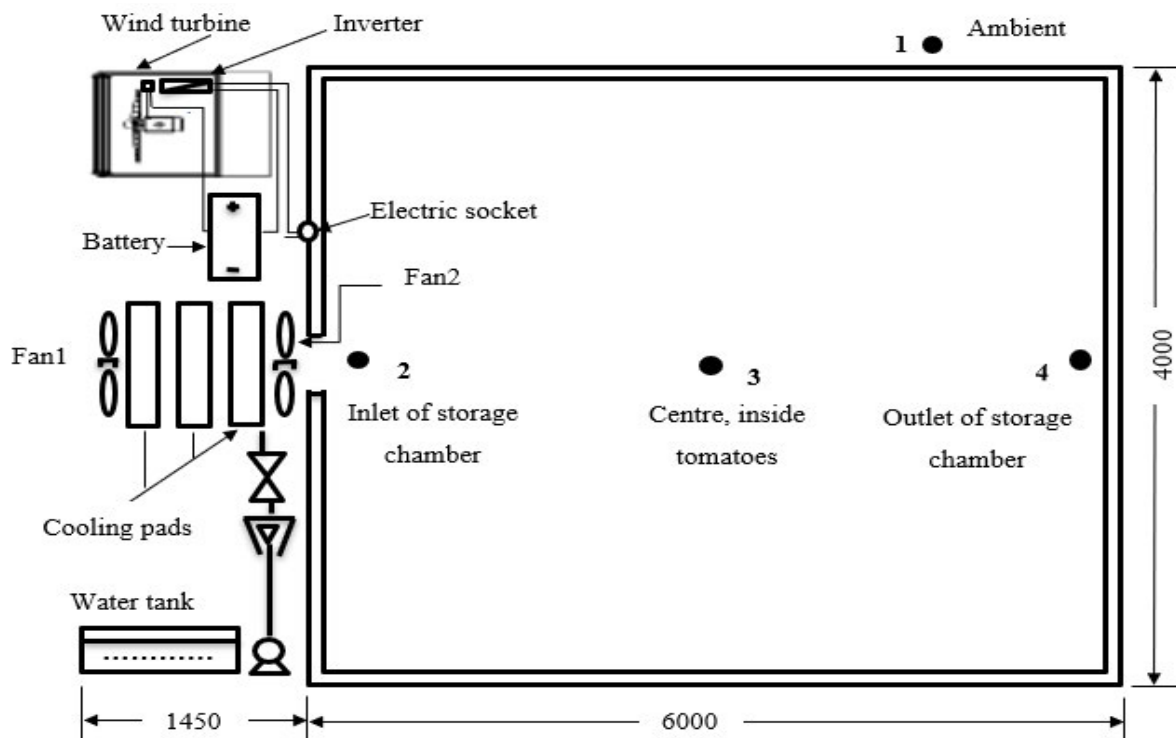


Figure 5.1 Top view of the evaporative cooler unit powered by the wind turbine showing different positions of the HOBO data loggers in the storage chamber.

5.2.3 Sample preparation

The tomato fruit test sample is shown in Figure 5.2. Temperature and relative humidity are recorded to assess the ability of the small wind turbine to power the ECS unit. These parameters will help to assess the quality of the tomatoes during transportation and therefore prove whether the wind turbine is competent to run the evaporative cooler unit. Two rounds of experimentation were done using different power sources, grid and wind turbine electrical energy. The experimentation duration is 2 hours for each power source.



Figure 5.2 Temperature and relative humidity data collection with tomato sample using a HOBOWare data logger sensor.

5.3 Experimental Design

The ECS unit experiments are divided into two parts, the wind turbine-powered ECS unit and the electric grid-powered ECS unit serving as the control as shown in Figure 5.3. The parameter studied is the efficiency of the power supply unit by analysing the condition of the test sample (tomatoes) in the initial and final stages of both parts. This study was conducted to validate that wind energy power achieves similar performance as the grid energy power in terms of temperature and relative humidity control along with the cooling efficiency of the fresh produce.

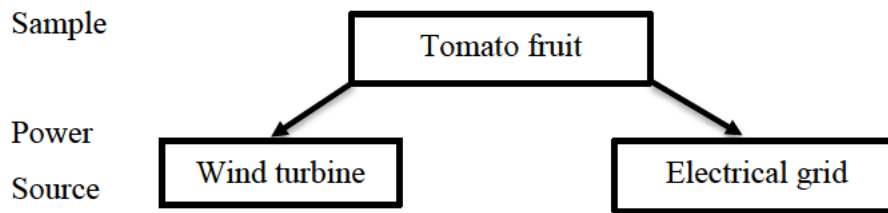


Figure 5.3 Experimental design to assess the performance of an evaporative cooler unit with different power source using tomato testing sample

5.4 Comparison of Wind Turbine and Grid Powered Evaporative Cooler Performance

The performance of the evaporative cooler unit powered by either the wind turbine or the grid was assessed based on changes in the temperature and relative humidity of the surrounding air. Four HOBOware data loggers were employed to collect the temperature and relative humidity data around the ECS unit and placed as follows: outside of the ECS unit to read ambient conditions, on the ECS storage chamber inlet, inside the tomato samples, and at the outlet of the ECS storage chamber in the far end. This is shown in Figure 5.1. The duration of each testing of the tomato fruit sample was for two hours to represent short transport travelling time around KwaZulu-Natal. The first testing part was done with the wind turbine used as the power source. Then, the second testing part used grid power as the power source and served as a control to measure the wind turbine power supply. To assess the performance of the evaporative cooling system, the cooling efficiency is also computed using the temperature difference ratio using Equation 5.1 (Jain, 2007).

$$\text{Cooling efficiency} = \frac{T_{db,a} - T_{db,c}}{T_{wb}} \times 100 \quad (5.1)$$

where

$T_{db,a}$ = Dry-bulb temperature of ambient conditions (°C),

$T_{wb,a}$ = Wet-bulb temperature of ambient condition (°C), and

$T_{db,c}$ = Dry-bulb temperature of inside air (°C).

5.5 Results and Discussion

This sub-section presents and discusses the results obtained from the testing of an evaporative cooler using wind turbine and grid electricity as a power source. The results presented include the temperature, relative humidity and cooling efficiency of the ECS unit.

5.5.1 Temperature

Figure 5.4 shows the temperature at different positions inside the evaporative cooler unit which was operated using wind turbine-generated electric energy power. The ambient temperature recorded during the experiment varied between 27.53 and 41.39 °C. The inside temperature varied between 24.68 - 30.80 °C, 24.68 - 31.87 °C, and 24.65 – 31.33 °C at the inlet of the cooling unit from the ECS, around the tomato sample and at the outlet of the evaporative cooling unit. The findings in this study are in agreement with the temperature changes reported by Cherono and Workneh (2020) which varied between 15-26 °C and 15-31°C in winter and summer seasons, respectively inside the truck during transportation. The appropriate temperature for tomato fruit storage facilities is 13-22 °C. Therefore, the obtained temperature (24.65 – 24.68°C) is slightly higher by 2.8 °C from the required temperature (22.0 °C). The graphs of the temperature inside the different positions of the ECS unit are closely lined which shows that the temperature inside the storage chamber is uniformly distributed. Unlike the refrigerator which maintains fixed internal temperature regardless of the ambient conditions, the ECS only offers a certain reduction in temperature, which is used to assess its performance.

The difference in the inside and outside temperature was determined between the outside and inside conditions. The reduction in temperature as a function of the ambient temperature was determined and found to range between 2.85 – 10.59 °C. Although these findings do not exactly match the desired temperature reduction range of 10 – 17 °C, the maximum temperature drop

obtained met the lowest set design specification value. These findings fall within the results obtained in the performance study done by Sibanda and Workneh (2020a) on the IAC + EC system who recorded an inside temperature of 7 – 16 °C lower than the ambient temperature. (Taha *et al.*, 1994) developed an evaporative cooler which achieved a 10 -13 °C temperature drop from the ambient temperature, which is similar to the findings of this study. Olosunde *et al.* (2016) developed a solar-powered evaporative cooling storage system (SPECSS) which was able to reduce the ambient temperature by 7.8 – 15.4 °C. Initially, the temperatures are similar but as time progresses the ambient temperature is high, and the inside temperature is low. This provides the tomatoes with an optimum environment for storage while in transit. This is sufficient to conclude that the wind turbine can support the ECS unit. From Figure 5.4 it can be seen that it takes approximately one hour to reach a stable temperature, therefore it is advisable to start the evaporative cooler one hour before loading

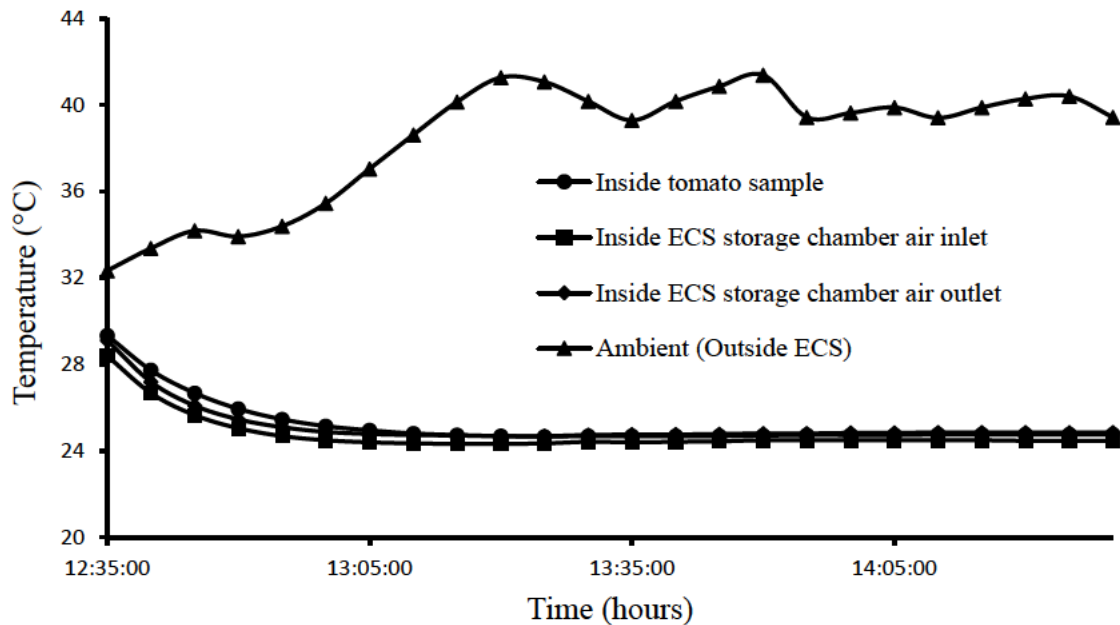


Figure 5.4 Temperature at different locations of the evaporative cooler unit using wind energy power source

Figure 5.5 shows the temperature at different locations of the evaporative cooler unit using a grid energy power source. The ambient temperature ranged between 28.35 – 40.4 °C. While the power source was provided by the grid electricity, the minimum and maximum inside temperature varied between 23.71 – 24.65 °C, 24.44 – 25.21°C, and 24.27 – 25.23 °C for the

ECS storage unit inlet, inside the tomatoes and at the outlet of the storage chamber. Then, the temperature depression varied between 4.63 – 15.75 °C, 3.91- 15.19 °C and 4.08 – 15.17 °C for the inlet, inside the tomato sample and outlet of the ECS unit. Therefore, the overall range of temperature drop inside the ECS unit storage chamber varied between 3.91 - 15.75 °C, which met the design specification for a temperature reduction around 10 – 17 °C, even though a much lesser temperature drop of 3.91°C was observed. These findings are still comparable to the results obtained by Cherono and Workneh (2020) (7 – 16 °C). Jain (2007) developed a two-stage evaporative cooler which was able to achieve a temperature drop ranging between 8 – 16 °C. The results reported by Jain (2007) are also similar to the findings of this study. In the late hours of the day the ambient temperature decreases but the inside temperature remains the same. This shows the dependence of the temperature reduction on the ambient temperature. There is more temperature drop or cooling with high ambient temperatures than there is for low ambient temperatures. This is because the ECS uses the principles of evaporation to bring cooling effect. These results show that both the wind turbine as well as grid electricity provide adequate power to run the ECS unit.

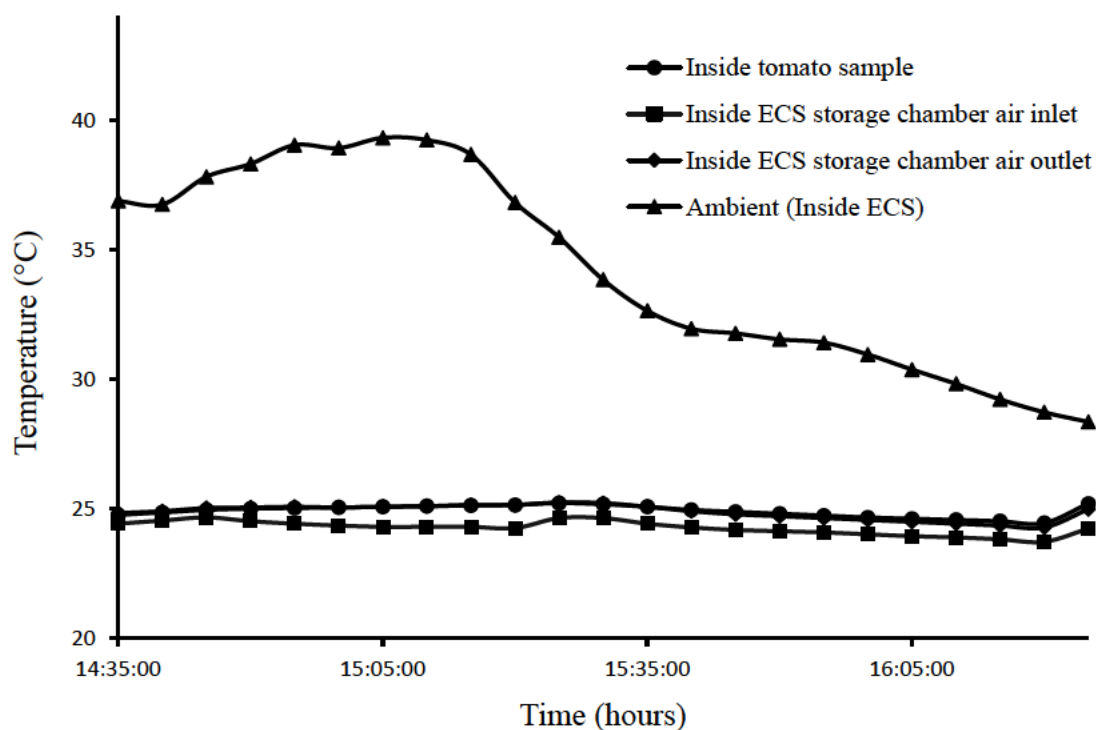


Figure 5.5 Temperature at different locations of the evaporative cooler unit using grid energy power source

5.5.2 Relative humidity (RH)

Figure 5.6 shows the relative humidity at different locations of the evaporative cooler unit using wind energy power source. The ambient relative humidity recorded when using the wind turbine power supply ranged between 35.62 – 59.73 %. The inside storage temperature ranged between 57.28 – 88.77 %, 58.21 – 86.36 %, and 58.16 – 85.01 % for the inlet, inside the tomatoes and outlet of the ECS unit, respectively. The appropriate storage RH for tomatoes is 90-95%. The maximum range of the relative humidity values (85.01, 86.36, and 88.77 %) recorded in this study are 2.33 – 5 % less than the required relative humidity, but it is sufficient to slow the metabolic rate and keep the tomatoes quality. The study done by Cherono and Workneh (2020) achieved a relative humidity of 40-100% in winter and 22-90% in summer, with most values between 20-40% inside the storage chamber, which is similar to the findings of this study. Other authors such as Olosunde *et al.* (2016), Jain (2007), and Nkolisa *et al.* (2018b) found a relative humidity range of 44 – 96.8 %, 50 – 75 %, and 79.84 – 83.91 % , respectively. The relative humidity increase for this study was determined and ranged between 21.66 - 29.04 %. These findings are comparable to those found by Sibanda and Workneh (2020a) (13.41 – 41 %).

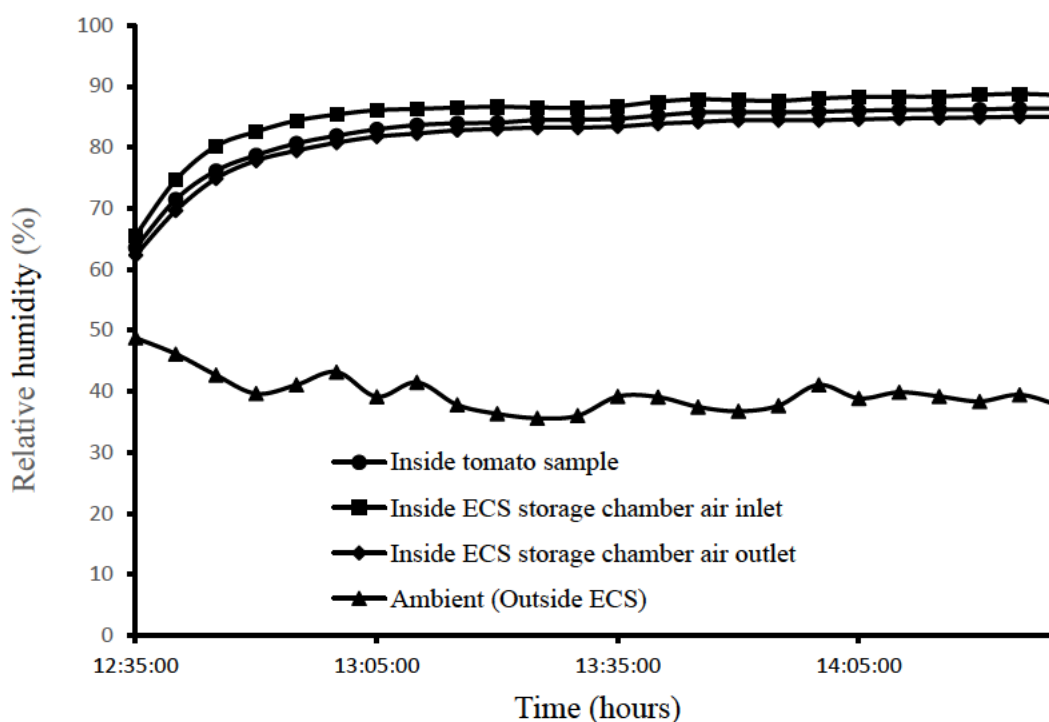


Figure 5.6 Relative humidity at different locations of the evaporative cooler unit using wind energy power source

Figure 5.7 shows the relative humidity at different locations of the evaporative cooler unit using grid energy power source. The ambient relative humidity varied between 33.44 – 56.95 %. The relative humidity inside the storage chamber varied between 81.68 – 89.11 %, 80.68 – 86.36 %, and 77.10 – 85.46 % for the inlet, inside the tomatoes and by the outlet of the storage chamber. The relative humidity increase varied between 28.52 – 47.66 %. This is comparable to the results obtained by Sibanda and Workneh (2020a) (13 – 41 %). The relative humidity range obtained in the grid powered ECS unit is similar to that obtained by the wind turbine powered ECS.

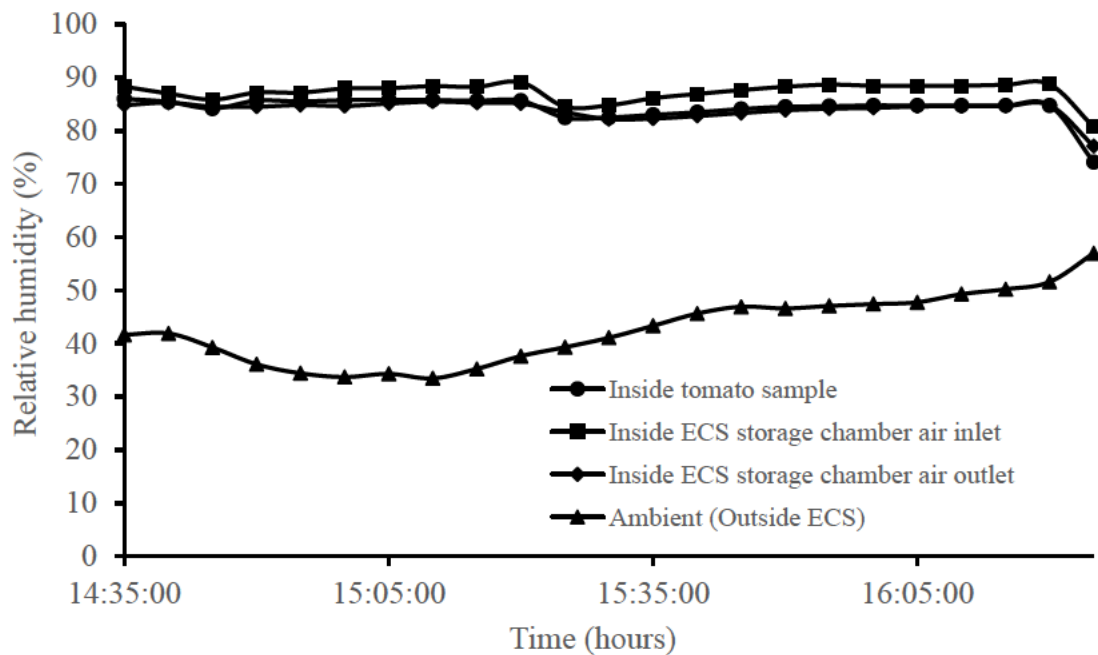
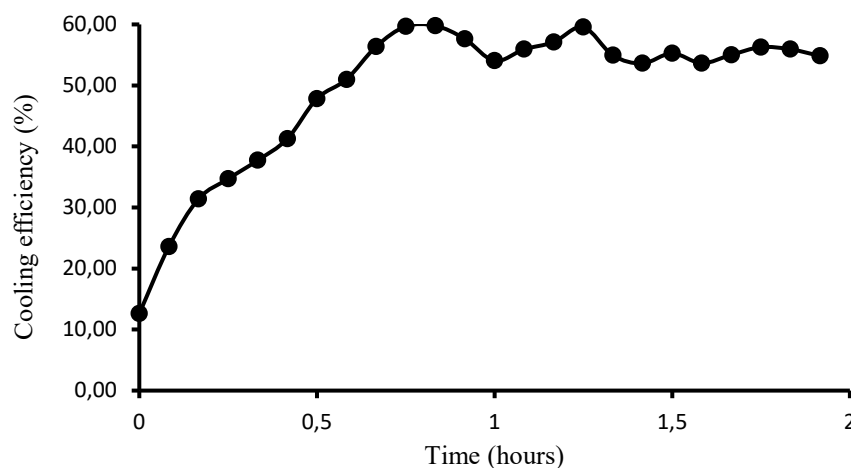


Figure 5.7 Relative humidity at different locations of the evaporative cooler unit using grid energy power source

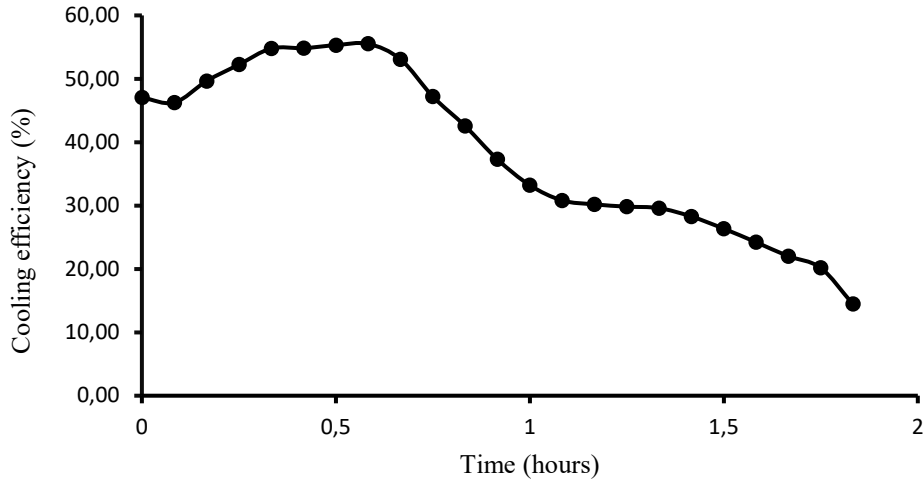
5.5.3 Cooling efficiency

Figure 5.8 shows the cooling efficiency of (a) the wind turbine-powered ECS unit and (b) the grid-powered ECS unit. The cooling efficiency of the wind turbine-powered ECS unit ranged between 12.62 – 59.78 %, and that of the grid-powered ECS unit varied between 14.46 – 55.93 %. The lowest cooling efficiency recorded of 12.62 % resulted due to not pre-cooling the ECS

unit for loading. The cooling efficiency found in this study is low but comparable to that reported by Nkolisa *et al.* (2018b) who obtained a cooling efficiency of 67.17 %. Sibanda and Workneh (2020a) found a cooling efficiency ranging between 88.04 – 95.6 %. However, this cooling efficiency is higher than that obtained in this study. The difference in the cooling efficiencies may be caused by the exclusion of the heat exchanger which may have improved the operation of the IAC + EC system. Regardless of the difference of these cooling efficiencies, the acquired cooling technology is sufficient to conclude that the wind turbine is a viable energy source for mobile cooling units. The distinct shapes of the cooling efficiency graphs for the grid- and wind turbine powered ECS unit can be attributed to the different but consistent time zones that the testing was performed at due to time constraints. The cooling efficiency of the wind turbine powered ECS unit was high because it was taken when the temperatures were high and that of the grid powered ECS unit was taken when the weather was having a mix of high and low temperatures. When the time of the day is factored out, the cooling efficiencies obtained should be similar provided that wind turbine and grid's only function is to provide electrical power and has no direct effect on cooling.



(a)



(b)

Figure 5.8 Cooling efficiency of (a) the wind turbine powered ECS unit and (b) the grid powered ECS unit

5.6 Conclusion

Both the power supply sources are able to adequately provide the required power to the ECS unit. This is evident from the temperature drop and relative humidity increase from the stored tomato sample. The temperature drop varied between 2.85 – 10.59 °C for the wind turbine powered ECS unit and 3.91 - 15.75 °C for the grid powered ECS unit. The relative humidity increase ranged between 57.28 – 88.77 % and 77.10 – 89.11 % for the wind turbine and grid electricity energy source, respectively. Lastly, the cooling efficiency of the wind turbine powered ECS system varied between 12.62 – 59.78 % and that of the grid powered ECS system ranged between 14.46 – 55.93 %.

From the findings in this study, it can be guaranteed that the electrical power generated using a wind turbine is adequate to operate the ECS unit which is not significantly different from the performance of the unit using grid electricity. This means that the wind turbine as a renewable energy alternative is a viable power source that can be used to power an evaporative cooling system or any cooling technology according to the power requirement of the cooling system. The ripening rate of sample tomatoes was reduced and tomatoes can be retained as marketable for an extended period without quality deterioration and therefore prolong their shelf life and smallholder farmers get more returns since consumers like to purchase good quality food.

5.7 References

- Cherono, K and Workneh, T. 2020. The Efficacy of Postharvest Biocontrol Treatments in Controlling Spoilage of Tomato Fruit in South African Commercial Supply Chains. *J. Eng. Agric. Environ* 5 19-25.
- Dorais, M, Ehret, DL and Papadopoulos, AP. 2008. Tomato (*Solanum lycopersicum*) health components: from the seed to the consumer. *Phytochemistry Reviews* 7 (2): 231-250.
- Haile, A and Safawo, T. 2018. Shelf life and quality of tomato (*Lycopersicon esculentum* Mill.) fruits as affected by different Packaging Materials. *African Journal of Food Science* 12 (2): 21-27.
- Ioannidi, E, Kalamaki, MS, Engineer, C, Pateraki, I, Alexandrou, D, Mellidou, I, Giovannonni, J and Kanellis, AK. 2009. Expression profiling of ascorbic acid-related genes during tomato fruit development and ripening and in response to stress conditions. *Journal of experimental botany* 60 (2): 663-678.
- Jain, D. 2007. Development and testing of two-stage evaporative cooler. *Building and Environment* 42 (7): 2549-2554.
- Kan, C, Gao, Y, Wan, C, Chen, M, Zhao, X, Liu, S and Chen, J. 2019. Influence of different cold storage times on quality of “Cuiguan” pear fruits during shelf life. *Journal of Food Processing and Preservation* 43 (12): e14245.
- Mothapo, M. 2022. Small-scale farmers and post-harvest losses. *Farmer's Weekly* 2022 (22030): 44-46.
- Nkolisa, N, Magwaza, LS, Workneh, TS and Chimphango, A. 2018. Evaluating evaporative cooling system as an energy-free and cost-effective method for postharvest storage of tomatoes (*Solanum lycopersicum* L.) for smallholder farmers. *Scientia Horticulturae* 241 131-143.
- Olosunde, WA, Aremu, AK and Onwude, DI. 2016. Development of a solar powered evaporative cooling storage system for tropical fruits and vegetables. *Journal of Food Processing and Preservation* 40 (2): 279-290.
- Porat, R, Lichter, A, Terry, LA, Harker, R and Buzby, J. 2018. Postharvest losses of fruit and vegetables during retail and in consumers’ homes: Quantifications, causes, and means of prevention. *Postharvest biology and technology* 139 135-149.
- Raut, R and Gardas, BB. 2018. Sustainable logistics barriers of fruits and vegetables: An interpretive structural modeling approach. *Benchmarking: An International Journal*.

- Sibanda, S and Workneh, TS. 2019. Effects of indirect air cooling combined with direct evaporative cooling on the quality of stored tomato fruit. *CyTA-Journal of Food* 17 (1): 603-612.
- Sibanda, S and Workneh, TS. 2020a. Performance evaluation of an indirect air cooling system combined with evaporative cooling. *Heliyon* 6 (1): e03286.
- Sibanda, S and Workneh, TS. 2020b. Potential causes of postharvest losses, low-cost cooling technology for fresh produce farmers in Sub-Sahara Africa. *African Journal of Agricultural Research* 16 (5): 553-566.
- Taha, A, Rahim, A and Eltom, O. 1994. Evaporative cooler using a porous material to be used for reservation of food. *Renewable Energy* 5 (1-4): 474-476.
- Tilahun, S. 2010. Feasibility and economic evaluation of low-cost evaporative cooling system in fruit and vegetables storage. *African Journal of Food, Agriculture, Nutrition and Development* 10 (8).
- Tongbram, T, Bora, J and Makroo, H. 2020. Fresh and Refrigerated Foods: Science, Shelf Life, and Quality. In: *Shelf Life and Food Safety*. CRC Press.
- Zhang, W-P, Yang, X-H, Mujumdar, A, Ju, H-Y and Xiao, H-W. 2022. The influence mechanism and control strategy of relative humidity on hot air drying of fruits and vegetables: a review. *Drying Technology* 40 (11): 2217-2234.

6. CONCLUSIONS AND RECOMMEDATIONS

6.1 Conclusion

The literature review in Chapter 2 revealed that smallholder farmers struggle with high post-harvest losses throughout the supply chain due to mishandling and unfavourable environmental conditions. This causes them to loss on market contracts as well as work on a loss. About 23 % of these PHL occur during transportation. Reefer units are available for storage and transportation of fresh produce, but due to their expensive nature, these are out of reach for use by smallholder farmers who rather use vans to save on expenses. Therefore, the main purpose of this was to develop and evaluate a small, portable wind turbine that can supply power to the proposed portable/mobile ECS unit or any other cooling technology as means to reduce the incurring costs of operating the cooling technology. Consequently, this helps reduce the purchase or hire costs of the cooling unit since it eliminates the dependence of fuels.

The use of small wind turbines on vehicles is a relatively new concept and there is limited literature on it. A moving vehicle gives rise to high wind energy on the road. This wind energy can be exploited to operate the wind turbine rotor and generate electrical energy. The literature reviewed for small wind turbine was on the general power output equation and its parameters. While air density does not have a significant effect on the power generation, the wind speed, swept area and power coefficient contribute greatly on the power generated. These parameters can be manipulated to obtain the required power output. The power coefficient is dependent on the tip speed ratio and pitch angle which are important for an optimum blade design. The Betz limit, approximated at 0.59 is the maximum power coefficient that a wind turbine can obtain. The permanent magnet synchronous generator (PMSG) and the doubly-fed induction generator (DFIG) are two of best variable speed generators since they can generate power at different wind speeds. Moreover, the PMSG can be directly coupled with the rotor, eliminating the need of a gearbox system. The BEM theory is employed for the design and optimisation of the blade with focus on each blade element. From this theory, the inflow angle, angle of attack, load coefficients, incoming flow and chord lengths were computed from which the maximum power output and power coefficient is obtained.

Chapter 3 focused on the BEM theory, QBlade and MATLAB Simulink modelling softwares which were used to adequately design the wind turbine blade and model the wind turbine system. The chord length for each section of the blade was determined for the SG6043 airfoil section using the BEM theory. QBlade further used the chord length to optimise the blade design while clearly defining the twist angles of each blade section that achieves maximum power. It was confirmed that a 600 mm diameter rotor requires a $3200 \text{ rev.min}^{-1}$ to support a 600 W load at a wind speed of 19.0 m.s^{-1} . Due to the unavailability of the specified PMSG in the market, a 600 rev.min^{-1} , 600 W PMSG was acquired. MATLAB Simulink was used to further model the rest of the wind turbine with the inclusion of the PMSG, three-phase rectifier, lead acid battery and the power inverter. The findings of MATLAB Simulink showed that a wind speed of 19.0 m.s^{-1} can achieve a power output of 611.8 W which validated the findings by QBlade.

Chapter 4 focused on the wind turbine prototype assemble using a 12 V, 600 rev.min^{-1} , 600 W permanent magnet synchronous generator. The furling mechanism was excluded in the design and a louvre mechanism was added to the design of the wind turbine along with a protective outer casing to control the airflow into the wind turbine. The vehicle speed and louvre opening levels were used as a treatment to assess the amount of power generated by each treatment combination. The maximum power output obtained was at a vehicle speed of 100 km.h^{-1} matching a power coefficient of 0.49. With the incorporation of a 230 VAC power inverter the battery voltage can be stepped up from 12 V to 230 V and thus make the system be able to provide the current required to operate a 33 W constant speed positive pressure fan, a 290 W fan for air transmission, and a 180 W water pump. Therefore, the findings of this chapter showed that the power output obtained in this study can continuously supply power to a 503 W load excluding electrical losses.

The results showed that unlike the vehicle speed of 60 km.h^{-1} which recorded low values of the wind turbine power output, the vehicle speed of 80 km.h^{-1} achieved high power output values which closely related to the power output obtained at a vehicle speed of 100 km.h^{-1} . Therefore, these findings suggest that in order to generate high power output, the vehicle speed of 80 and 100 km.h^{-1} should be used to transport fresh produce. Depending on the power output required, the louvre opening level can be opened on different levels to control the airflow into the wind turbine. The findings of this study validate that due to the size limitation of the rotor and

understanding the aerodynamic power output equation, the vehicle speed, which ultimately refers to the wind speed, has to be increased to meet the power requirement by the load.

Chapter 5 focused on the integration of the assembled wind turbine prototype with the 53 m³ ECS unit to assess its ability to continuously power the system. The grid electricity testing was used as a control measure. The cooling efficiency of 59.78 % and 55.93 % were obtained for the wind turbine-and grid-powered ECS unit, respectively. These cooling efficiencies were comparable and matched to the results obtained in other performance studies done by other researchers. This is proof that a wind turbine can successfully power an ECS system and other cooling technologies. This technology is also relatively affordable compared to the market value of a 600 W wind turbine. The wind turbine system can be easily modified to generate the required power of the load through using the BEM theory equation provided in this study and optimising the blade design through QBlade and lastly using MATLAB Simulink to model the entire wind turbine system together. Considering the abundance of wind energy for moving vehicles, the wind turbine can be adopted with definite success for any mobile cooling technology operation.

6.2 Recommendations

Based on the findings of this study, the following recommendations are suggested:

1. Investigate the aerodynamic effect of the wind load on the mounted wind turbine and the vehicle.
2. Perform the fatigue analysis of the blades to determine the life span of the PVC blades.
3. Develop a trailed ECS unit powered by the wind turbine instead of a portable, bakkie mounted ECS unit.
4. Investigate possible aerodynamic/drag effect of the wind turbine on overall performance of the vehicle and fuel efficiency
5. Add a wire mesh or net at the back of the wind turbine as safety measure to ensure that in the case of the blades breaking or any other component it does not fly to the following vehicles and potentially cause accidents
6. Automate the louvre mechanism to improve the ease of operation with the assistance of wind speed sensors.

7. APPENDIX

Table 7.1 Lead-acid voltage and charge capacity (Beale, 2022)

Voltage	Charge capacity
12.89 V	100%
12.78 V	90%
12.65 V	80%
12.51 V	70%
12.41 V	60%
12.23 V	50%
12.11 V	40%
11.96 V	30%
11.81 V	20%
11.70 V	10%
11.63 V	0%

Table 7.2 Battery charge measurements

Time (min)	Voltage (V)	Capacity charge (%)	Electrical energy (Wh)	Power (W)	Accumulated power (W)
0	11.7	10	60	0	0
5	11.78	17	102	42	42
10	11.86	23	138	36	78
15	11.91	27	162	24	102
20	11.94	29	174	12	114
25	12	33	198	24	138
30	12.07	37	222	24	162
35	12.16	44	264	42	204

40	12.23	50	300	36	240
45	12.3	54	324	24	264
50	12.38	58	348	24	288
55	12.45	64	384	36	324
60	12.49	68	408	24	348
65	12.54	72	432	24	372
70	12.61	77	462	30	402
75	12.66	81	486	24	426
80	12.72	85	510	24	450
85	12.79	91	546	36	486
90	12.86	97	582	36	522

Table 7.3 Average voltage readings at different opening levels of the louvre mechanism for different vehicle speed

Louvre opening level	Time (min)	Vehicle speed (km.h ⁻¹)		
		60	80	100
1	0	12.20	12.2	12.2
	15	12.22	12.23	12.27
	30	12.25	12.29	12.35
	45	12.30	12.34	12.41
	60	12.35	12.42	12.46
2	0	12.20	12.20	12.20
	15	12.27	12.29	12.28
	30	12.32	12.38	12.40
	45	12.36	12.46	12.51
	60	12.40	12.51	12.53

Table 7.4 Accumulated power of the small wind turbine with different louvre opening level subjected to different vehicle speeds

Louvre level	opening	Time (min)	Vehicle speed (m.s^{-1})		
			60	80	100
1	0		0.0(0.00) ^a	0.0(0.00) ^a	0.0(0.00) ^a
	15		8.4(7.27) ^a	29.4(7.27) ^{ab}	54.6(7.27) ^{bcd}
	30		42.0(7.27) ^{bc}	58.8(7.27) ^{bcd}	109.2(7.27) ^{fgh}
	45		75.6(0.00) ^{cde}	100.8(37.80) ^{efg}	147.0(7.27) ^{ijk}
	60		113.4(0.00) ^{fghi}	159.6(26.23) ^k	210.0(14.55) ^l
2	0		0.0(0.00) ^a	0.0(0.00) ^a	0.0(0.00) ^a
	15		58.8(7.27) ^{bcd}	84.0(14.55) ^{def}	63.0(0.00) ^{bcd}
	30		121.8(7.27) ^{ghij}	138.6(21.82) ^{hijk}	138.6(0.00) ^{hijk}
	45		151.2(54.92) ^{jk}	210.0(56.82) ^l	277.2(0.00) ^m
	60		142.8(7.27) ^{hijk}	268.8(38.49) ^m	294.0(7.27) ^m



(a)



(b)

Figure 7.1 (a) 1st level opening and (b) 2nd level opening of the louvre mechanism



Figure 7.2 Small wind turbine prototype